

STUDY ON PLASMA SHAPING AND CONTROL IN STEADY STATE SUPERCONDUCTING TOKAMAK (SST-1)

By

**SUBRATA JANA
ENGG06201404002**

Institute for Plasma Research, Gandhinagar.

*A thesis submitted to the
Board of Studies in Engineering Sciences
In partial fulfillment of requirements
for the Degree of*

DOCTOR OF PHILOSOPHY

of

HOMI BHABHA NATIONAL INSTITUTE

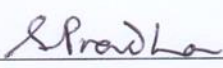
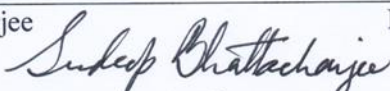
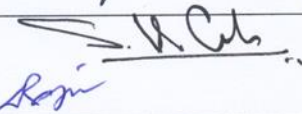


November, 2017

Homi Bhabha National Institute¹

Recommendations of the Viva Voce Committee

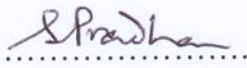
As members of the Viva Voce Committee, we certify that we have read the dissertation prepared by Subrata Jana entitled “Study on Plasma Shaping and Control in Steady State Superconducting Tokamak (SST-1)” and recommend that it may be accepted as fulfilling the thesis requirement for the award of Degree of Doctor of Philosophy.

Chairman - Dr. R. Srinivasan		Date: 16/05/2018
Guide / Convener - Dr. Subrata Pradhan		Date: 16/05/2018
Co-guide - Prof. Amita Das		Date: 16/05/2018
Examiner - Prof. Sudeep Bhattacharjee		Date: 16/05/2018
Member 1- Dr. Suryakant Gupta		Date: 16/05/2018
Member 2- Dr. Daniel Raju		Date: 16/05/2018
Technology Advisor- Mr. Chet Narayan Gupta		Date: 16/05/2018

Final approval and acceptance of this thesis is contingent upon the candidate's submission of the final copies of the thesis to HBNI.

I/We hereby certify that I/we have read this thesis prepared under my/our direction and recommend that it may be accepted as fulfilling the thesis requirement.


.....
Prof. Amita Das
(Co-guide)


.....
Dr. Subrata Pradhan
(Guide)

Date: 16/05/2018

Place: Institute for Plasma Research, Gandhinagar.

¹ This page is to be included only for final submission after successful completion of viva voce.
Version approved during the meeting of Standing Committee of Deans held during 29-30 Nov 2013

STATEMENT BY AUTHOR

This dissertation has been submitted in partial fulfillment of requirements for an advanced degree at Homi Bhabha National Institute (HBNI) and is deposited in the Library to be made available to borrowers under rules of the HBNI.

Brief quotations from this dissertation are allowable without special permission, provided that accurate acknowledgment of the source is made. Requests for permission for extended quotation from or reproduction of this manuscript in whole or in part may be granted by the Competent Authority of HBNI when in his or her judgment the proposed use of the material is in the interests of scholarship. In all other instances, however, permission must be obtained from the author.

Subrata Jana.

.....
Subrata Jana

DECLARATION

I, hereby declare that the investigation presented in the thesis has been carried out by me. The work is original and has not been submitted earlier as a whole or in part for a degree/diploma at this or any other Institution / University.

Subrata Jana.

.....
Subrata Jana

List of Publications arising from the thesis

Journal

1. “Vessel eddy current characteristics in SST-1 tokamak”, Subrata Jana, Subrata Pradhan, Jasraj Dhongde, Harish Masand and SST-1 Team, *Fusion engineering and design*, **2016**, Vol. 112, 380-387.
2. “Magnetic flux surfaces and radial Shafranov shifts in SST-1 tokamak plasma”, Subrata Jana, Subrata Pradhan*, Jasraj Dhongde, Harish Masand, Manoj Kumar, Sameer Kumar, Praveenlal Edappala, Hitesh Patel, Debashis Ghosh, SST- 1 Team, *Fusion engineering and design*, **2017**, Vol. 120, 39–48.
3. “Electromagnetic modeling of SST-1 plasma start-up”, Subrata Jana, Debashis Ghosh, Subrata Pradhan and Jasraj Dhongde. (To be Submitted)

Conferences

1. “Vessel eddy current measurement in SST-1 tokamak”. Subrata Jana, Subrata Pradhan, Jasraj Dhongde, Harish Masand and SST-1 team, 30th National Symposium on Plasma Science & Technology (PLASMA-2015), 1st to 4th December 2015, Saha Institute of Nuclear Physics, Kolkata, West Bengal, India
2. “The Determination of Plasma Radial Shafranov Shift (ΔR) and Vertical Shift (ΔZ) experimentally using Magnetic probe and Flux loop Method for SST-1 tokamak”, Subrata Jana, Jasraj Dhongde, Harish Masand, Subrata Pradhan, Sameer Kumar and SST-1 Team. 10th Asia Plasma Fusion Association Conference (APFA-2015), 14- 18th December 2015, Institute for Plasma Research, Bhat, Gandhinagar, Gujarat, India
3. “Electromagnetic field study and computation for SST-1 tokamak”, Subrata Jana, Debashis Ghosh, Jasraj Dhongde, Subrata Pradhan, CPP-IPR Silver Jubilee Symposium, 21st -22nd April 2016, Centre for Plasma Physics, Sonapur, Assam, India.
4. “Plasma Start-up Studies and Electromagnetic Field Computation for SST-1 tokamak”, Subrata Jana, Debashis Ghosh, Subrata Pradhan, Jasraj Dhongde, 26th IAEA Fusion Energy Conference (FEC-2016), 17th – 22nd October 2016, Kyoto International Conference Center, Japan.

Subrata Jana.

.....
Subrata Jana

Dedicated to my family and teachers.

ACKNOWLEDGEMENT

First and foremost, I would like to thank my thesis supervisor, Dr. Subrata Pradhan who has constantly inspired me for the completion of this thesis. It is impossible to detail all that I have learned from him, particularly working in an organized and time-bound manner, taking the initiative, being self-reliant, teamwork, having a positive outlook, being passionate about my work, a sense of patriotic duty and devotion. I thank him for the freedom that he has given me to do research and availability for discussion at any time. I consider myself extremely fortunate to work under his leadership and guidance and will forever owe a debt of gratitude for the time I have spent.

I would like to pay my sincere regards to my co-guide Prof. Amita Das for constant inspiration and various technical ideas.

I am also thankful to my doctoral committee Chairman Dr. R Srinivasan and the other committee members Dr. Daniel Raju, Dr. Suryakant Gupta and Mr. Chet Narayan Gupta for their valuable suggestions to improve the quality of this work.

I would like to convey my sincere regards to my senior colleagues and co-workers Mr. Jasraj Dhongde, Mr. Debashis Ghosh, Mr. Harish Masand, Mr. Kirit B Patel, Mrs. Kirti Mahajan, Mr. Sameer Kumar, Mr. Manoj Kumar, Mr. Praveenlal Edappalla, Mrs. Manisha Bhandarkar, Mr. Aveg Kumar, Mr. Hitesh Gulati, Mr. Hitesh Chudasma and other colleagues of the SST-1 team for their assistance during this period of research. I have enjoyed many stimulating discussions and learned various experimental and numerical techniques from them.

I am also thankful to Dr. Vipul L. Tanna, Prof. Subroto Mukherjee, Dr. Mainak Bandyopadhyay, Mr. Ritesh Sugandhi, Dr. Nirmal K Bisai, Mr. Yuvakiran Paravastu , Mr. Dilip C. Raval, Dr. Ziauddin Khan, Dr. Bharat Kakati, Mr. Tejas J. Parekh, Mr. Kirit R Vasava, Dr. Santanu Banerjee, Mr. Upendra Prasad, Mr. Azadsinh Makwana and Mr. Hitesh Patel for their kind support during my Ph.D. tenure.

I am also indebted to my teachers, Prof. Koushik Ghosh, Prof Amitava Gupta and Prof Achintya Mukhopadhyay for their encouragement to pursue a career in research, especially in nuclear fusion.

I would like to thank all of my hostel friends who have always wished me well. I have enjoyed the time that I have spent with them. Thanks to my batchmates, especially Gaurav Kumar Singh, Arun Pandey, Anirban Chakraborty, Rupak Mukherjee, Shivam Kumar Mishra, Avnish Kumar Pandey for their constant encouragement and enjoyable hostel atmosphere. I also like to thank my juniors Bhumi Chowdhury and Jal Patel for

their constant support. I am also thankful to all my TTP batchmates Hardik Mistry, Rohit Kumar, Jagabandhu Kumar, Prasad Rao, Arvind Tomar, Uday Maurya and Ratnesh Manu for their help and support. I like to thank some of my close friends especially Sankha, Abhijit, Arijit, Deberghya, Himadri, Soumyodeep, Prabeerda, Debashis, Arijit, Sourav, Anjani, Purnam, Suman, Madhushree, Sumona, Sutirtha, Iftikar, and Gourab for their encouragements for their kind support.

I would also like to convey my best wishes and thanks to the IPR scholar community specially to Kshitish Barada, Pravesh Dhyani, Sayak Bose, Manjit Kaur, Aditya Krishna Swamy, Soumen Ghosh, Vikram Dharodi, Neeraj Choubey, Vara Prasad Kella, Bibhu Prasad Sahoo, Rupendra Rajawat, Chandrasekhar Shukla, Mangilal Chowdhury, Meghraj Senguta, Akanksha Gupta, Vidhi Goyal, Deepa Verma, Harish Charan, Sonu Yadav, Debraj Mandal, Ratan Kumar Bera, Narayan Behera, Arghya Mukheree, Umesh Shukla, Modhugamba Laishram, Amit Patel, Bhumika Thakur, Sagar Sekhar Mahalik, Atul Kumar, Deepak Verma, Alamgir Mandal, Prabhakar Srivastava, Jervis Mendonca, Sandeep Shukla, Pallavi Trivedi, Meenakshee Sharma, Harshita Raj, Pranjal Singh, Srimanta Maity, Arnab Deka, Mayank Rajput, Priti Kanth, Gariama Arora, Dipshika Borah for creating a friendly ambience around me.

My family especially my maa, baba, didibhai, dadabhai and pupu have supported me with their patience, fun, and encouragement during the tenure of successful completion of this research and I am extremely thankful to them.

Last but not the least, I am also thankful to the library, administration and computer center staff for their kind support during my Ph.D. tenure.

Subrata Jana.

Subrata Jana

CONTENTS

<i>Chapter</i>	<i>Subtitle</i>	<i>Page</i>
	SYNOPSIS	i
	List of Figures	xxv
	List of Tables	xxix
	List of Abbreviations	xxix
	List of Symbols	xxxi
	Chapter I: Introduction of Fusion, Plasma & SST-1	1
	1.1 Nuclear Fusion	3
	1.1.1 Brief History of Nuclear Fusion	4
	1.1.2 Basic fusion equation	6
	1.1.3 Fusion vs. Fission.....	7
	1.1.4 Magnetic confinement of plasma.....	9
	1.1.5 Methods of plasma heating	12
	1.1.6 The role of fusion energy	14
	1.2 Plasma	16
	1.2.1 Application of plasma	19
	1.2.2 Different types of plasma.....	19
	1.3 Steady-state Superconducting Tokamak	24
	1.3.1 Basic Parameter of Steady State Superconducting Tokamak (SST-1)	25
	1.3.2 Magnet System.....	26
	1.3.3 Cryogenic System	28
	1.3.4 Vacuum Vessel and Pumping System	29
	1.3.5 Plasma Facing Components (PFC)	31
	1.3.6 High Power Radio Frequency Systems.....	32
	1.3.7 Diagnostics for SST-1 Tokamak.....	32
	1.3.8 SST-1 Control and data acquisition system	33
	1.3.9 Present status of SST-1	36
	Chapter II : Study of Vessel Eddy current in SST-1 Tokamak	37
	2.1 Basics of Eddy Current and its importance	39
	2.2 Motivation and Literature Survey	40
	2.3 Study of Vessel Eddy current in SST-1 Tokamak	43
	2.3.1 Model	45

2.3.2 Circuit Equations	47
2.3.3 Reconstruction of the B-field.....	49
2.3.4 Computational procedure.....	50
2.4 Results	51
2.5 Experiment for Validation using RCC coil	56
2.6 Summary and Conclusion	57
Chapter III : Electromagnetic Modeling of SST-1 Plasma start-up	59
3.1 Motivation and Literature Survey	61
3.2 Type of plasma start-up.....	64
3.2.1 Central solenoid based inductive (Ohmic) start-up	65
3.2.2 Ohmic with ECRH pre-ionization start-up.	66
3.2.3 Radio frequency (RF) driven non-inductive start-up or Solenoid free inductive startup.....	66
3.3 SST-1 Magnet System.....	67
3.4 Description of ANSYS Model	70
3.5 Result and Analysis.....	72
3.5.1 Validation of simulation model using known vertical field (VF) coil current	72
3.5.2 Different scenarios for SST-1 Start-up	74
3.5.3 Computation of Dynamic Null.....	77
3.5.4 Effects of Radial Control Coil (RCC).....	79
3.7 Summary and Conclusion	79
Chapter IV: Electromagnetic Diagnostics for SST-1	81
4.1 Motivation and literature survey.....	83
4.2 Importance of magnetic diagnostics and their challenges in tokamak study.	86
4.3 Brief description of various magnetic diagnostics	87
4.3.1 Rogowski coil	89
4.3.2. Diamagnetic Loop.....	91
4.3.3 Flux loops.....	95
4.3.4 Magnetic Probes:	96
4.4 Study and Installation of SST-1 Magnetic probe diagnostics.....	98
4.5 Results and Discussion.....	101
4.6 Observations & Conclusions.....	102
Chapter V: Plasma Radial Shift in Steady State Superconducting Tokamak (SST-1)	103
5.1 Motivation and literature survey.....	105

5.2 Principle	110
5.2.1 Radial Shafranov shifts Calculation.....	110
5.3 Results and Analysis	111
5.5 Comparison with imaging diagnostics	112
5.6 Observations & Conclusions.....	115
Chapter VI : Computation of magnetic flux surfaces using the magnetic diagnostics.....	117
6.1 Motivation and Literature Survey	119
6.2 Principle of Plasma Equilibrium	121
6.2.1 Plasma flux surface	121
6.2.2 Flux surface Calculation	123
6.3 Application for SST-1 Tokamak	127
6.3 Results and Analysis	129
6.4 Summary and Conclusions	130
Chapter VII : Study on Plasma Feedback Control related issues in SST-1.....	131
7.1 Motivation and literature survey.....	133
7.2 Basics of plasma position control.....	135
7.3 Basics of plasma Shaping	138
7.4 Initial implementation plasma radial position control in SST-1	140
7.4.1 Feedback methodology used in SST-1	140
7.4.2 Hardware for feedback methodology.....	143
7.4.3 Simulation Scenarios in open loop	145
7.5 Results and Discussion.....	145
7.6 Observations & Conclusions.....	148
Chapter VIII: Summary and future work.....	149
8.1 Summary and Conclusion	151
8.2 Future Work.....	155
Appendix I	157
Appendix II.....	158
Bibliography	161

SYNOPSIS

The demand for clean and abundant energy is continuously increasing in developing nations necessitated by rapid industrial development and escalating environmental sustainability issues. At present, a significant portion of energy [1] comes from fossil fuels i.e. oil, gas, and coal. Fossil fuels sources are finite. Further, fossil fuels add to environmental pollution. Therefore, considerable attention has been focussed on alternate sources of energy and especially on non-polluting and green form of energies. Many alternative energy sources [2] such as solar, wind, water, geothermal, biofuel and hybrid seem to be attractive from an ecological point of view. However, there exists serious scepticism about alternative energy sources [3] because of their limited energy density in a scenario where energy demands are growing monotonically. Fusion energy [4] can offer the world a nearly endless, economically viable source of energy with a very low environmental impact. For these reasons, ‘Nuclear Fusion’ could be a leading candidate amongst all forms of alternative energy resources if it succeeds. The magnetic confinement concept based on the ‘Tokamak’ [5] configuration is a promising contender towards achieving thermo-nuclear fusion with a Deuterium and Tritium plasma. For the last few decades, intensive research has been going on in the field of plasma start-up, plasma stability, plasma confinement, disruption and instability control etc. in Tokamaks. These studies are critical towards achieving thermo-nuclear fusion in reactor relevant tokamak devices including the ongoing international initiative ITER [6]-[7]. As a matter of fact, the deployment of advanced feedback control is mandatory for control of plasma position, current and shape etc. apart from kinetic control aspects. The present study is a maiden attempt in the first Indian Steady State Tokamak (SST-1) addressing some of the basic aspects of plasma initiation, plasma evolution, preliminary plasma controls and so forth. The spectrum of this scientific investigation can be divided into two broad parts.

The first module addresses the basis of plasma formation in SST-1 and its subsequent evolution as per the prevailing constraints of the device. Apart from explaining the observed plasma shots, desirable steps towards increasing the plasma currents have also been studied under this module. The next module studies the factors and measures that would improve the performance, specifically the duration of the SST-1 plasma. This study is important for the generation of useful inputs [8] towards implementation of a robust and precise feedback control system 0 that would contribute towards long-duration confinement of the SST-1 plasma column in the future. The thesis is organized as follows. The **first chapter** is an introduction to the basic study of nuclear fusion related technologies with the Tokamak as a flagship of fusion-based research reactors. This chapter also describes the first Indian Steady-state Superconducting Tokamak (SST-1). **Chapter-II** contains results on the characterization of Vessel eddy current characteristics in the SST-1 Tokamak and its effects on plasma start-up and poloidal null in the present operating scenario. Detailed studies on plasma start-up and electromagnetic modeling in SST-1 have been described using finite element analysis in **chapter -III**. This chapter also explains various experimental situations using operational combinations of the central solenoid, vertical field coil, the radial control coil and vessel eddy currents etc. In **chapter -IV**, details of the experimental set-up and associated magnetic diagnostics such as Rogowski coils, flux loops, magnetic probes and diamagnetic loops have been described. The utilization of these diagnostics in the present study has been described. **Chapter -V** contains the detailed description of plasma position measurement using magnetic diagnostics. The comparison between magnetic diagnostics with visible imaging diagnostics has also been described. Various analytical, numerical and experimental equilibrium studies have been presented in **chapter- VI**. It also contains results related to characteristics of the plasma column such as flux surfaces using

magnetic diagnostics under the prevailing constraints of the measurement of the pressure profile. In **chapter – VII**, the concept of a simple position feedback loop and its implementation towards position control using the vertical magnetic field and shift calculated from EM diagnostics have been described. Concluding remarks and a discussion about possible future extensions of the work reported have been described in **chapter - VIII**. The content of each of the chapter of the thesis is summarized below:

The Steady-state Superconducting Tokamak (SST-1)

Chapter-1 is a brief introduction to the basic study of nuclear fusion related technologies with the tokamak as a flagship of a fusion-based research reactor. This chapter also describes the first Indian tokamak, Steady-state Superconducting Tokamak (SST-1). The SST-1 is a plasma confinement experimental device (at the Institute for Plasma Research, Gandhinagar, Gujarat, India) employing Superconducting Magnets. The SST-1 was commissioned in June 2013 and has been in operation since then. The SST-1 [9] repeatedly produces a circular ohmic plasma having plasma current ~ 100 kA in a central field of 1.5 T for a typical duration of ~ 450 ms. Presently, experimental efforts are underway towards extending the SST-1 plasma duration. SST-1 plasma formation is dependent upon synchronization among its different systems and sub-systems. The primary magnetic configuration is provided by Super-Conducting Magnet [10] Systems (SCMS), comprising of sixteen superconducting D-shaped toroidal field (TF) magnets and nine superconducting poloidal field (PF) magnets [11][12]. An air core ohmic transformer (OT), together with an ECRH system is used for pre-ionization, break-down and initial current start-up. A pair of resistive vertical field magnets, located outside the cryostat and placed symmetrically around the midplane, provides the initial equilibrium conditions. The particle environment within the plasma chamber is maintained using gas

puffing. The eddy current distribution and the impurity level in the vacuum vessel needs to be precisely controlled for successful plasma shots with high current and repeatable.

Study of Vessel Eddy current in SST-1 Tokamak

Chapter-II of the thesis contains results on the characterization of Vessel eddy current characteristics in SST-1 Tokamak and its effects on plasma start-up and poloidal null in the present operating scenario. There is a lot of evidence that an unfavorable eddy current [13]-[14] can affect the null position significantly and hence the initial plasma breakdown characteristics can alter in a significant fashion. An important objective of our work has been to determine vessel current distribution and its influence on the overall null characteristics. Eddy current distribution [15] in the vacuum vessel of the SST-1 tokamak has been determined from the experimental data obtained, using an array of internal voltage loops (flux loop) installed inside the vacuum vessel. A simple circuit model has been employed. The model takes into account the geometric and constructional features of the SST-1 vacuum vessel. SST-1 vacuum vessel [16]-[17] is a modified 'D' shaped vessel having a major axis of 1.285 m and minor axis of 0.81m and has been manufactured from non-magnetic stainless steel. The plasma facing components installed inside the vacuum vessel are graphite blocks mounted on Copper Chromium Zirconium (CuCrZr) heat sink plates on inconel supports. During the discharge of the central solenoid, eddy currents get generated in the vacuum vessel and passive supports mounted on the vacuum vessel. These eddy currents influence early magnetic NULL dynamics, plasma breakdown and start-up characteristics. In this model, the SST-1 vacuum vessel has been divided into several segments, similar to a filament model for calculation purpose. In order to determine the eddy currents, the line average electric field around each segment needs to be measured. The flux generated by the central solenoid magnets in SST-1 is measured by the magnetically coupled in-vessel installed internal flux loops.

In this model, we have considered multiple simple circular shaped flux loops installed inside the SST-1 vessel section. The estimation of the magnitude and contour patterns of the net axisymmetric eddy current flowing in the vessel has been determined by the circuitual model. The well-known Kirchhoff's voltage equations have been used to measure induction effects on two concentric conducting loops such as the vessel segments and voltage measurement loop. The equivalent circuit contains the respective resistance, self and mutual inductances for each section. The computed results obtained from the model have been benchmarked against experimental data obtained in a large number of SST-1 plasma shots. The results are in good agreement. Once benchmarked, the calculated eddy current based on the flux loop signal and circuit equation model has been extended to the reconstruction of the overall B- field contours of SST-1 Tokamak in the vessel region. The individual normal and radial components of the magnetic field are computed for each vessel section using the off-axis formulation. These iso-B contours have helped to shape the profiles of the ohmic and equilibrium coils towards initiating the plasma column at the right location. A comparison of the field lines with and without the plasma column in identical conditions of the central solenoid and equilibrium field profiles have also been done with an aim to quantify the responses of the diagnostics. The rate of change of current in the central solenoid and sudden disappearance of plasma current during the disruptions are the main reasons causing substantial eddy currents on the vessel, cryostat, and in-vessel supports structures. The eddy currents have been found to be influencing the poloidal field null significantly and hence the breakdown characteristics of the plasma.

In the absence of a detailed filamentary model, a formalism with an associated code has been developed on a MATLAB platform which has provided critical inputs towards

plasma initiation and operation in the SST-1 device. This study of eddy current distributions can provide useful information for plasma equilibrium modeling.

Electromagnetic Modelling of SST-1 Plasma start-up

Chapter-III of the thesis describes studies on plasma start-up and electromagnetic modeling in SST-1 using finite element analysis. This chapter also explains various experimental situations employing operational combinations of the central solenoid, vertical field coil, the radial control coil and vessel eddy currents etc. Detailed studies of electromagnetic fields including field errors influencing Tokamak operation especially towards plasma break down, start-up and plasma controls are still areas of intense research [18]-[19]. SST-1 start-up studies and the development of an appropriate model have been performed using electromagnetic field computations for an active current carrying conductor and SST-1 vacuum vessel eddy characteristics. This electromagnetic model has been employed to predict individual electromagnetic field contours (iso-field) for active electromagnets such as vertical field coil (VF), poloidal field coil (PF), radial control coil (RCC), central solenoid (CS) and other active current carrying coil. This model can be also used to determine some other breakdown parameters such as connection length, ionization length, electric field etc. A static field Null calculation has been performed for initial magnetization stage. The 'eddy current' distribution in the vacuum vessel of the SST-1 tokamak has been used to compute the null region during the dynamic scenario; as during discharge of the central solenoid, eddy currents get generated in the vacuum vessel and on the passive supports mounted on it. These eddy currents influence early magnetic null dynamics, plasma breakdown and start-up characteristics. A study of the iso-field lines in various different scenarios has been computed using experimental profiles of the ohmic solenoid and vertical field coils which have been compared subsequently. Comprehensive research in the area of plasma

breakdown, start-up, and plasma controls are critical areas of tokamak research even today. Plasma current ramp-up and feedback control depend critically on the electromagnetic fields created by both active currents carrying coils and circulating currents in the passive elements in a tokamak. The initial stage of a tokamak discharge are generally divided into three phases: breakdown, plasma formation and current ramp up. Thereafter, a plasma flat-top is achieved using optimized current feedback control. Plasma initiation in a tokamak is most commonly achieved [20] with a Townsend avalanche. The gas inside the vacuum vessel is maintained at a certain pressure (P) and is ionized by applying a toroidal electric field (E). This toroidal electric field is induced by the variation of the current in the central solenoid. Alternative methods, [21]-[24] such as the Electron Cyclotron (EC) assisted pre-ionizations have also been adopted for tokamak plasma break down, especially where the devices are superconducting or in cases where the vacuum vessel and the cryostats are electrically continuous. In any successful plasma breakdown the connection length, L_C should be much greater than the ionization length, λ_i . The L_C , is defined as the distance an electron travels prior to its escape from the helical magnetic field of the tokamak. The λ_i denotes the distance an electron travels to gain sufficient kinetic energy from the toroidal electric field in order to ionize a neutral atom.

Ohmic or pre-ionization assisted plasma breakdown and the subsequent start-up remain very keenly investigated aspects of a tokamak. These issues have been attracting significant attention in recent years. A number of review articles have listed various formulations as well as methods of calculations. A two-dimensional FEM electromagnetic model has been employed to predict the stray field configuration explaining the Tokamak JET breakdown characteristics [25]. Specific experiments and corresponding modeling have been carried out to optimize the magnetic field null during

the breakdown at JET. An investigation of the field null for HL-2M Tokamak start-up has been performed by J. Liu [26] et. al. using the finite element method. This paper presents dynamic modeling of the inductive plasma start-up using an ohmic solenoid (CS) coil and some of the shaping (PF) coils currents. An ECRH assisted ITER start-up model has been described by B. Lloyd et al [27]. In this work, it has been predicted that in ITER the electric field applied for ionization and for ramping up the plasma currents may be feasible at a field value of 0.3 V m^{-1} . A zero-dimensional (0-D) code has been developed to analyze burn through in ITER. A similar type of analysis has been performed for SST-1 by Aveg Kumar et al. [28], explaining the successful plasma start-up under low loop voltage conditions. SST-1 has successfully achieved plasma break down and start-up assisted with EC in both the second harmonic mode as well in fundamental modes of operation [29]. In all these SST-1 experiments, successful plasma breakdown has been achieved at loop voltages of $\sim 3.0 \text{ V}$ that corresponds to $\sim 0.35\text{--}0.4 \text{ V/m}$ of a toroidal electric field in SST-1. Efficient ECH-assisted plasma start-up with low loop voltage and low volt-second consumption utilizing the trapped particles has been previously demonstrated by Young Hwa An [30] et al in spherical torus experiments. Operational scenarios involving plasma breakdown and current ramp-up phases in JT-60SA tokamak have been developed by H. Urano et al. [31]. In this work, it is shown that the operational scenarios for plasma breakdown and current ramp-up phase can be optimized by considering a large eddy current induced by the current ramp-up. Electron cyclotron heating (ECH)-assisted start-up experiments have been successfully performed by K. Kajiwara et al [32] in JT-60U following model predictions. Breakdown loop voltage was successfully reduced from 25 to 4V ($E = 0.26 \text{ V m}^{-1}$) by 200 kW ECH assisted pre-ionization. The plasma start-up designs of fully Superconducting tokamaks like EAST and KSTAR with implications for ITER have been described by J. A. Leuer et al [33]-

[34]. The COMPASS magnetic field originating from the poloidal field coils was computed using numerical integration of Biot-Savart law by J. Havlicek et al [35]. Finally, an attractive solenoid-free start-up scenario exploiting economic issues involving a tokamak based power plant has been performed by Wonho Choe [36] et. al. Thus, such a study involving the electromagnetic modeling is necessary in the case of SST-1 to ramp up plasma current. In this study, we have described a model that has captured the electromagnetic details of the SST-1 device during its EC assisted plasma breakdown and subsequent ohmic plasma start-up. The electromagnetic modeling of complex structures like tokamak could be performed accurately on Finite Element Analysis platforms such as ANSYS Maxwell. ANSYS Maxwell incorporates finite element method solvers to solve static, frequency-domain, and time-varying electromagnetic and electric fields. Here, in this model, the actual orientations and parameters of the coils have been given as inputs. The model also takes into account detailed geometric and constructional features of the SST-1 vacuum vessel and cryostat. Necessary material properties for this have also been appropriately incorporated in the modeling. Few structural constraints such as the viewports of the SST-1 have not been considered for this analysis. At first, the magnetic field generated by the Vertical field (VF) coil has been computed and compared with the experimental signals obtained from magnetic probe diagnostics during the 'VF only' shots. In that comparison, we have observed that the simulated results nearly match with the average magnetic field within the vessel. This has been used for benchmarking purposes in our electromagnetic model. After being benchmarked, the model has been extended to study various experimental situations considering operational combinations such as (a) only the Central solenoid (b) Central solenoid with combination of vertical field coil (c) the central solenoid with combination of vertical field coil and vessel eddy currents and (d) the central solenoid with a combination of vertical field coil,

the radial control coil and vessel eddy currents etc. The dynamic null i.e. evolution of the null has been computed using a time-dependent 3D transient model, accounting for vacuum vessel eddy currents induced by the changes in various external coils currents. These results have been subsequently validated against experimental results obtained from the magnetic diagnostics. Finally, the contribution of the radial control coil has been added, which demonstrates to be favoring to the plasma start-up scenarios. These predictions would serve plasma control measures during the plasma ramp up and flat-top to a certain extent.

This is a first-of-its-kind of study for SST-1. These studies would provide critical inputs towards the plasma control in SST-1 in future during the current ramp up as well as in the flat-top regime.

Study and Installation of SST-1 Magnetic diagnostics

Chapter-IV of this thesis describes the details of the experimental set-up and associated magnetic diagnostics such as Rogowski coils, flux loops, magnetic probes and diamagnetic loops etc. regarding their utilization in the context of studies in SST-1. Sources of the magnetic field in tokamaks are of various kinds. Usually, different profiles of currents need to be generated by the power supplies for activating current carrying coils towards initial magnetization and plasma control scenarios. Vessel eddy currents generated by induced voltages and the plasma current give rise to magnetic fields in the poloidal and toroidal directions inside a tokamak. The accurate measurements of these current and their fields employing magnetic diagnostics are simple, cost-effective and reasonably accurate. Various plasma parameters such as total plasma current, plasma position, plasma shape, plasma conductivity, total energy content and MHD instabilities [37]-[38] could be measured using specific magnetic diagnostics. Here, some of these

basic studies related employing these magnetic diagnostics, which have been used in the course of our investigation have been outlined.

Rogowski coil: A Rogowski coil is an electrical device for measuring alternating current (AC) or high-speed current pulses. It consists of a helical coil of wire with the lead from one end returning through the center of the coil to the other end, so that both terminals are at the same end of the coil. The whole assembly is then wrapped around the current carrying entity whose current is to be measured. Rogowski coil has been used in SST-1 to measure the plasma current (I_p). Two full Rogowski coils and two pairs of half Rogowski coils have been used to measure the SST-1 plasma current in present operating scenario. Different sets of Rogowski coil have been used to measure the different TR coils, Vertical field (VF) coil and radial control coil (RCC) currents.

The Rogowski coil outputs have been calibrated with a known source and known current profiles first. Once calibrated with sources like that of a RCC current profile, the SST-1 plasma currents have been measured in actual plasma shots.

Magnetic Probes: The SST-1 tokamak [39] is equipped with eighteen pairs of identically designed magnetic probes (tangential and normal). It consists of multi-turn coils oriented in a way that they intercept magnetic field lines and the resulting voltage is proportional to the rate of change of magnetic field. According to Faraday's law, the output of the magnetic probe is proportional to the derivatives of the magnetic flux passing through it ($V = -NA \frac{dB_i}{dt}$) where, NA is the actual magnetic section and i=t, n stands for tangential or normal direction. Each of these probes have been calibrated against a known field of a Helmholtz coil in a laboratory test setup. After installation, all probes were calibrated using an in-vessel control coil (RCC) and vertical field (VF) coil currents. An extensive study has been carried out, and it has been found that the probe's signals have a maximum deviation of less than 5% between expected fitted signals and experimentally obtained

signals for identical vacuum shots. These are reproducible over a large number of vacuum shots as well as with plasma shots. The hardware comprises of multichannel signal conditioning with an isolation amplifier and a noise removal filter with a selectable gain controller. In SST-1, a numerical integrator (with DC offset and integrating drift correction is required after the integration) is used for integration purposes. For the experimental measurement of the radial shift (ΔR) and vertical shift (ΔZ) in the SST-1 plasma, the sets of magnetic probes installed inside the SST-1 vacuum vessel has been used. Traditionally, these standard diagnostics have been installed at specific in-vessel locations have been used for accurate measurement of plasma positions in a Tokamak. In SST-1, four sets of probes have been used for this purposes. With due compensations, these measurements have been used for the radial and vertical shifts of the present SST-1 plasma column. An ultra-high vacuum compatible single core copper conductor has been used in the winding of these probes. Necessary metallic shielding has been added to avoid unwanted noise pick up. A compensation technique has been used to compensate OT and VF current field contributions on probe diagnostics signals during plasma shift measurements.

Flux loops: A flux loop is a loop of wire placed inside the plasma at a right angle. The magnetic field passes through the wire loop. As the field is varied inside the loop, it generates a voltage, driving a current. This is measured from the signal, from which the magnetic flux was measured. The induced voltage is determined by using Faraday's law.

SST-1 has eleven sets of in-vessel flux loops installed inside the vessel. A voltage is induced from the flux variation in the central solenoid and the vertical field. The plasma position and shape could then be computed from the magnetic probes and flux loop data, and subsequently validated with the analytical solution of the Grad-Shafranov equation (GSE). We have used a set of particular in-vessel flux loops for the measurement of

inboard (φ_{IN}) outboard flux (φ_{OUT}) and hence the radial Shafranov shift measurements in SST-1 plasma. An appropriate compensation technique has been used to estimate the plasma position information. A reference signal has been generated using non-plasma shots but having exactly the same parameters (profiles) such as an ohmic transformer (OT) and vertical field (VF) and other active coils. The contribution of plasma has been calculated from the difference between the reference signal and the signal from plasma shot.

Diamagnetic Loop: The diamagnetic flux measurement [40] using a simple poloidal coil can give us a significant amount of information about the tokamak plasma. Poloidal beta (β_p) is defined as the ratio of plasma kinetic pressure to the poloidal magnetic field pressure created by plasma current and can be measured directly from diamagnetic flux change. Poloidal beta and internal inductance (l_i) can be used for the measurement of $\beta_p + l_i/2$, which gives us information about Shafranov parameter and plasma shape. Plasma pressure and total stored pressure energy or diamagnetic energy has been determined using poloidal beta and plasma current. In SST-1, the diamagnetic flux change has been measured by taking the difference of the diamagnetic loop and compensating loop signals.

The Determination of Plasma Radial Shift (ΔR) in the Steady State Superconducting Tokamak (SST-1)

Chapter-V contains a detailed description of plasma position measurement using magnetic diagnostics. A comparison between magnetic diagnostics with visible imaging diagnostics has also been described in this chapter. The radial shift (ΔR) and vertical shift (ΔZ) have been calculated [8] for SST-1 experimentally using magnetic probes [41]-[42] and Flux loops [43]-[44]. The SST-1 plasma in the current phase of operations is circular

in shape and leans against the limiters and its position is calculated using this method. The radial and vertical shift formulated from the Shafranov equation have been used for computation. We have selected the best possible pairs of flux loops and magnetic probes location for the measurements. The comparison of results obtained from these two methods have also been performed for numerous shots for repeatability and reliability test for validation purpose. We have seen that results of this method are in good agreement for the SST-1 campaign. Since the control of plasma position plays an important role in plasma confinement and optimized tokamak operations, this ΔR could be used later as a plasma position feedback control parameter in long-duration SST-1 plasma experiments. In ohmically heated low beta tokamaks, the plasma equilibrium is achieved by balancing the outward hoop force against the radial force produced by the vertical field. These opposite forces may not be equal and hence the plasma undergoes a radial shift (ΔR) and vertical shift (ΔZ). These have been long considered as one of the fundamental problems of tokamak plasma control and equilibrium studies. The real-time computation of plasma position from magnetic diagnostics (i.e. flux loop and magnetic probes data after compensation techniques) has been used the vertical field control or B_v control. An error signal has been generated as proportional to plasma position and if that error signals magnitude exceeds the defined threshold limit then position controller output would adjust vertical field current to stabilize the plasma position.

Comparison with imaging diagnostics: An optical imaging system has been employed to detect the boundary of the plasma column formed, from which the plasma center has been inferred. The exact relation between the magnetic boundary, which is the Last Closed Flux Surface (LCFS), and the optical plasma boundary is unclear and difficult to compare quantitatively with great accuracy. However, scientists have tried these comparisons with acceptable accuracy [45]-[47]. In this study, the radial shift obtained from the plasma flux

surface contours computed from the Grad-Shafranov equations have been compared with the radial shift inferred from the optical imaging system. This comparison shows a good agreement between the plasma position shift from the flux surface contours and that from the imaging system.

The computation of flux surfaces using magnetic diagnostics

Various analytical, numerical and experimental equilibrium studies have been presented in chapter- VI. It also contains results related to characteristics of the plasma column such as flux surfaces using the magnetic diagnostics under the prevailing constraints of the measurement of the pressure profile. In tokamak physics, plasma equilibrium is a fundamental and essential element to understand not only basic equilibrium properties but also various plasma phenomena such as MHD instabilities, transport, turbulence, flows, waves etc. Recognizing the immense importance of these aspects, various analytical, numerical and experimental equilibrium studies have been conducted and tools have been developed. The necessary conditions for an axisymmetric toroidal plasma to be in an equilibrium have been first obtained by H. Grad et al [48] and V. D. Shafranov et al [49]-[51], called the Grad Shafranov equation (GSE). Its solutions are expanded in terms of the aspect ratio a/R of a tokamak, where 'a' and 'R' denotes the minor radius and major radius of the toroidal plasma column respectively. This equation does not include contributions due to current and longitudinal magnetic field over the plasma cross section. They have presented a formulation of plasma displacement by considering plasma as a conducting shell. A general analytical solution of the Grad Shafranov equation (GSE) has been presented by Zheng et al [52]. This work shows that if we possess a parametric description of a plasma, then an equilibrium can be computed with enough freedom to independently control pressure and plasma current, for arbitrary choices of plasma size, aspect ratio, elongation, and triangularity. This paper also

explains the scaling relations to produce a new solution with identical shape and poloidal beta, but with a rescaled value of the plasma current. Their solution has limitations, however, in the form of fixed boundary conditions and poloidal beta. In the works of Atanasiu et al [53], two families of exact analytical solutions of the Grad-Shafranov equation have been presented by specifying the highest polynomial dependence of plasma current density on the flux function. This solution uses the pressure profile and poloidal current density parameterizations with four degrees of freedom. Thus, an independent choice of the plasma current, the poloidal beta, internal inductance and the safety factor can be made. These solutions are applicable for both a D-shaped plasma and diverted plasma.

The study of poloidal beta and internal inductance by solving the GSE has been carried out for a circular cross-section tokamak by M. Asif et al [54]. They have shown that the calculated poloidal beta and plasma internal inductance depends on the plasma current. Remi G. Lefrançois et al [55] have presented a numerical solution for a three-dimensional nonlinear equilibrium equation for single species plasma confined on an equipotential boundary. An algorithm nearly identical to standard equilibrium techniques are presented by J. R. Ferron et al [56] could be used to identify tokamak equilibrium parameters for discharge control in real time scenarios. There are various other procedures to solve the Grad-Shafranov equation [57]-[58] and experimental methods to calculate plasma shift [59]-[61].

In this thesis, studies have been carried out to determine the equilibrium flux surfaces in SST-1 tokamak [8]. An experimental method has been presented and discussed to compute magnetic flux surface contours of the SST-1 tokamak plasma by fitting experimental measurements obtained from magnetic probes and flux loops measurements in the analytical solutions of the Grad-Shafranov equation for the first time in the context

of SST-1 plasma column. Here, we have chosen the Solov'ev [62] equilibrium solution for a circular plasma cross-section. Since the Solov'ev solution does not require an explicit profile of poloidal beta and plasma internal inductance, we have adopted the above family of solutions [63]. Nevertheless, the Solov'ev equilibrium solution has been used extensively to benchmark numerical equilibrium codes. It contains four unknowns; therefore, we need at least four boundary conditions. The boundary conditions is the magnetic flux measured at three poloidal positions of 0^0 , 90^0 and 180^0 and the magnetic field found by a magnetic probe at an angle of 90^0 within the machine cross-section. In order to determine these boundary conditions, we have used experimental magnetic diagnostics data. These have been provided by the fitting data obtained by the in-vessel probes and flux loops at four particular boundary locations inside the SST-1 vacuum vessel.

The theoretical and experimental flux surfaces thus computed for the present SST-1 operating conditions from magnetic diagnostics with the prevailing constraints of the pressure profile. A quantitative comparison has been done between the two. It has been observed that the computed flux surfaces using the experimental values agree well with those predicted from the theory [64]. A comparative study has then been carried out, between the shift computed from the magnetic diagnostics and that obtained from the synchronized visual imaging signal.

Study on Plasma Feedback Control related issues in SST-1

In chapter – VII of the thesis, the concept of a simple position feedback loop and its implementation towards position control using the vertical magnetic field and shift calculated from EM diagnostics has been described. Adequate control of the position of the plasma column within the tokamak is a primary requirement for quality discharges.

The use of advanced feedback control [65]-[66] in plasma position, current and shape are mandatory for an optimized tokamak performance. The profile of vertical field current (I_{VF}) is a function of plasma current, plasma position and poloidal beta; hence plasma pressure and temperature etc. A simple position feedback loop 0 has been implemented to contribute towards long-duration confinement of SST-1 plasma column. In our present feedback loop design, we have generated a reference vertical field current as proportional to the profile of plasma current. In that model, real-time plasma position computed from magnetic diagnostics (i.e. flux loop and magnetic probes) has been used after compensation technique. In the feedback loop, radial position direction is considered as +ve if plasma is moving outwards and -ve if plasma is moving inwards in reference to initial plasma position. An error signal has been generated proportional to plasma position and if that error signal's magnitude exceeds the defined threshold limit, then position controller output would adjust vertical field current (I_{VF}) by changing the actuator signal ($I_{VF} \pm \Delta I_{VF}$). ΔI_{VF} is generated as proportional to plasma position factor calculated from EM diagnostics. In this experiment, our efforts were to maintain the plasma position within the limit of ± 2 cm from the magnetic axis or, the position where the maximum plasma current has been achieved. The implementation of this basic feedback loop has helped to stabilize the plasma position in a particular position for a longer duration, consequently elongating the total plasma flat-top duration. The longest plasma duration (~450ms) has been achieved using the initial implementation of the position feedback loop with the prevailing constraints. As per the present status of the SST-1 machine, due to the non-availability of the in-vessel fast feedback coil only the vertical field current profile control has been used with the limitation of vessel time constant.

During this phase, all the quantities that characterize the plasma should remain as constant as possible. Therefore, control requirements are very stringent. Optimal control over tokamak discharge parameters, including plasma position, is very difficult to achieve. This is largely due to the difficulty in modeling tokamak discharge parameters, as they are highly nonlinear and time-varying in nature. Upgradation of the SST-1 tokamak incorporating advanced position control implementation is being considered for the future [67]-[68] which uses the vertical magnetic field and the in-vessel fast feedback coil.

Concluding remarks and a discussion about possible future extensions of the work reported have been described in the last chapter of this thesis work.

The most significant achievement of this study is the improvement of the physical performance of the SST-1 plasma specifically in achieving the highest current ($>110\text{kA}$), optimizing the initial start-up scenario and longest duration plasma ($\sim 450\text{ms}$) and using the initial implementation of the position feedback loop possible under the prevailing constraints.

Bibliography

- [1] Zou Caineng et al., Energy revolution: From a fossil energy era to a new energy era, *Natural Gas Industry B* 3 (2016) 1-11
- [2] N.L. Panwar, S.C. Kaushik, Surendra Kothari., Role of renewable energy sources in environmental protection: A review, *Renewable and Sustainable Energy Reviews* 15 (2011) 1513–1524.
- [3] Javid Mohtasham, Review Article-Renewable Energies, *Energy Procedia* 74 (2015) 1289 – 1297.
- [4] Abbas Azarpour et al., A Review on the Drawbacks of Renewable Energy as a Promising Energy Source of the Future, *Arabian Journal for Science and Engineering* 38 (2013) 317–328.
- [5] Mitsuru Kikuchi, A Review of Fusion and Tokamak Research Towards Steady-State Operation: A JAEA Contribution, *Energies* 3 (2010) 1741-1789
- [6] O. Motojima., The ITER project construction status, *Nucl. Fusion* 55 (2015) 104023 (20pp)
- [7] R.J. Hawryluk et al., Principal physics developments evaluated in the ITER design review, *Nucl. Fusion* 49 (2009) 065012 (15pp).
- [8] S. Jana et al., Magnetic flux surfaces and radial Shafranov shifts in SST-1 tokamak plasma, *Fusion engineering and design* 120 (2017) 39–48.
- Kirit Patel, et al., Design and Architecture of SST-1 basic plasma control system, *Fusion engineering and design* 112 (2016) 703-709.
- S. Pradhan et al., The First Experiment in SST-1, *Nuclear Fusion* 55 (2015) 104009.
- [9] S. Pradhan et al., Initial results in SST-1 after up-gradation, *Journal of Physics: Conf. Series* 1234567890 823 (2017) 012004
- [10] Pierluigi Bruzzone, Superconductivity and fusion energy—the inseparable companions, *Superconductor Science and Technology* 28 (2015) 024001 (6pp).
- [11] S. Pradhan et al., SST-1 Poloidal Field Magnets. *Proc. 17th IEEE NPSS Symp. on Fusion Engg*, California (1997), 665-668.
- [12] Ashoo N. Sharma, Thesis: Studies on quench characteristics of superconducting magnets of SST-1 (2015).
- [13] L.R Turner, Eddy current analysis in fusion device, *ANL/FPP/223 DE* 88013326
- [14] D.A. Gates, J. E. Menard and R. J. Marsala., Vessel eddy current measurement for the National Spherical Torus Experiment, *Review of Scientific Instruments* 75(12) (2004) 5090-5093.

- [15] S. Jana, et al., Vessel eddy current characteristics in SST-1tokamak, *Fusion Eng. Des.* 112 (2016) 380-387.
- [16] Ziauddin Khan et al., Vacuum system of SST-1 Tokamak, *Fusion engineering and design* 88 (2013) 692-695.
- [17] Ziauddin Khan et al., Overall Performance of SST-1 Tokamak Vacuum System, *IEEE transactions on plasma science*, 42(4) (2014) 1006-1011.
- [18] L.R Turner, Electromagnetic computations for fusion devices, *COMPUMAG-Tokyo Conference*, Tokyo, Japan, September 3-7, 1989.
- [19] Makoto Hasegawa et al., Experiments of Tokamak Discharge and Simulation of Magnetic Field Configuration in Tokamak-Helical Hybrid Device TOKASTAR-2, *Plasma and Fusion Research* 7 (2012) 2402116
- [20] R. Papoular., The genesis of toroidal discharges, *Nuclear fusion* 16 1 (1976) 37-45.
- [21] B Lloyd et al, Low voltage ohmic and electron cyclotron heating assisted start-up in DIII-D, *Nucl. Fusion* 31 (1991) 2031.
- [22] G. L. Jackson et al., Second harmonic electron cyclotron pre-ionization in the DIII-D tokamak, *Nucl. Fusion* 47 (2007) 257–263.
- [23] G. L. Jackson et al., ITER start-up studies in the DIII-D tokamak, *Nucl. Fusion* 48 (2008) 125002.
- [24] G. Granucci et al., Experiments and modeling on FTU tokamak for EC assisted plasma start-up studies in ITER-like configuration, *Nucl. Fusion* 55 (2015) 093025 (10pp)
- [25] R. Albanese et al., Experimental results with an optimized magnetic field configuration for the JET breakdown, *Nucl. Fusion* 52 (2012) 123010.
- [26] J. Liu et al., Investigation of field null for HL-2M tokamak start-up, *2013 IEEE 25th Symposium on Fusion Engineering (SOFE)*.
- [27] B. Lloyd et al., ECRH-assisted start-up in ITER, *Plasma Phys. Control. Fusion* 38 (1996) 1627–1643.
- [28] Aveg Kumar et al., 0-D modeling of SST-1 plasma break-down & start-up using ECRH assisted pre-ionization, *Fusion Engineering and Design* 105 (2016) 22–28
- [29] Kirit Patel et al., Observation on fundamental and second harmonic mode ECRH assisted plasma startup in SST-1 experiments, *Fusion Engineering and Design* 106 (2016) 99–102.
- [30] YoungHwa An et al., Efficient ECH- assisted plasma start-up using trapped particle configuration in the versatile experiment spherical torus, *Nuclear Fusion* 57(2017) 016001(11pp)

- [31] H. Urano et al., Development of operation scenarios for plasma break down and current ramp-up phases in JT-60SA tokamak, *Fusion engineering and design* 100 (2015) 345-356.
- [32] K. Kajiwara et al., Electron cyclotron heating assisted start-up in JT-60U, *Nucl. Fusion* 45 (2005) 694–705.
- [33] J. A. Leuer et al., Plasma Start-up Design of Fully Superconducting Tokamaks EAST and KSTAR With Implications for ITER, *IEEE transactions on plasma science* 38(3) (2010) 333-340.
- [34] J. A. Leuer et al., Tokamak start-up modeling and design for EAST first plasma campaign, *Fusion Sci. Tech.* 57 (2010) 48–65.
- [35] J. Havicek and O. Hronova., Characterization of the Magnetic field in the COMPASS tokamak, *WDS,08 Proceedings of Contributed papers,2* (2008) 110-114.
- [36] WonhoChoe et al., solenoid free toroidal plasma start-up concepts utilizing only the outer poloidal field coils and a conducting center-post, *Nuclear Fusion* 45 (2005) 1463-1473.
- [37] Jasraj Dhongde et al., Study of MHD activities in the plasma of SST-1, *Fusion Engineering and Design* 108(2016) 77-80
- [38] Jasraj Dhongde et al., MHD mode evolutions prior to minor and major disruptions in SST-1 plasma, *Fusion Engineering and Design* 114(2017) 6–12
- [39] D. Raju, et al., Design of magnetic diagnostics for SST-1, *Fusion Engineering and design* 34-35 (1997) 717-720
- [40] Sameer Kumar et al., Diamagnetic flux measurement in Aditya tokamak, *The Review of scientific instruments* 81(12) (2010)123505
- [41] H. Ninomiya and Norio Suzuki, Estimation of plasma position and $\beta_{p+li/2}$ from magnetic measurements under High $-\beta$ condition in JFT-2, *Japanese Journal of Applied Physics* (1982) 21(9) 1323-1327.
- [42] A. SalarElahi., et al., Measurement of plasma boundary shift and approximation of magnetic surfaces on the IR-T1 tokamak, *Brazilian Journal of physics*, (2010) 40(3).
- [43] A. Salar Elahi, et al., Estimation of plasma horizontal displacement using Flux loops and comparison with analytical solution in IR-T1 tokamak, *Journal of Nuclear and Particle Physics* 2(6) (2012) 142
- [44] A. Salar Elahi and M. Ghoranneviss, High-temperature plasma equilibrium analysis by remote magnetic diagnostics in large aspect ratio tokamaks, *International Journal of Hydrogen Energy*. (2016) 1-8.

- [45] G. Hommen, et al., Optical boundary reconstruction of tokamak plasmas for feedback control of plasma position and shape, *Review of scientific instruments* (2010) 81113504.
- [46] G. Hommen, et al., Real-Time optical plasma boundary reconstruction for plasma position control at the TCV tokamak, *Nucl. Fusion* 54 (2014) 073018.
- [47] P. Hacek, et al., Plasma boundary reconstruction using the Fast camera on COMPASS Tokamak, *WDS 14 Proceedings of contributed paper-physics* (2014) 221-226.
- [48] H. Grad and H. Rubin., Hydromagnetic equilibria and force-free fields, *Proceedings of the Second United Nations Conference on the Peaceful Uses of Atomic Energy, United Nations, Geneva, Vol. 31* (1958) 190-197.
- [49] V. D. Shafranov., On magneto-hydrodynamical equilibrium configurations, *Soviet J. Exp. Theor. Phys.* 6(1958) 545-554.
- [50] V. D. Shafranov, Equilibrium of a toroidal plasma in a magnetic field, *Journal of nuclear energy* 5 (1963) 251-258.
- [51] V. S. Mukhovatav and V. D. Shafranov, Plasma equilibrium in a tokamak, *Nucl. Fusion* 11 (1971) 605.
- [52] S. B. Zheng, A.J. Wootton and E. R. Solano, Analytical tokamak equilibrium for shaped plasmas, *Phys. Plasmas* 3 (1996) 1176.
- [53] C. V. Atanasiu, S. Gunter, K. Lackner and I. G. Miron, Analytical solutions to the Grad Shafranov equation, *Physics of Plasmas* 11(7) (2004).
- [54] M. Asif, A. Asif, Study of poloidal beta and internal inductance by solving the simplest Grad Shafranov equation for a tokamak with a circular cross-section, *Journal of applied mechanics and technical physics* (2014) 55(6) 927.
- [55] Remi G. Lefrancois, et al., Numerical investigation of three-dimensional single-species plasma equilibria on magnetic surfaces, *Physics of plasma* (2005)12 072105.
- [56] J. R. Ferron, et al., Real-time equilibrium reconstructions for tokamak discharge control, *Nuclear Fusion* 38(7) (1998).
- [57] L.L. Lao, et al., Equilibrium Analysis of Current Profiles in Tokamaks, *Nucl. Fusion* 30 (1990) 1035.
- [58] Z. Amerian, et al., Control of heat and mass transfer processes by plasma equilibrium reconstruction in toroidal magnetic confinement nuclear fusion devices, *International Journal of Thermal Sciences* (2016) 110 299-303.

- [59] R. Lopez- Callejas, et al., Plasma position measurement on Novillo Tokamak, *Fusion Eng. Des.* 54 (2001) 21-29.
- [60] Seong-Heon Seo., Plasma current Position measurement in the Korea Superconducting Tokamak Advanced research device, *Physics of plasmas* (2009), 16032501.
- [61] S. V. Mirnov, A probe method for measuring the displacement of the current channel in the cylindrical and toroidal discharge vessel, *Journal of nuclear energy* 7 (1965) 7325.
- [62] L. S. Solov'ev, et al., *Soviet Physics JETP* 26(2) (1968) 400.
- [63] A. Rahimirad, et al., Demonstration of Shafranov Shift by the Simplest Grad-Shafranov Equation Solution in IR-T1 tokamak, *Journal of fusion energy* 29 (2010) 73.
- [64] D. Nath, and M. S. Kalra, Solution of Grad –Shafranov equation by the method of fundamental solutions, *Journal of plasma physics* 80(3) (2014) 477-494.
- [65] Akihisa Kameari and Setsuo Niikura, Control of plasma vertical position in Tokamak reactors, *Nuclear Engineering and Design/Fusion* 2 (1985) 365-373
- [66] V. A. Belyakov et al., Plasma position and current control in a T-15 tokamak, *Plasma Devices and Operations* 2(1) (1992) 61-75.
- [67] W Z Yu et al., Plasma horizontal position control for the J-TEXT tokamak-based on feedforward density compensation, *Plasma Phys. Control. Fusion* 56 (2014) 045002 (7pp).
- [68] Giuseppe Ambrosino et al., Design of the Plasma Position and Shape Control in the ITER Tokamak Using In-Vessel Coils, *IEEE Transactions on Plasma Science* 37 (2009). 7 1324.

List of Figures

<u>Figure No</u>	<u>Description of Figure</u>	<u>Page</u>
<u>Chapter I</u>		
Figure 1.1	A basic fusion reaction of Deuterium with Tritium	3
Figure 1.2	Advances in fusion research with time and type.	5
Figure 1.3	Advances in Fusion Research.	5
Figure 1.4	Tokamak, Spherical Tokamak and Stellarator.	11
Figure 1.5	The Schematic diagram of Fusion Power plants.	15
Figure 1.6	Conceptual illustration of matter becoming plasma.	18
Figure 1.7	A Photograph of SST-1	24
Figure 1.8	A 3-D cut view of SST-1 Machine.	27
Figure 1.9	SST-1 2D cross-section view.	27
Figure 1.10	SST-1 Vacuum vessel sector.	30
Figure 1.11	Basic SST-1 plasma control Subsystem network interface.	35
<u>Chapter II</u>		
Figure 2.1	Schematic of Eddy current generation.	40
Figure 2.2	The orientation of flux loops (Red dot) and SST-1 vacuum vessel.	45
Figure 2.3	The Segments of SST-1 vacuum vessel used for calculation purpose.	46
Figure 2.4	The schematic representation of single vessel segments and corresponding flux loop used for Calculation purpose.	47
Figure 2.5	The Circuit Model between flux loops and SST-1 vacuum vessel Segments.	47
Figure 2.6	The Flow chart of Eddy Current Measurements.	50
Figure 2.7	(a) The actual flux loop signals and (b) The corresponding segmental eddy current calculated from flux loop signals for vacuum Shot#6059.	52
Figure 2.8	The total eddy current with $I_p = 0$ and I_{OT} , I_{VF} (green) for vacuum Shot# 6059.	52
Figure 2.9	(a) The actual flux loops signal and (b) The segmental eddy current of SST-1 vacuum vessel for plasma Shot # 6063.	53
Figure 2.10	The total eddy current with I_p , I_{OT} and I_{VF} (green) for plasma shot no 6063	53
Figure 2.11	The comparison of the eddy field line between vacuum Shot# 6059 and plasma Shot #6063 at 30ms, 220ms and 475ms.	55
Figure 2.12	(a) The Predefined RCC current pulse and measured eddy current for before and after PFC installation. (b) The Comparison of Internal (blue) and External (red) Rogowski voltage signal and their comparison for before and after PFC installation. (c) The Comparison of Internal (blue) and External (red) Rogowski signal Current and their comparisons for before and after PFC installation.	57

Chapter III

Figure 3.1 Schematic block diagram up ohmic start-up using central solenoid.	65
Figure 3.2 Schematic block diagram of solenoid free inductive start-up.	67
Figure 3.3 a) Top View of SST-1 Tokamak b) The Cross-sectional View of SST-1 Machine.	69
Figure 3.4 a) The actual drawing of SST-1 current carrying coil b) Side view with actual dimension, c) The actual TR1 coils, d)The cross sectional view of individual rectangular single turn copper coil and e) The dimension of rectangular single turn coil.	69
Figure 3.5 The Flow chart of FEM Modelling.	71
Figure 3.6 The ANSYS model a) Overall 3D transient model with selected boundary region	71
Figure 3.7 (a) The evolution of vertical field current for Pure VF Shot # 8573.(b)The comparison between measured magnetic field from probe diagnostics and simulated magnetic field using finite element modelling for Pure VF Shot # 8573.	73
Figure 3.8 (a) The Iso – B field line and (b) The B vector field line for Pure VF Shot # 8573 at 3.2kA.....	74
Figure 3.9 The evolution of simulated magnetic field in different experimental scenario for SST-1.	76
Figure 3.10 (a) Plasma current (I_P), (b) Central solenoid current (I_{OT}) (c)Vertical field current (I_{VF}) (d) Vessel pressure (e) ECRH Power (f) H_{Alpha} signal for SST-1 shot # 8707 during startup.	76
Figure 3.11 The evolution of Dynamic null region simulated using FEM modelling tools for specimen shot # 8707.....	78
Figure 3.12 (a) The magnetic field measured using magnetic probe diagnostics and its magnified representation shown below. (b) The profile of vessel eddy current field measured using flux loop diagnostics and its magnified representation has been shown below.....	78
Figure 3. 13 The evolution of simulated magnetic field with contribution of the RCC coil.	79

Chapter IV

Figure 4.1 Schematic figure of a plasma magnetic diagnostics.....	89
Figure 4.2 Structure of Rogowski coil	90
Figure 4.3 Diamagnetic and compensating loop positioning in SST-1 poloidal plane. .	94
Figure 4.4 Schematic of typical magnetic coil and integrators	97
Figure 4.5 Structure of Magnetic Probes.....	97
Figure 4.6 (In left) The design parameter of magnetic diagnostics and (in right) a photograph of installed magnetic probe within the SST-1 vessel has been presented. ...	99
Figure 4.7 The basic blocks of magnetic diagnostics.	100
Figure 4.8 The schematic orientation of magnetic probe diagnostics with.	100
Figure 4.9 Layout of SST-1 existing magnetic diagnostics.....	101
Figure 4.11 The comparison between theoretical and experimentally obtained signals.	102

Chapter V

Figure 5.1 (a) Plasma current (I_P), (b) Central Solenoid current (I_{OT}), (c) Vessel Pressure, (d) ECRH Power, (e) Internal Loop Voltage, (f) Internal Loop Voltage for SST-1 Shot No: 7712.	108
Figure 5.2 (a) The Schematic orientation of Magnetic Probe (Red Dot and Circle) is used for measurement. (b) The Actual orientation of flux loops (Red Dot).....	109
Figure 5.3 Schematic diagram of Flux loop orientation.	109
Figure 5.4 Plasma current [top], comparison of radial shift [middle] and applied vertical field current (I_{VF}) [lower] for SST-1 Shot no 7712.	112
Figure 5.5 The boundary approximation of camera image.....	113
Figure 5.6 Horizontal image Profile for shot # 7916.....	113
Figure 5.7 Comparison between the shifts of imaging with Magnetic.....	114

Chapter VI

Figure 6.1 Magnetic flux surfaces forming a set of nested toroids.	123
Figure 6.2 Schematic diagram of flux loop orientation.	126
Figure 6.3 Plasma position control feedback loop.....	127
Figure 6.4 (a) Magnetic flux surface and (b) maximum flux value position for SST-1 shot #7916 ($I_P \approx 90\text{kA}$) (experimental) c) Magnetic flux surface as an ideal case and (d) maximum flux value position at maximum plasma current ($I_P \approx 90\text{kA}$)(theoretical) ..	129

Chapter VII

Figure 7.1 Basic blocks of control loop.....	135
Figure 7.2 Typical use of vertical field coil to maintain plasma position	136
Figure 7.3 Typical sequence of event in a plasma experiment in Tokamak.....	137
Figure 7.4 Magnetic field for basic plasma shaping.....	139
Figure 7.5 Some of standard form of shaped plasma a) circular, b) D- shaped, c) Vertically elongated and d) modified D-shaped plasma.....	140
Figure 7.6 Schematic of B_V Feedback Control Loop	142
Figure 7.7 Comparison of plasma shot # 7024(blue) and shot#7026(red) (position control loop applied. The Subplots represent a) plasma current b) Loop voltage c) OT current d) Radial shift and e) vertical field current.	146
Figure 7.8 A longer duration plasma shot using position control loop. SST-1 plasma shot # 7812. The Subplots represent a) plasma current b) Loop voltage c) Radial shift and d) vertical field current.....	147

List of Tables

Page

Table 1.1: Nuclear Fission vs. Nuclear Fusion	7
Table 1.2: Different types of plasma	19
Table 1.3: Typical parameters of different types of plasma	23
Table 1.4: SST-1 Basic Plasma parameters	25
Table 1.5: SST-1 CRYOSTAT Parameter	29
Table 1.6: SST-1 Vacuum vessel parameter.....	30
Table 2.1: Computed Parameters of SST-1 Vessel.....	48
Table 3.1: SST-1 Magnet parameter (TRs and VFs)	68
Table 4.1: List of Plasma Diagnostics	88

List of Abbreviations

ITER	-----	International Thermonuclear Experimental Reactor.
SST-1	-----	Indian Steady State Superconducting Tokamak.
IPR	-----	Institute for Plasma Research.
SCMS	-----	Super-Conducting Magnet Systems.
OT	-----	Ohmic transformer.
EDDY	-----	Eddy Current.
EC	-----	Electron Cyclotron
ECRH	-----	Electron Cyclotron Resonance Heating.
NBI	-----	Neutral-beam injection.
RF	-----	Radio-frequency.
TF	-----	Toroidal Field
VF	-----	Vertical Field.
PF	-----	Poloidal Field.
PFC	-----	Plasma Facing Component.
CuCrZr	-----	Copper Chromium Zirconium.
KVL	-----	Kirchhoff's voltage equations.
RCC	-----	Radial Control Coil.
CS	-----	Central Solenoid.

0-D	-----	Zero-dimensional.
FEM	-----	Finite Element Method.
JET	-----	Joint European Torus.
DIII-D	-----	Doublet III (D-Shaped) Tokamak.
DEMO	-----	Demonstration Power Plant.
KSTAR	-----	Korea Superconducting Tokamak Advanced
Research.		
EAST	-----	Experimental Advanced Superconducting
Tokamak		
COMPASS	-----	COMPact ASSEMBly Tokamak.
JT-60U	-----	Japan Torus-60.
START	-----	Small Tight Aspect Ratio Tokamak.
MAST	-----	Mega Ampere Spherical Tokamak.
TCV	-----	Tokamak à Configuration Variable.
NSTX-U	-----	National Spherical Torus Experiment Upgrade.
ASDEX	-----	Axial symmetrisches Divertor experiment
W7-X	-----	Wendelstein 7-X
HSX	-----	Helically Symmetric Experiment
ANSYS	-----	ANalysis SYStem
GSE	-----	Grad-Shafranov equation.
EM	-----	Electromagnetic Diagnostics.
B _v	-----	Vertical Field Control.
LCFS	-----	Last Closed Flux Surface.
a/R	-----	Aspect Ratio.
I _{vF}	-----	Vertical Field Current.
I _p	-----	Plasma current
D-T	-----	Deuterium Tritium Reaction.
MeV	-----	Mega electron volt.
keV	-----	Kilo electron volt.
eV	-----	Electron volt (1.6×10^{-19} Joules).
B _T	-----	Toroidal Field.
CICC	-----	Cable-In-Conduit Conductor.
LN2	-----	Liquid Nitrogen.
HRL	-----	Helium Refrigerator/liquefier.
She	-----	Supercritical helium.
SCADA	-----	Supervisory Control and Data Acquisition system.
PLC	-----	Programmable Logic Controller.
RP	-----	Radial ports.
VP	-----	Verticals ports.
LHCD	-----	Lower hybrid current drive system.
ICRF	-----	Ion Cyclotron Resonance Frequency system.
FIR	-----	Multichannel Far Infrared interferometer.
VUV	-----	Vacuum-ultraviolet.

DAQ	-----	Data Acquisition System.
DAS	-----	Data Acquisition systems.
NAS	-----	Network Attached Server.
SAN	-----	Storage Area Network.
CCS	-----	Central control system.
FPGA	-----	Field-Programmable Gate Array
CAMAC	-----	Computer-Aided Measurement And Control
VME	-----	Virtual Machine Environment.
PXI	-----	PCI eXtensions for Instrumentation
TCP/IP	-----	Transmission Control Protocol/Internet Protocol
DSP	-----	Digital signal processor
MATLAB	-----	Matrix laboratory.
RFM	-----	Reflective Memory.
SCSI HDD	-----	Small Computer System Interface Hard Disk Drive.
GPS	-----	Global Positioning System.
MHD	-----	Magnetohydrodynamics.
EFIT	-----	Equilibrium Fitting code.

List of Symbols

λ_i	-Ionization length.
L_c	-Connection length.
ΔR	-Radial Shift.
ΔZ	-Vertical Shift.
φ_{IN}	-Inboard flux.
φ_{OUT}	-Outboard flux.
β_p	-Poloidal beta of plasma.
l_i	-Internal inductance of plasma.
A	-Minor radius of Tokamak.
R	-Major Radius of Tokamak.
$K(k)$	-The complete elliptic integral function of the first kind.
$E(k)$	-The complete elliptic integral function of the second kind.
P	-Pressure kinetic pressure.
E_ϕ	-Toroidal electric field.

W_d	-Stored energy.
Φ_D	-Flux picked up by the diamagnetic loop.
Φ_C	-Flux picked up by compensating loop.
Φ_{DV} current.	-Flux due to vacuum field contribution from TFs, VFs, PFs and eddy current.
$(\Phi_C)_{TF}$	-Vacuum flux picked up by compensating loop due to Toroidal field.
$(\Phi_C)_{OH}$	-Vacuum flux picked up by compensating loop due to Ohmic field
$(\Phi_C)_{VF}$	-Vacuum flux picked up by compensating loop due to Vertical field
$(\Phi_C)_{ED}$	-Vacuum flux picked up by compensating loop due to Eddy field.
k	-Balance coefficient $\left(\frac{\Phi_{DV}}{\Phi_C}\right)$
F	-Flux function associated with the poloidal current.
ψ	-Poloidal flux of plasma.
ψ_{in}	-Flux measured using inboard flux loop.
ψ_{out}	-Flux measured using outboard flux loop.
B_i (LCFS).	-Average magnetic field between inner flux loops and plasma surface
B_o (LCFS).	-Average magnetic field between outer flux loops and plasma surface
ΔS_i	-The intervening area for internal loop.
ΔS_o	-The intervening area for external loop.
ΔB_θ	$= B_\theta(\theta = 0) - B_\theta(\theta = \pi)$
ΔB_r	$= B_r\left(\theta = \frac{\pi}{2}\right) - B_r\left(\theta = \frac{3\pi}{2}\right)$

CHAPTER – I

Introduction of Fusion, Plasma & SST-1

Fusion

- Basics of fusion and its basic equation
- Fusion vs. Fission
- Magnetic confinement of plasma
- Tokamak
- Stellarator
- Spherical device
- Methods of plasma heating
- The role of fusion energy

Plasma

- A brief history of plasma physics
- Definition of plasma
- Condition of plasma
- Important Plasma parameter
- Application of plasma

SST-1 Machine

- SST-1 Magnet
- SST-1 Vacuum System
- SST-1 Cryogenics
- SST-1 Plasma heating
- SST-1 Data acquisition
- SST-1 Operation Control
- Present Status of SST-1

1.1 Nuclear Fusion

Nuclear fusion [1.1] is a reaction in which two or more atomic nuclei come close enough to form one or more different atomic nuclei and subatomic particles (neutrons or protons). The difference in mass between the products and reactants is manifested with the release of large amounts of energy. This difference in mass arises due to the difference in atomic binding energy between the atomic nuclei before and after the reaction. Fusion is the process that powers active stars.

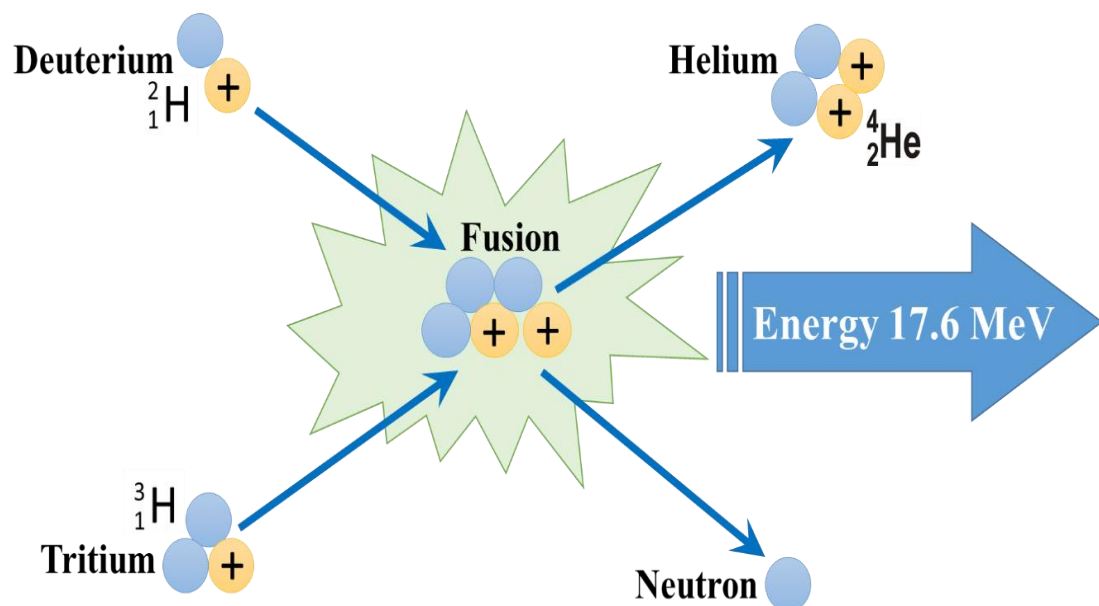


Figure 1.1 A basic fusion reaction of deuterium with tritium

In a famous fusion reaction (Shown in Figure 1.1) of deuterium with tritium, helium- 4 has been created with a neutron. This reaction releases 17.6 MeV as kinetic energy, while a corresponding amount of mass disappears, in agreement with kinetic $E = \Delta mc^2$, where Δm is the decrease in the total rest mass of particles.

1.1.1 Brief History of Nuclear Fusion

Nuclear fission and fusion have been the subject of intense research since the World War II. It has been seen that the devastating energy released in a nuclear explosion can be used to produce electrical power. Currently, 80 percent of the world's primary energy is generated by burning fossil fuels, a resource that is rapidly dwindling. Nuclear fusion is a promising source of energy. Nuclear fission has already been used for electrical energy production in various countries including India. Two main concerns with nuclear fission are accidents and a large amount of radioactive waste produced in the fission power plant. In comparison, nuclear fusion [1.2-1.3] research hopes to produce economically viable clean energy with a very small probability of accidental disaster and significantly less amount of radioactive waste in future. Fusion researchers have already made significant advances in their efforts. Notably, researchers at the JET Tokamak [1.4-1.5] demonstrated the production of over a megawatt of fusion power with the release of two megajoules of fusion energy in 1991. Researchers at JT-60U [1.6-1.8] showed a power gain of 1.25 for D-T equivalent fuel in 1999. Power gain greater than unity is an essential criterion for fusion power plant. This means that more energy gets produced than it requires towards sustaining a nuclear fusion reaction. A schematic diagram (shown in [Figure 1.2](#) and [Figure 1.3](#)) has represented the advancement in fusion research worldwide. At present, worldwide current efforts focuses on the development of ITER (International Thermonuclear Experimental Reactor) Tokamak to bridge the gap between current fusion research and achieving the goal to develop commercial nuclear power plants.

1.1.2 Basic fusion equation

The fusion reaction powers the sun and other stars. In a fusion reaction, principal reactions involve deuterium (D) and tritium (T) nuclei are as follows [1.3][1.9]:



The third reaction has been chosen because of large cross section and least demanding condition ($n \geq 10^{20}/\text{m}^3$ and $T \geq 10 \text{ keV}$). Of the 17.6 MeV energy produced in the fusion reaction 14.1 MeV energy is carried by neutron and 3.5 MeV by the alpha particle. The alpha particles confined in the magnetic field and provide heating to the plasma. Deuterium is abundantly available. Sea water is a natural deuterium source. On the other hand Tritium is a fast-decaying radioactive isotope of hydrogen, that occurs only in traces in nature. In a typical fusion reactor, the tritium can be produced during the fusion reaction. A tritium is produced as neutrons escaping from the burning plasma interact with lithium in the blanket wall of the tokamak reactor. This is often referred as 'tritium breeding'.



1.1.3 Fusion vs. Fission

Nuclear fusion and nuclear fission are different types of reactions that release energy. The difference in mass between the products and reactants is manifested as the release of large amounts of energy. The presence of high-powered atomic bonds between particles found within a nucleus. In fission, an atom is split into two or more smaller, lighter atoms. Fusion, in contrast, occurs when two or smaller atoms fuse together, creating a larger, heavier atom. The main differences between fusion and fission have been elaborated in tabular form in Table 1.1.

Table 1.1: Nuclear Fission vs. Nuclear Fusion

	Nuclear Fission	Nuclear Fusion
Definition	Fission is the splitting of a large atom into two or more smaller ones.	Fusion is the fusing of two or more lighter atoms into a larger one.
Natural occurrence	Fission reactions do not normally occur in nature.	Fusion occurs in stars, such as the sun.
By-products of the reaction	Fission produces many highly radioactive particles.	Very small radioactive particles are produced by the fusion reaction.
Conditions	A critical mass of the substance and high-speed neutrons are required.	High density, high-temperature environment is required.

Energy Requirement	Little energy is required to split two atoms in a fission reaction. Easy to attain this requirement.	Extremely high energy is required to bring two or more protons close enough that nuclear forces overcome electrostatic repulsion.
Energy Released	The energy released by fission is a million times greater than that released in chemical reactions but lower than the energy released by nuclear fusion.	The energy released by fusion is three to four times greater than the energy released by fission.
Nuclear weapon	One class of nuclear weapon is a fission bomb, also known as an atomic bomb or atom bomb.	One class of nuclear weapon is the hydrogen bomb, which uses a fission reaction to "trigger" a fusion reaction.
Energy production	Fission is used in nuclear power plants.	Fusion is an experimental technology for producing power.
Fuel	Uranium is the primary fuel used in power plants.	Hydrogen isotopes (Deuterium and Tritium) are the primary fuel used in experimental fusion power plants.

1.1.4 Magnetic confinement of plasma

Magnetic confinement fusion is an approach towards generating thermonuclear fusion power that uses magnetic fields to confine hot fusion fuel in the form of a plasma. Magnetic confinement is one of the two major branches of fusion energy research, the other being inertial confinement fusion. The magnetic approach is more highly developed and is usually considered more promising for practical power production.

Fusion reactions combine light atomic nuclei such as hydrogen to form heavier ones such as helium and high amount of energy is released during that. In order to overcome the electrostatic repulsion between them, the nuclei must have a temperature of several tens of millions of degrees, conditions under which they no longer form neutral atoms but exist in the plasma state. In addition, sufficient high density and energy confinement are required for fusion reaction, as specified by the Lawson criterion.

Magnetic confinement fusion attempts to create the conditions needed for fusion energy production by using the electrical conductivity of the plasma to contain it with magnetic fields since no solid container could withstand the extreme heat of the plasma. The basic concept can be thought of in a fluid picture as a balance between magnetic pressure and plasma pressure, or in terms of individual particles spiraling along magnetic field lines. There are various established approaches today for achieving the same. A schematic picture of the conceptual tokamak, spherical device, and stellarator is shown in [Figure 1.4](#).

Tokamak

A tokamak (Russian: ТОКАМА́К) is a device that uses a powerful magnetic field to confine the plasma in the shape of a torus. Tokamaks were invented in the 1950s by

Soviet physicists Igor Tamm and Andrei Sakharov, inspired by an original idea of Oleg Lavrentiev. Experimental research of tokamak systems started in 1956 in the Kurchatov Institute, Moscow, by a group of Soviet scientists led by Lev Artsimovich. The tokamak is one among several types of magnetic confinement devices being developed to contain the hot plasma needed for producing controlled thermonuclear fusion power. In a tokamak, closed magnetic field lines are used to confine plasma. When charged particles are moving along the magnetic field they spiral around the magnetic field lines due to Lorentz force. This prevents their collision from the enclosure and allows usage of different heating mechanism to heat plasma to required temperature. Examples of well-known tokamaks are EAST, KSTAR, JT-60SA, DIII-D, ITER etc.

Spherical device

A spherical tokamak [\[1.5-1.7\]](#) is a type of fusion power device based on the tokamak principle. It is notable for its very narrow profile or aspect ratio. A traditional tokamak has a toroidal confinement area that gives it an overall shape similar to a donut, complete with a large cavity in the middle. The spherical tokamak reduces the size of the cavity as much as possible, resulting in a plasma shape that is almost spherical, often compared with a cored apple. The spherical tokamak is sometimes referred to as a spherical torus and is often shortened to ST. The spherical tokamak is an offshoot of the conventional tokamak design. It was believed by some to have a number of substantial practical advantages over other devices in some respects. For this reason, the ST has generated considerable interest since the late 1980s. However, its development remains effectively one generation behind traditional tokamak efforts like JET. Major experiments in the Spherical Tokamak field include the pioneering START and MAST at Culham in the UK, the US's NSTX-U and Russian Globus-M etc.

Stellarator

The stellarator was invented by Lyman Spitzer of Princeton University in 1951. The basic concept is to lay out the magnetic fields so that particles circulating around the long axis of the machine follow twisting paths. This type of configuration may cancel out instabilities seen in purely toroidal machines. This would further keep the fuel confined long enough to allow it to be heated to the point where fusion would take place.

Since the 1990s, there has been renewed interest in the stellarator design. New methods of construction have improved the quality and power of the magnetic fields, improving the performance. A number of new devices have been built to test these concepts. Major examples include Wendelstein 7-X in Germany, the Helicly Symmetric Experiment (HSX) in the USA, and the Large Helical Device in Japan.

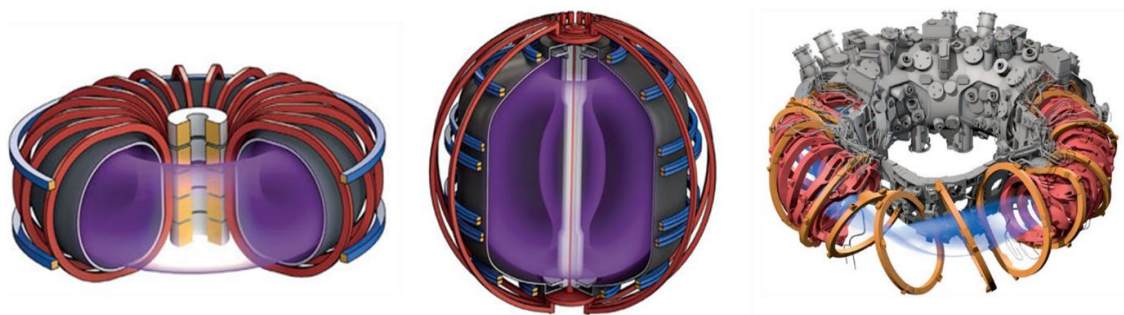


Figure 1.4 Tokamak, Spherical Tokamak, and Stellarator.

[**Image Source:** <http://fuelrfuture.com>. **Image credit:** James Provost and C. Bickel].

1.1.5 Methods of plasma heating

Heating of the plasma confined in a Tokamak configuration is essential to attain the necessary fusion temperature condition in the plasma. In an operating fusion reactor, part of the energy generated will serve to maintain the plasma temperature as fresh deuterium and tritium are introduced. In current tokamak magnetic fusion experiments, insufficient fusion energy is produced to maintain the plasma temperature. So, the plasma needs to be additionally heated to its operating temperature of greater than 10 keV. At present, there are several ways to heat the plasma.

Ohmic heating or inductive mode

The plasma is electrically conductive and heats up when a current is passed through it (due to electrical resistance). This method is only used for initial heating, as resistance is inversely proportional to plasma temperature. The plasma can be viewed as the secondary winding of a transformer. Current in the plasma is induced by slowly increasing the current through an electromagnetic winding linked with the plasma torus. This is inherently a pulsed process because there is a limit to the current through the primary. Tokamaks must therefore either operate for short periods or rely on other means of heating and current drive. The heating caused by the induced current is called ohmic (or resistive) heating. It is similar to the heating that occurs in an electric light bulb or in an electric heater. The heat generated depends on the resistance of the plasma and the amount of electric current running through it. However, as the temperature of heated plasma rises, the resistance decreases and ohmic heating becomes less effective. It appears that the maximum plasma temperature attainable by ohmic heating in a tokamak is 20-30 million degrees Celsius. In order to obtain still higher temperatures, additional heating methods must be used.

Radio-frequency heating (RF)

High-frequency electromagnetic waves are generated by oscillators (often by Gyrotrons or Klystrons) outside the torus. If these waves have the correct frequency or wavelength and polarization, their energy can be transferred to the charged particles in the plasma by resonance. This collides with other plasma particles, thus increasing the temperature of the bulk plasma. Various techniques exist including electron cyclotron resonance heating (ECRH) and ion cyclotron resonance heating. This energy is usually transferred by microwaves. The plasma absorbs energy when electromagnetic waves are applied to it.

Neutral-beam injection (NBI)

A neutral particle beam injector produces ions and accelerates them with an electric field. Neutralised ions are then injected into the plasma. Their high kinetic energy is transferred to the plasma particles by collisions and heating up the plasma. Neutral-beam injection involves the introduction of high energy atoms into the ohmically heated, magnetically confined plasma within the tokamak. The high energy atoms originate as ions in an arc chamber before being extracted through a high voltage grid set. The "ion source" is an assembly consisting of a set of electron emitting filaments, an arc chamber volume, and a set of extraction grids. The extracted ions travel through a neutralizer section of the beam line where they gain enough electrons to become neutral atoms but retain the high velocity imparted to them from the ion source. Once the neutral beam enters the tokamak, interactions with the main plasma ions occur which significantly heat the bulk plasma and bring it closer to fusion-relevant temperatures. Ion source extraction voltages are typical of the order 50-100 kV. NBI

can also be used as a diagnostic tool and in feedback control. Deuterium is a primary fuel for neutral beam heating systems although hydrogen and helium are sometimes used for selected experiments.

1.1.6 The role of fusion energy

Fusion power is a form of power generation in which energy is generated by using fusion reactions to produce heat for electricity generation. Various scenarios have been envisioned predicting the effect of the commercialization of fusion power on the future of human civilization. ITER and later DEMO are envisaged to bring online the first commercial nuclear fusion energy reactor by 2050.

Fusion power commonly proposes the use of deuterium and tritium, isotopes of hydrogen, as fuel. Several current designs also use additionally lithium. It has been proposed to use neutrons as a way to regenerate spent fission fuel or as a way to breed tritium using a breeder blanket consisting of lithium. Large-scale reactors using neutronic fuels (e.g. ITER) and thermal power production (turbine-based) are the most similar among other designs to fission power from an engineering and economics viewpoint. Both fission and fusion power stations involve a relatively compact heat source powering a conventional steam turbine-based power station. The main distinction is that fusion power produces no high-level radioactive waste. Steam turbines have been proposed to convert the heat from the fusion chamber into electricity. The heat is transferred into a working fluid that turns into steam, driving electric generators.

Fusion power has many benefits such as being a long-term energy supply and emitting no greenhouse gases as well as some of the benefits of resource-limited energy sources as a hydrocarbon. The fusion power could provide very high power-generation density

and uninterrupted power delivery because it does not depend on the weather like wind and solar power. Another aspect of fusion energy is that its cost of production is not adversely affected by economies of scale as its production cost will not increase much even if large numbers of stations are built because of the availability of the resource. A schematic block diagram of nuclear power plant has been shown in Figure 1.5.

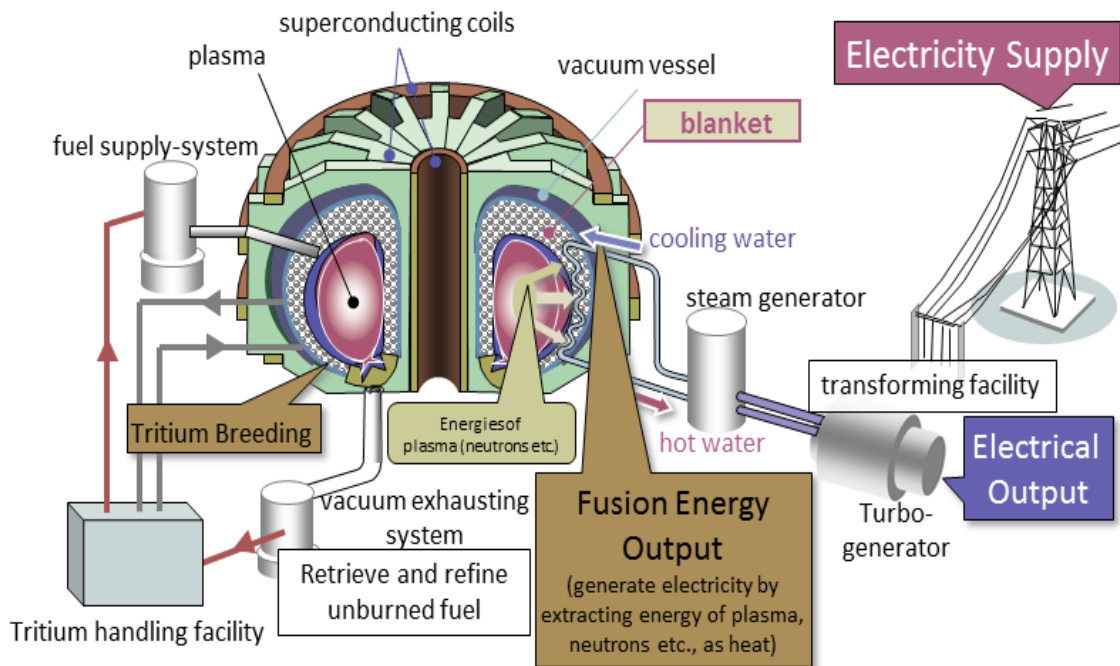


Figure 1.5 The Schematic diagram of Fusion Power plants.

[Image Source- <http://www.fusion.qst.go.jp>].

1.2 Plasma

The word ‘Plasma’ comes from a Greek word ‘πλάσμα’ which means something molded. A useful definition of plasma is as follows:

"Plasma is a quasi-neutral gas of charged and neutral particles which exhibit collective behavior."

Plasmas are also known as the fourth state of matter. A hefty percentage (~90 %) of the matter in the universe is in a plasma. The other three states are solids, liquids, and gases.

A conceptual illustration of matter becoming plasma has been shown in [Figure 1.6](#).

Usually, plasma is observed in lightning, in fluorescent lamps, in the laboratory, and in the Aurora Borealis. Each atom in a solid, liquid or gas is electrically neutral, with a positively charged nucleus surrounded by negatively charged electrons. In plasma, the electrons are stripped from the nuclei of the atoms resulting in an ionized gas where positively and negatively charged particles move independently. The amount of ionization in a gas is found from the Saha ionization equation [\[1.11\]](#).

$$\frac{n_i}{n_n} = 2.4 \times 10^{21} \frac{T^{3/2}}{n_i} e^{-U_i/KT} \quad (1.6)$$

Where, n_i and n_n is the number density of ions and neutrals, T is the gas temperature in K, U_i is the ionization energy for the gas and K is the Boltzmann constant.

Hence, since the particles in the plasma are charged, they conduct electricity and interact with magnetic field. This characteristic has ensured the application of plasma in nuclear fusion based experimental device specifically tokamak and Stellarator etc.

The main properties of Plasma are as follows:

- i) Plasma is a gas of ionized charged particles electrons and ions.

The first condition says the transition of neutral gas to plasma when a gas is energized enough to separate it into electrons and ions it becomes a plasma.

ii) Plasma is quasi-neutral.

The plasma is quasi-neutral, which means neutral enough so that

$$n_i \sim n_e \sim n \quad (1.7)$$

Where, 'n' is called plasma density.

If we see plasma from outside the Debye sphere, it seems to be nearly neutral because of an approximately equal number of positively charged ions and negatively charged electrons. However, the plasma is not so neutral that all the electromagnetic forces vanish. Actually, it subsists within plasma region. This phenomenon is known as quasi-neutrality of plasma.

(iii) The collective behavior of plasma

In order to understand the 'Collective Behavior', let us consider the force acting on a molecule of ordinary air. Since the molecules are neutral, therefore, there is no net force on them. Also, the gravitational force is negligible. Thus, the molecules move without any disturbance until they collide with each other and due to these collisions, the motion of the particle is changed.

However, in case of plasma, the situation is totally different because of the existence of charged particles. These charge particles exert long-range Coulomb force on each other. Due to this long-range force, plasma has many possible motions. In plasma, the long-range Coulomb forces are so much larger than the force due to the ordinary collision. Therefore, we neglect the forces due to ordinary collisions. When a single particle is

disturbed, the whole plasma will be disturbed. This is referred as collective behavior of plasma.

Criteria for plasma:

Plasma Criteria I: An ionized gas is called plasma if Debye length (λ_D) is much smaller than dimensions (L). ($\lambda_D \ll L$)

Plasma Criteria II: If, number of particles in a Debye sphere is ' N_D ' then plasma collective behaviour requires $N_D \gg 1$.

Plasma Criteria III: If ω_p is the frequency of typical plasma oscillation and τ is the mean time between collisions then, $\omega_p \tau > 1$ is a necessary criterion to qualify as 'plasma' state.

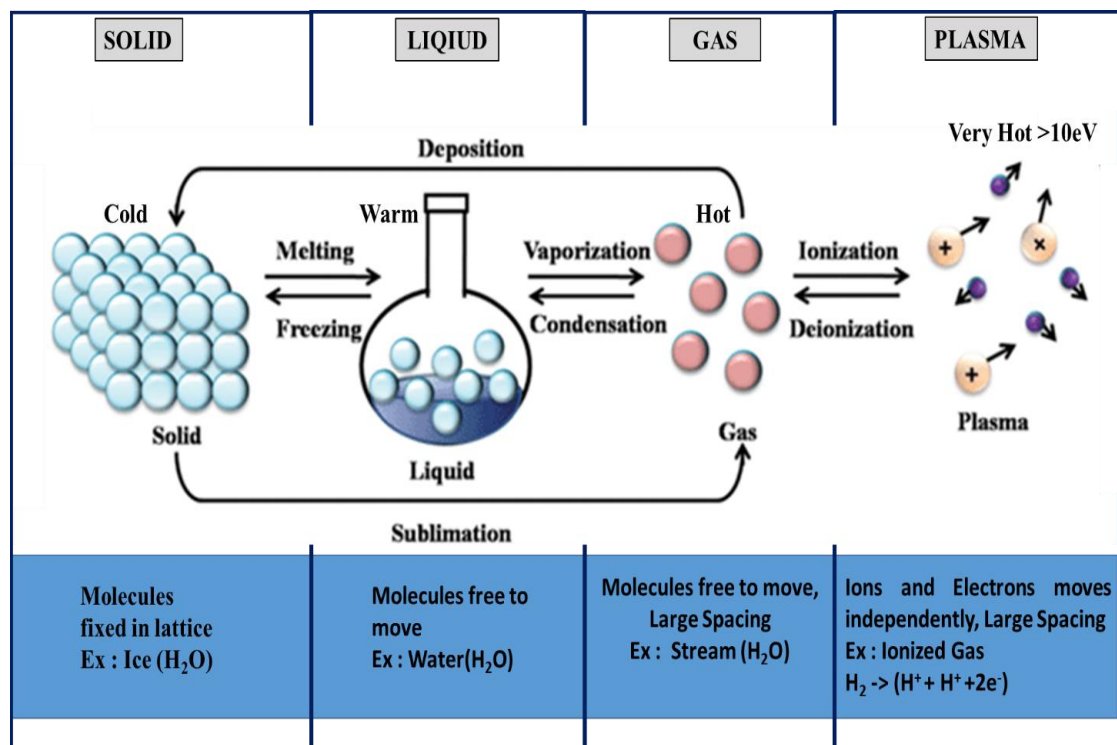


Figure 1.6 Conceptual illustration of matter becoming plasma. Water begins with solid (ice) with heat becomes liquid, with further heating it becomes a gas. With continued heating, the gas molecules dissociate to atoms and finally ionize to become plasma.

1.2.1 Application of plasma

There is a large spectrum of technological applications of plasma in industrial applications across many fields spanning from nuclear power, satellite technology to plasma etching. Most artificial plasmas are generated by the application of electric and/or magnetic fields through a gas. RF and microwave sources are used to generate plasmas in a laboratory or industry for applied purposes. Plasma is successfully used in industrial and extractive metallurgy, surface treatments such as plasma spraying (coating), etching in microelectronics, metal cutting and welding, exhaust cleanup and fluorescent/luminescent lamps etc. Plasma is even used in supersonic combustion engines for aerospace engineering. The more recent and emerging areas in plasma applications are biomedical application of plasma, atmospheric pressure plasma jets and plasmas for CO₂ dissociation for environmental applications.

1.2.2 Different types of plasma

Plasmas are also available in nature in innumerable forms and locations, which can be broadly summarized in the following Table 1.2.

Table 1.2: Different types of plasma

Space and Astrophysical Plasmas	
Stars	A Star as like Sun is an almost entirely ionized ball of plasma. Mainly it consists of electrons and ions, in which there are hardly any neutral gas atoms.
The solar wind	The solar wind is a stream of charged particles released from the upper atmosphere of the Sun. This plasma consists of mostly

	electrons, protons and alpha particles with thermal energies between 1.5 to 10 keV. The solar wind varies in density, temperature, and speed over time and over solar latitude and longitude.
The Io-Jupiter flux tube	Jupiter's Galilean moon Io has multiple active volcanoes on its surface. These spew a gas of particles into space that becomes ionized as Io moves about its orbit in the strong magnetic field of Jupiter and through the plasma torus. A huge electrical current is set up between Io and Jupiter in a cylinder of highly concentrated magnetic flux called the Io Flux Tube.
Accretion discs	An accretion disk is a structure formed by a diffused material in orbital motion around a massive central body. The central body is typically a star.
Interstellar nebulae	The interstellar medium is the matter and radiation that exists in the space between the star systems in a galaxy.
Terrestrial Plasmas	
Lightning St. Elmo's fire	St. Elmo's fire is a weather phenomenon in which luminous plasma is created by a coronal discharge from a sharp or pointed object in a strong electric field in the atmosphere.
Upper-atmospheric lightning	Blue jets, Blue starters, Gigantic jets, ELVES.
Sprites	Sprites are large-scale electrical discharges that occur high above thunderstorm clouds. They are triggered by the discharges of

	positive lightning between an underlying thundercloud and the ground.
The ionosphere	The ionosphere is ionized by solar radiation, plays an important part in atmospheric electricity and forms the inner edge of the magnetosphere. It influences radio propagation to distant places on the Earth.
Plasmasphere	The plasmasphere is a region of the Earth's magnetosphere consisting of low energy (cool) plasma. It is located above the ionosphere.
Polar wind	The polar wind or plasma fountain is a permanent outflow of plasma from the polar regions of Earth's magnetosphere, Usually, it is caused by the interaction between the solar wind and the Earth's atmosphere.
Industrial Application	
Plasma etching	Plasmas used in semiconductor device fabrication including reactive-ion etching, sputtering, surface cleaning and plasma enhanced chemical vapour deposition.
Plasma Torch	The electric arc in an arc lamp, an arc welder.
Tesla coil's arc	The resonant air core transformer or disruptor coil that produces arcs similar to lightning, but with alternating current rather than static electricity.

Plasma waste treatment processes	It is a process of controlled burning of waste with very less residue using plasma.
Surface modifications of the materials	Thermal and cold plasmas can be used for the surface modification of the materials in order to confer functional properties to the treated surfaces.
Research Application	
Fusion energy research	The study to confine plasma by using strong magnetic fields at the high temperatures and pressures required for practical fusion energy. Application in the generation of a fusion reactor, i.e. tokamak, stellarator etc.
Laser Plasmas	Laser produced plasmas are plasmas produced by firing high-intensity beams of light (power lasers) interacts with materials. Laser-produced plasmas have been used to create short bursts of x-rays and to accelerate particles in so-called plasma-based accelerators. It is also useful for recreating astrophysical plasmas in the laboratory.
Rocket exhaust and ion thrusters	A plasma propulsion engine is a type of electric propulsion that generates thrust from a quasi-neutral plasma. Plasma engines are better suited for long-distance interplanetary space travel missions as it has a much higher specific impulse value than most other types of rocket technology.

Emerging areas in plasma applications

Medical	Atmospheric plasma is widely used for medical applications including sterilization, skin treatment, selective killing of tumor cells, gene transfection, and healing wounds.
Biological and Environmental applications	Plasma is used to clean water from biological contaminants. Plasma related study is effective for ozone formation in atmospheric pressure discharges, abatement of volatile organic compounds (VOC), plasma-assisted abatement, plasma catalysis and many other areas.

The approximate value of typical key plasma parameters are mentioned below

Table 1.3: Typical parameters of different types of plasma

Plasma Type	Density $n_e(\text{m}^{-3})$	Electron temperature T(K)	Magnetic field B(T)	Debye length λ_D (m)
Solar Core	$\sim 10^{32}$	$\sim 10^7$	-	$\sim 10^{-11}$
Inertial Confinement	$\sim 10^{28}$	$\sim 10^8$	-	$\sim 10^{-8}$
Tokamak	$\sim 10^{20}$	$\sim 10^8$	$\sim 1-10$	$\sim 10^{-4}$
Gas discharge	$\sim 10^{16}$	$\sim 10^4$	-	$\sim 10^{-4}$
Ionosphere	$\sim 10^{12}$	$\sim 10^3$	$\sim 10^{-5}$	$\sim 10^{-3}$
Magnetosphere	$\sim 10^7$	$\sim 10^7$	$\sim 10^{-8}$	$\sim 10^2$
Solar wind	$\sim 10^6$	$\sim 10^5$	$\sim 10^{-9}$	~ 10
Interstellar medium	$\sim 10^5$	$\sim 10^4$	$\sim 10^{-10}$	~ 10
Intergalactic medium	$\sim 10^1$	$\sim 10^6$	-	$\sim 10^5$

1.3 Steady-state Superconducting Tokamak

The Steady-state Superconducting Tokamak (SST-1) [1.12-1.26] (A photograph of SST-1 has shown in Figure 1.7) is a medium-sized plasma confinement experimental device at the Institute for Plasma Research (Gandhinagar, India) employing Superconducting Magnets. The SST-1 was commissioned in June 2013 and has been in operation since then. SST-1 is designed to address some of the physics and technological issues relevant to the steady-state operation of fusion machines. The SST-1 successfully produces a circular ohmic plasma having plasma current ~ 110 kA in a central field of 1.5 T for a typical duration of ~ 450 ms. Presently, experimental efforts are underway towards extending the SST-1 plasma duration.

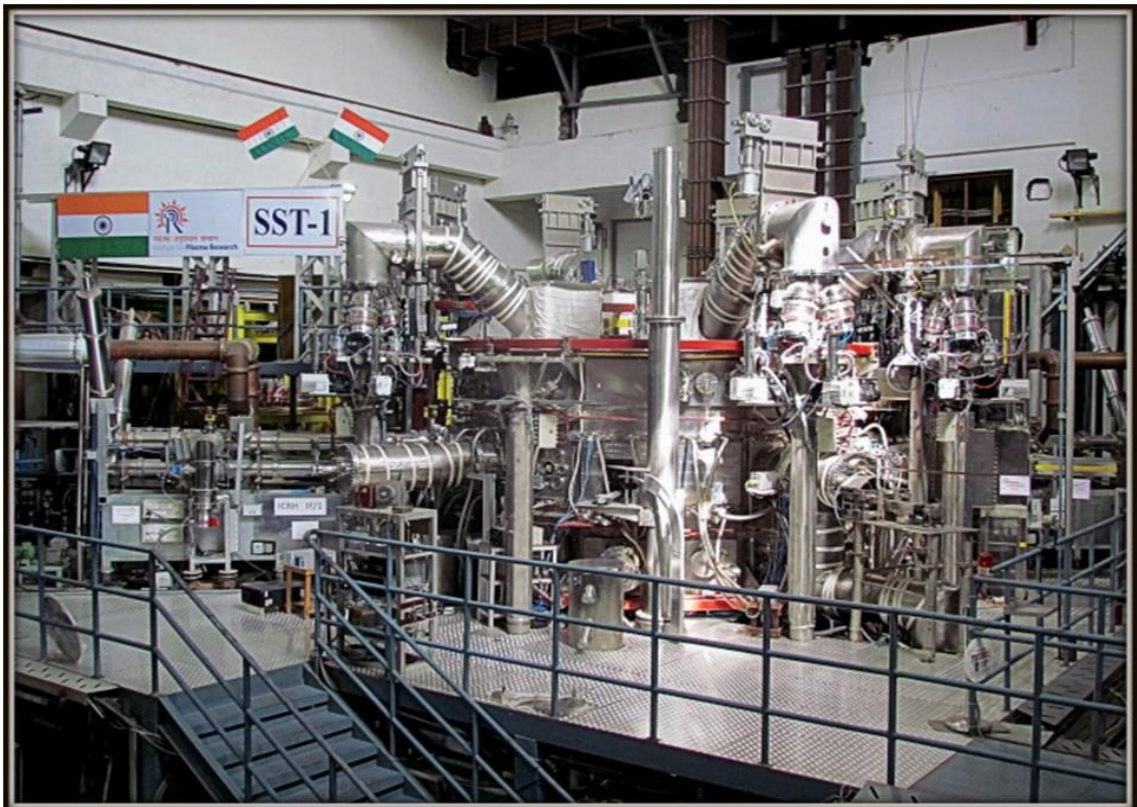


Figure 1.7 A photographic view of SST-1

SST-1 plasma formation is dependent upon synchronization among its different systems and sub-systems. The primary magnetic configuration is provided by Super-Conducting Magnet Systems (SCMS), comprising of sixteen superconducting D-shaped toroidal field (TF) magnets and nine superconducting poloidal field (PF) magnets. An air core ohmic transformer (OT), together with an ECRH system is used for pre-ionization, break-down and initial current start-up. A pair of resistive vertical field magnets, located outside the cryostat and placed symmetrically around the midplane, provides the initial equilibrium conditions. The particle environment within the plasma chamber is maintained using gas puffing. Eddy current distribution and the impurity level in the vacuum vessel need to be precisely controlled for successful high current and repeatable plasma shots.

1.3.1 Basic Parameter of Steady State Superconducting Tokamak (SST-1)

SST-1 has a major radius (R_0) of 1.1 m, minor radius (a) of 0.2 m, toroidal field of 1.5 T at the plasma center and plasma current up to 110 kA. The basic plasma parameters have been mentioned in Table 1.4. The auxiliary current drive and heating are based on Lower Hybrid Current Drive, Ion Cyclotron Resonance Heating, Electron Cyclotron Resonance Heating and Neutral Beam Injection. Major systems and subsystem of SST-1 tokamak (shown in [Figure 1.8](#) and [Figure 1.9](#)) has been described in details following sections.

Table 1.4: SST-1 Basic Plasma parameters

PLASMA PARAMETER	Value
Major Radius (R_0)	1.1m
Minor Radius (a)	0.2m
Toroidal Field (B_T)	1.5T
Plasma current (I_p)	~110kA
Plasma Duration	~450ms

1.3.2 Magnet System

The magnet system [1.12-1.16] comprises the TF coil system, the PF coil system, the ohmic transformer, the vertical field coils and the radial control coils. A cross-section of SST-1, indicating various magnets, is shown in Figure 1.9.

Toroidal Field Magnets:

The SST-1 Toroidal Field magnet system [1.15-1.16] comprises of sixteen superconducting magnets. These are modified 'D' shaped coils arranged symmetrically around the major axis and spaced 22.5 degrees apart. The TF system is designed to produce 3.0 T at plasma axis. The TF coil magnets are NbTi based CICC with wedge-shaped casing. A cylindrical vault structure is formed when all the 16 coils are assembled together. The cylindrical vault structure would resist the expected forces (in-plane and out of plane) on the TF magnet system during SST-1 operation. Presently TF Magnet system successfully operated at 1.5 T during the campaign. This TF field provides the primary mechanism of confinement of the SST-1 plasma.

Central solenoid:

The central solenoid system is consists of the main transformer (TR1) and three pairs of compensating coils (TR2, TR3, and TR4). These coils are made from oxygen free high conductivity copper conductor with a central channel for cooling with water. This central solenoid assembly is used for plasma start-up and initial current ramp-up.

Other coils:

In addition to the above-mentioned coils, a pair of the copper conductors (VF coil) is located outside the cryostat and placed symmetrically around the midplane. This coil provides the necessary field to maintain the initial equilibrium conditions. In addition, there is a pair of single turn active radial control coils (RCC) placed inside the vacuum vessel to provide feedback for plasma position control. The SST-1 PF magnet system

has nine superconducting coils, which can be used for radial position control, in addition to equilibrium and shaping in future.

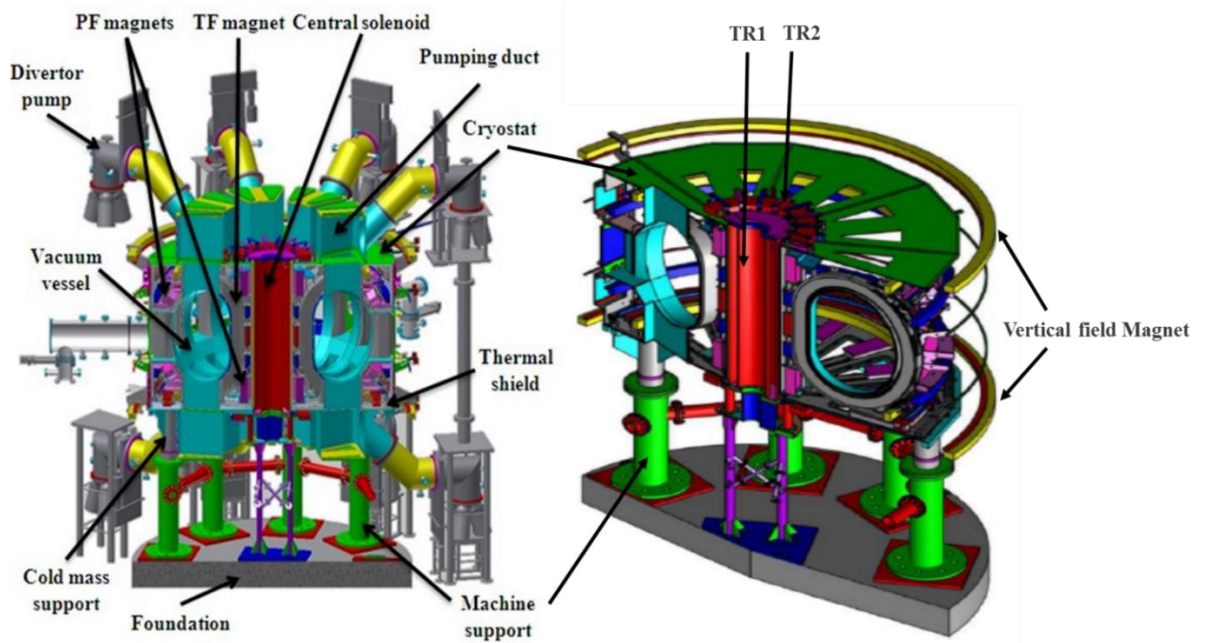


Figure 1.8 A 3-D cut view of SST-1 machine

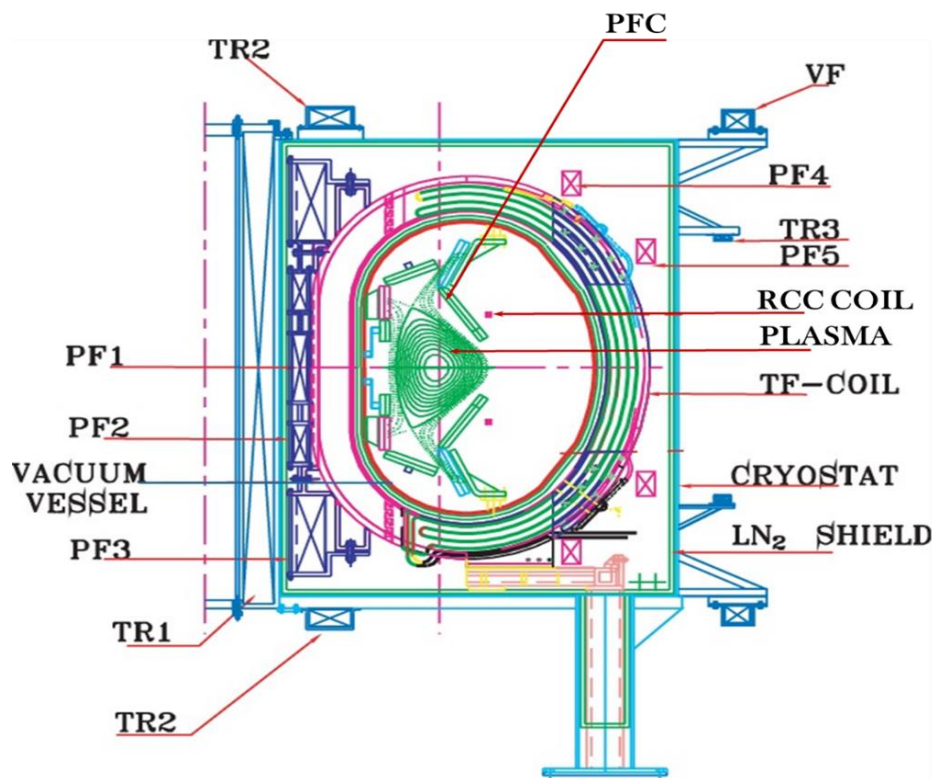


Figure 1.9 SST-1 2D cross-section view.

1.3.3 Cryogenic System

The SST-1 cryogenic system [1.17-1.18] is used to cool all the superconducting magnets. The cryogenic system of SST-1 consists of the helium cryogenic system and the nitrogen cryogenic system. A 1.3 kW Helium refrigeration and liquefaction (HRL) at 4.5 K along with its distribution network facilitates the cooling down of the cold mass and cryo-stable operation of SST-1TF magnets. The HRL has different operating modes like controlled cool down & warm-up of the Super-Conducting Magnet Systems (SCMS), maintaining SCMS at 4.5K during tokamak operation, safe handling of the SCMS quench, higher SHe flow rate at higher pressure drop in the SCMS, absorption of high transient heat loads of the SCMS, compressor power saving for lower cooling requirements in standby mode, and operation without liquid nitrogen. The main components of the HRL are the compressors with an oil removal system, an on-line purifier, a cold box, the main control dewar (MCD) and the warm gas management system.

A liquid nitrogen (LN2) management system has been installed to take care of the LN2 requirement during the campaign. The main system consists of 3 LN2 storage tanks with 300m long super-insulated vacuum transfer lines, followed by a phase separator before that LN2 is distributed to the cryogenic sub-systems. All the cryogenic systems have been automated with a Supervisory Control and Data Acquisition system (SCADA) on Programmable Logic Controller (PLC).

The SST-1 Cryostat is a sixteen-sided polygon shaped outer vessel made of SS 304L. The cryostat houses the superconducting toroidal field (TF) and poloidal field (PF) magnets isolates these coils from ambient pressure and temperature. It also provides a high vacuum barrier around plasma vacuum vessel and surrounding cold mass. Some of the cryostat parameters have been mentioned in Table 1.5.

Table 1.5: SST-1 CRYOSTAT Parameter

CRYOSTAT Parameter	Value
Vertical Height	2.6m
Wall Thickness	0.1m
Total Surface Area	59m ²
Total Volume	39m ³
Material	SS304L
# <u>Modular Construction</u>	
Sixteen sided polygon connected to vacuum vessel at the radial top and bottom ports.32 ports for SCMS diagnostics and pumping.	

1.3.4 Vacuum Vessel and Pumping System

The SST-1 vacuum vessel [1.19-1.21] has been designed to be ultrahigh vacuum compatible while the cryostat is compatible with a high vacuum environment. The vacuum vessel is an ultra-high vacuum, the fully welded SS304L chamber made of sixteen modules, each module consisting of a vessel sector, an interconnecting ring and three ports. The ring sector sits in the bore of TF coil, while the vessel sector with ports is located between two TF coils. It has a height of 1.62 m, the mid-plane width of 1.07 m, a total volume of 16 m³ and a surface area of 75 m². The Plasma facing components (PFC) installed inside the vacuum vessel are graphite blocks mounted on Copper Chromium Zirconium (CuCrZr) heat sink plates on inconel supports. SST-1 vacuum vessel is a welded continuous torus structure fabricated using SS 304L material having sixteen of rectangular radial ports (RP) and thirty-two numbers triangular verticals ports (VP). Each vessel module is made up of one wedge shape sector along with a radial port, two vertical ports, and one interconnecting ring. The entire structure is welded together by sixteen interconnecting rings to form a complete torus. In order to achieve the desired ultra-high vacuum inside the chamber, the vacuum vessel is baked at 150°C

for a longer duration. (Some of the vacuum vessel basic parameters are described in Table 1.6)

Table 1.6: SST-1 Vacuum vessel parameter

VESSEL Parameter	Value
Vertical Semi Axis	0.81m
Radial Semi Axis	0.535m
Total Surface Area	75m ²
Total Volume	16m ³
Material	SS304L
# Modular Construction	
Sixteen vessel sectors, each with one radial port and two vertical ports and Sixteen interconnecting rings.	

A vacuum vessel sector along with different attached components is shown in Figure 1.10

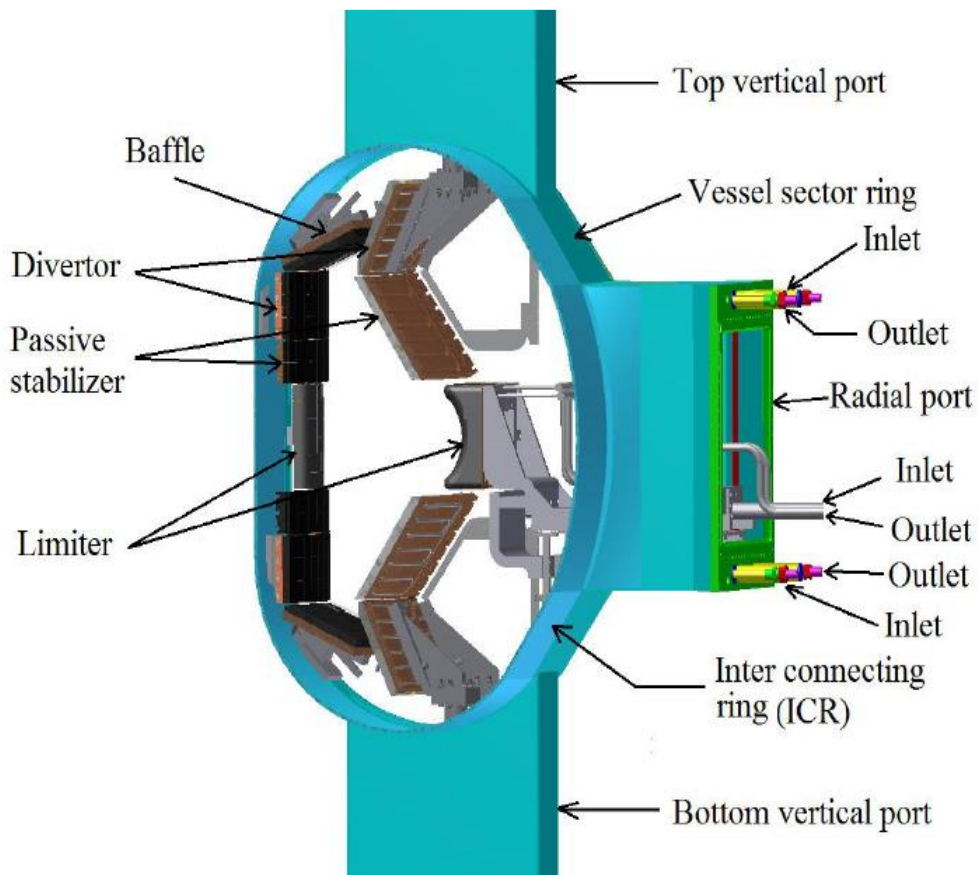


Figure 1.10 SST-1 Vacuum vessel sector [1.22]

1.3.5 Plasma Facing Components (PFC)

The PFC [1.22] of SST-1 comprise of divertors and baffles, poloidal limiters, and passive stabilizers. The normal incident peak heat flux on the inboard and outboard strike point is 1.6 MW/m^2 and 5.6 MW/m^2 respectively. The poloidal inclination of the outboard divertor plates is adjusted so as to have the average heat flux at the strike point to be less than the allowed limit of 0.6 MW/m^2 . The target points of inboard, as well as outboard divertor plates, have been chosen at a distance as large as practicable from the null point. A baffle has been incorporated into the design so as to form a closed divertor configuration that helps in increasing the neutral pressure in the divertor region. A pair of poloidal limiters is provided to assist plasma breakdown, current ramp-up, and current ramp-down and for the protection of RF antenna and other in-vessel components during normal operation and during VDEs and disruptions. The outboard limiters are made movable to protect the RF antenna. On the inboard side, a safety limiter is placed away from the separatrix. Passive stabilizers comprised of conducting structures surrounding the plasma are provided to reduce the growth rate of the vertical instability. The stabilizers are located close to the plasma to have a greater mutual coupling with it when the plasma moves from its equilibrium position. The top and the bottom stabilizers are connected in saddle configuration. Pressed fine-grain graphite is chosen as the baseline armour material for PFC of SST-1 tokamak. The PFCs are actively cooled so as to keep the temperature of the plasma facing surfaces less than $1000 \text{ }^\circ\text{C}$. The PFCs are also designed for baking up to $250 \text{ }^\circ\text{C}$.

1.3.6 High Power Radio Frequency Systems

SST-1 has three different high-power radio frequency systems to additionally heat and non-inductively drive plasma current to sustain the plasma in steady-state for a long duration.

Electron Cyclotron Resonance Heating system [1.23] is based on a 500 kW, continuous-wave gyrotron at 42.2 GHz. Beam launching systems have been designed, fabricated and tested for microwave compatibility for radial and top launch. The system would be used for initial breakdown and heating of the plasma. The localized current drive would also form a part of experimentation.

The lower hybrid current drive system is being planned to operate at 3.7 GHz. The system is based on two 500 kW, continuous wave Klystrons with four outputs. Power at these arms is further divided successively into sixty-four channels which then finally deliver the power to a grill type window positioned at the equatorial plane on a radial port at the low field side of SST-1.

Ion Cyclotron Resonance Frequency system would operate in a range between 22 to 91 MHz to accommodate various heating schemes at 1.5 T and at 3.0 T operation of SST-1. The same system would also be used for initial breakdown and wall conditioning experiments. Fast wave current drive in the center of the plasma is also planned at a later stage. A multi-stage 1.5 MW continuous wave radio frequency system is being built to meet these goals. All the system components require active cooling.

1.3.7 Diagnostics for the SST-1 Tokamak

The SST-1 diagnostics and measurement system has been designed to measure plasma parameters like plasma current, position, shape, density, electron and ion temperatures in the core and edge. Additional diagnostics have been used to measure impurity

concentrations, radiated power and surface temperatures of various PFCs and limiters. Some of the very important diagnostics such as FIR interferometer, Thomson scattering, ECE, charge exchange, thermography, soft and hard x-ray monitoring, visible and VUV spectroscopy are planned to be used to characterize the plasma in the foreseeable future.

1.3.8 SST-1 Control and data acquisition system

SST-1 Data Acquisition (DAQ) System [1.24] is focused on establishing communication interfaces between the front end signal conditioning and electronics, data acquisition, and controls for automated information exchanges during the SST-1 operation under the command of Central Control. A dedicated network attached data storage server has been implemented to store the diagnostics data for post-shot analyses. SST-1 Data Acquisition systems (DAS) is capable to cover a wide range of slow to fast channels interfaced with a large set of diagnostics. The DAS also provides the essential user interface for data acquisition to cater to both on and off-line data usage. The SST-1 DAS is heterogeneously configured in a distributed architecture system. The central archiving and retrieval service is based on a dual step architecture involving a combination of Network Attached Server (NAS) and a Storage Area Network (SAN). SST-1 Data Acquisition Systems have been reliably operated in the SST-1 experimental campaigns. At present different distributed DAS caters to the needs of around 130 channels from different SST-1 diagnostics and its subsystems. PXI based DAS and CAMAC based DAS have been chosen to cater to the need, with sampling rates varying from 10Ksamples/ sec to 1Msamples/sec. For these large sets of channels acquired from the individual diagnostics and subsystems have been a combined setup, subjected to a gradual phase of optimization and tests resulting in a series of improvisations over the

recent operations. In order to facilitate reliable data acquisition, the model further integrates the objects of the systems with the Central Control System of SST-1 using the TCP/IP communication. The focus is also on the need of a loss-less data acquisition for various slow and fast SST-1 diagnostics channels along with the synchronization of DAS elements with the central timing system. Additional aspects of the system include a service subsystem responsible for data retrieval and analysis of diagnostics data, which integrates a facility to view diagnostics/subsystem signals across the network using a centralized MATLAB based plotting and analysis tool for the SST-1 diagnostics data.

The primary objective of the SST-1 Plasma control system [1.25-1.26] is to achieve plasma position, shape and current profile control. The architecture of the control system for SST-1 is distributed in nature. The fastest control loop time requirement of 100 μ s is achieved using VME based simultaneous sampling ADCs, PMC based quad-core DSP, Reflective Memory [RFM] based real-time network, and VME based real-time trigger distribution network and Ethernet network. All the control loops for shape control, position control, and current profile control share common signals from the magnetic diagnostics. It is planned to accommodate all algorithms on the same PMC based quad-core DSP module TSC-43. The Reflected Memory RFM based real-time data network replicate data from one node to next node in a ring network topology at a sustained throughput rate of 13.4MBps. Monitoring and configuration of different systems participating in the operation of SST-1 are done by Ethernet network.

Magnetic sensors data are acquired using Pentek6802 simultaneously sampling ADC card at the rate of 10KSPS. All real-time raw data along with the control data will be archived using RFM network and SCSI HDD for the experiment duration. The RFM network is also planned for the real-time plotting of key parameter of Plasma during

the long experiment. After the experiment, this data is transferred to the central storage server for archival purpose. This paper discusses the architecture and hardware implementation of the control system by describing all the involved hardware and software along with future plans for up-gradation.

All the essential subsystems (Shown below [Figure 1.11](#)) of SST-1 will be monitored through a central machine control. Various subsystems of SST-1 operate in heterogeneous platforms such as VME, PXI, and SCADA etc. This diversity issue was addressed with a GPS-based time synchronization system in a master-slave configuration. The reference time for all synchronous and asynchronous events for the plasma shots are derived from a precision crystal oven oscillator. A terabyte-level data storage system had also been implemented for data handling and manipulation purposes. An electronic logbook system had been introduced aimed at logging all the experiments and campaigns also.

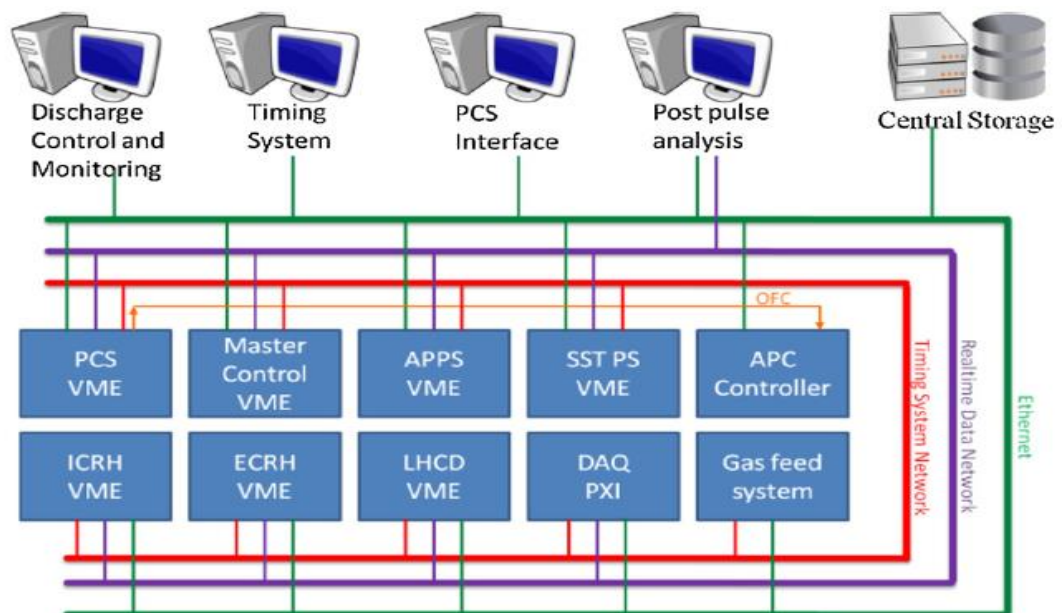


[Figure 1.11](#) Basic SST-1 plasma control subsystem network interface. [1.25]

1.3.9 Present status of SST-1

Steady-state Superconducting Tokamak (SST-1) has been commissioned after the successful experimental and engineering validation of its critical sub-systems. During the ‘engineering validation phase’ of SST-1, the cryostat was demonstrated to be leak tight to superconducting magnets system operations in all operational scenarios, the 80 K thermal shield was demonstrated to be uniformly cooled without regions of ‘thermal runaway and hotspots’, the superconducting toroidal field magnets were demonstrated to be cooled to their nominal operational conditions and charged up to 1.5 T of field at the major radius. A successful plasma breakdown in SST-1 assisted with electron cyclotron pre-ionization in second harmonic mode was obtained in June 2013, thus marking the ‘First Plasma’ in SST-1.

Subsequent to the first plasma, successful repeatable plasma start-ups with $E \sim 0.4$ V/m, plasma currents in excess of 110 kA for 450ms assisted with ECH pre-ionization at a field of 1.5 T have been so far achieved. Lengthening the plasma pulse duration with LHCD, confinement, and transport in SST-1 plasmas and MHD activities typical to large aspect ratio SST-1 discharges are presently being investigated in SST-1. In parallel, SST-1 has uniquely demonstrated reliable cryo-stable high field operation of TF magnets in two-phase cooling mode. SST-1 is also upgraded with first wall integration.

CHAPTER -II

Study of Vessel Eddy current in SST-1 Tokamak

- **Basics of Eddy Current and its importance**
- **Motivation and Literature Survey**
- **Method Description**
- **Circuit Equations**
- **Reconstruction of the B-field**
- **Computational procedure**
- **Experiment for Validation using RCC coil**
- **Observations & Conclusions**

2.1 Basics of Eddy Current and its importance

Eddy currents are loops of electrical current induced within conductors generated by a changing magnetic field in the conductor due to induction. The French physicist Léon Foucault discovered eddy currents and its characteristics. In Lenz's law, Heinrich Lenz stated that the direction of induced current flow in an object will be such that its magnetic field will oppose the change of magnetic field that caused the current flow [2.1]. Eddy currents produce a secondary field that cancels a part of the external field and causes some of the external flux to avoid the conductor.

The term eddy current comes from analogous currents seen in water when rowing using a paddle boat, causing localized areas of turbulence known as eddies which give rise to persistent vortices. Somewhat analogously, eddy currents can take time to build up and persist for very short times in conductors due to their inductance.

Eddy currents flow in closed loops within conductors, in planes perpendicular to the magnetic field. The field can be induced within nearby stationary conductors by a time-varying magnetic field created by an AC electromagnet or transformer as shown in Figure 2.1 or by relative motion between a magnet and a nearby conductor. The magnitude of the current in a given loop is proportional to the strength of the magnetic field, the area of the loop, and the rate of change of flux, and inversely proportional to the resistivity of the material.

The eddy currents are present in a lot of different industrial applications [2.2] ranging from the induction heater, metal crack detection techniques to advanced vehicle systems. Eddy currents in conductors of non-zero resistivity generate heat as well as electromagnetic forces. The heat can be used for induction heating. Electromagnetic

forces can be used for levitation, creating movement, or to give a strong braking effect. Self-induced eddy currents are responsible for the skin effect in conductors and can be used for non-destructive testing of materials for geometry features, like micro-cracks. Eddy currents can also have undesirable effects, for instance, power loss in transformers. Here in this chapter, we will discuss the effects of eddy current in a specific fusion experimental device i.e. tokamak.

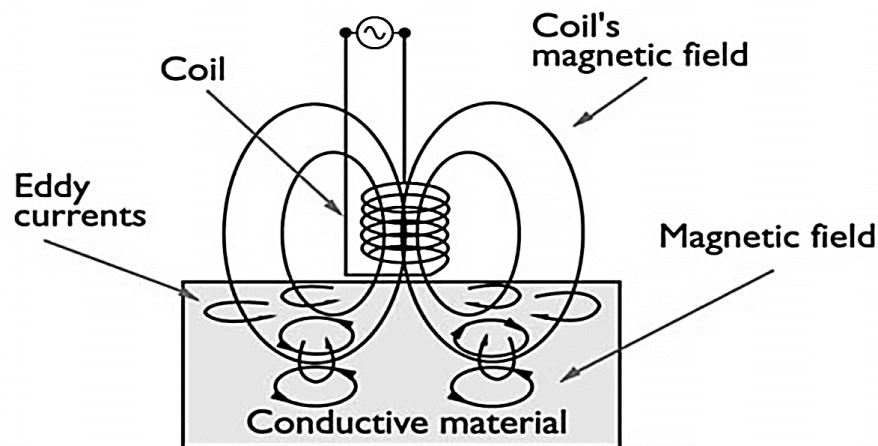


Figure 2. 1 Schematic of eddy current generation.

2.2 Motivation and Literature Survey

In a tokamak, time-varying magnetic fields usually induce transient eddy currents into the surrounding structures. In tokamak case, the computation of eddy currents is very important because of the eddy current produce localized magnetic field [2.3], which may affect the desired magnetic field within the vacuum vessel during tokamak plasma start-up. In central solenoid based inductive start-up the large eddy current is generated in surrounding structure during flux swing in ohmic phase. This leads to shielding effects which delay the build-up of necessary loop voltage and its reduction in some extent. The generation of eddy current is one of the primary reasons to think of a low loop voltage start-up in a present-day tokamak. In recent times, the vacuum vessel and

cryostat are toroidally continuous in most of the superconducting tokamak. This type of tokamak configuration increases the effects of eddy currents significantly, so that affects the static poloidal null position and shape hence the start-up parameter. The eddy current has various other effects (i.e. error field generation, diagnostic error, unnecessary heat generation etc.) during plasma break-down, current ramp-up even in the plasma flat top region because of their mechanical and thermal effects, especially for tokamaks having superconducting magnets. In fact, plasma shape identification is affected by the presence of eddy currents as this identification is based on magnetic measurements. So the study related eddy current computation is important as it differs with machine specification, material selection, and structure of vacuum vessel.

The eddy current distribution is usually modeled by two types of methodologies. In the first method, passive conducting structures in the tokamak are replaced by toroidally symmetric passive filaments [2.4]. This approach will be referred to as the filament model. An alternative approach is to use the finite element method (FEM) [2.5] to model the structures. The filament model is generally used in plasma simulations and is relatively easier to handle. There are various numerical methods available such as in the Tore Supra tokamak [2.6], eddy current calculations have been computed by a finite element method where the variational formulation in terms of the electric vector potential has been used to solve the eddy current for the vessel. In their hypothesis, the structures are assimilated to thin shells which are small compared to the skin depth of the phenomenon. Guglielmo Rubinacci [2.7] has explained a numerical finite elements method, stated in terms of the surface current density vector and of the scalar electric potential. The resulting mathematical model is described in detail with reference to a nuclear fusion device. A computer program, EDDYTOR (eddy current analysis and evaluation code system for a tokamak reactor), has been developed [2.8] to calculate

eddy currents, electromagnetic forces, stress and deformation, and plasma position control properties. The eddy currents calculation resulting from the OH flux change in the CTH vacuum vessel and conducting structures for the CTH vacuum vessel has been demonstrated [2.9] by two separate methods. The MAXWELL and SPARK codes were used for the Electromagnetic modeling and simulation. M. Mattei et al [2.10] has described a method to use an H-infinity observer to estimate eddy currents in the passive structures of a tokamak have been tested in view of a possible application to ITER. G.A. Evans [2.11] has computed time-dependent eddy currents in tokamaks using a numerical solution of Maxwell's equations. This has explained the expected physical phenomena such as the build-up of eddy currents with rapidly varying driving fields and the skin-effect near the metal interface. A simple analog circuit model has been designed [2.12] for NSTX tokamak for the computation of eddy current distribution to use in equilibrium reconstruction. The model has also been validated using a spatial axisymmetric code and benchmarked using numerous vacuum shots.

Whereas in our model we have calculated eddy currents with the help of experimental flux loop signal which has been placed on the vacuum vessel with the help of MATLAB numerical platforms and validated using numerous plasma and vacuum shots. In addition, we have computed the time evolution of approximate eddy field characteristics within the vessel. The important objective of our work has been to determine the vessel current distributions and its influence on the overall null characteristics for the SST-1 tokamak. In the absence of a detailed filamentary model, the code and formalism developed on a MATLAB platform has provided critical inputs towards plasma initiation and operation in the SST-1 device. These findings are extremely useful towards the magnetic null evolutions control as well as for the plasma break down in SST-1. The time evolution study on eddy current characteristics has

contributed to optimizing the initial start-up condition which significantly helps to increase the plasma current from 60kA to 100kA in recent campaigns. This eddy current profile has helped us to calibrate in-vessel magnetic diagnostics especially magnetic loops and probes used for plasma position measurements. This study about eddy current distributions will be useful information to plasma equilibrium modeling.

2.3 Study of Vessel Eddy current in SST-1 Tokamak

In SST-1 tokamak case, the computation of eddy current is very important because of the toroidal continuity of its vacuum vessel and cryostat [2.13]. Substantial eddy currents are generated in the cryostat and vacuum vessel (because they are electrically continuous) in response to the rapid flux swings of the central solenoid coil, compensating coils and equilibrium field coils of SST-1. As a result, these eddy current patterns significantly influence the field null and hence plasma break-down characteristics such as location and spatial region of the null. There is considerable evidence [2.4-2.7] that an unfavorable eddy current can affect the null position significantly, and this can influence initial plasma breakdown characteristics significantly. An important objective of our work has been to determine vessel current distribution and its influence on overall null characteristics. The eddy current distribution in the vacuum vessel of the SST-1 tokamak has been determined using an array of internal voltage loops (flux loop) installed inside the vacuum vessel. A simple circuit model has been employed for the same. This model takes into account the geometric and constructional features of the SST-1 vacuum vessel. The SST-1 vacuum vessel is a modified 'D' shaped vessel having a major axis of 1.285 m and minor axis of 0.81m and has been manufactured from non-magnetic stainless steel. The plasma

facing components installed inside the vacuum vessel are graphite blocks mounted on Copper Chromium Zirconium (CuCrZr) heat sink plates on inconel supports. During the discharge of the central solenoid, eddy currents get generated in the vacuum vessel and passive supports on the vacuum vessel. These eddy currents influence early magnetic null dynamics, plasma breakdown and start-up characteristics. In our model, the SST-1 vacuum vessel has been divided into several segments similar to a filament model for the purpose of calculation. In order to determine the eddy currents, the line average electric field around each segment needs to be measured. The flux generated by the central solenoid magnets in SST-1 are measured by the magnetically coupled in-vessel installed internal flux loops. In this model, we have considered multiple simple circular shaped flux loops installed inside the SST-1 vessel section. The estimation of the magnitude and contour patterns of the net axisymmetric eddy current flowing in the vessel has been determined by the circuit model. The standard Kirchhoff's voltage equations have been used to measure induced voltage for two concentric conducting loops such as the vessel segments and the voltage measurement loop. The equivalent circuit has taken into account the respective resistance, self and mutual inductance of each section. The results computed from the model have been benchmarked against experimental data obtained in a large number of SST-1 plasma shots. These results are in good agreement. Once benchmarked, the calculated eddy current based on the flux loop signal and the circuit equation model has been extended to the reconstruction of the overall B- field contours of SST-1 tokamak in the vessel region. The individual normal and radial components are computed for each vessel section using the off-axis formulation. These iso-B contours have helped to shape the profiles of the ohmic and equilibrium coils towards initiating the plasma column at the right location. A comparison of the field lines with and without the plasma column in identical conditions

of the central solenoid and equilibrium field profiles have also been done with an aim to quantify the diagnostics' responses. The rate of change of current in the central solenoid and the sudden disappearance of plasma current during disruptions are the main reasons leading to the generation of substantial eddy currents on the vessel, cryostat, and in-vessel supports structures.

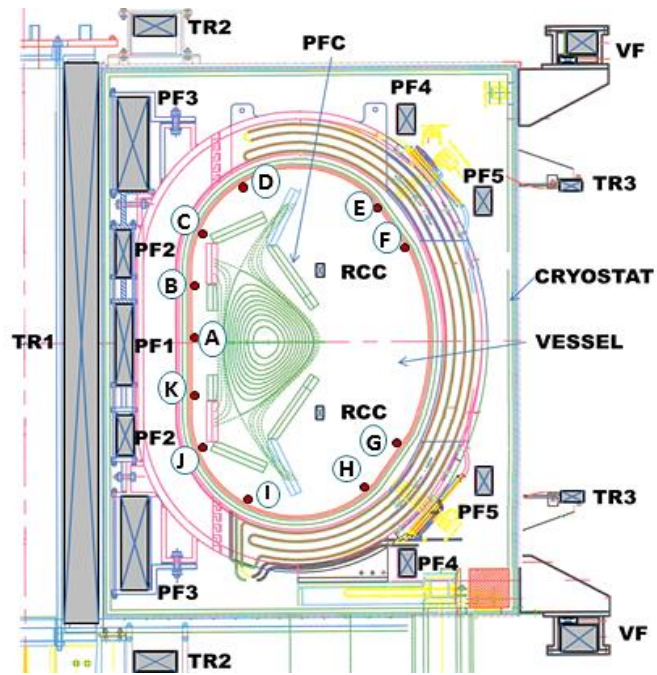
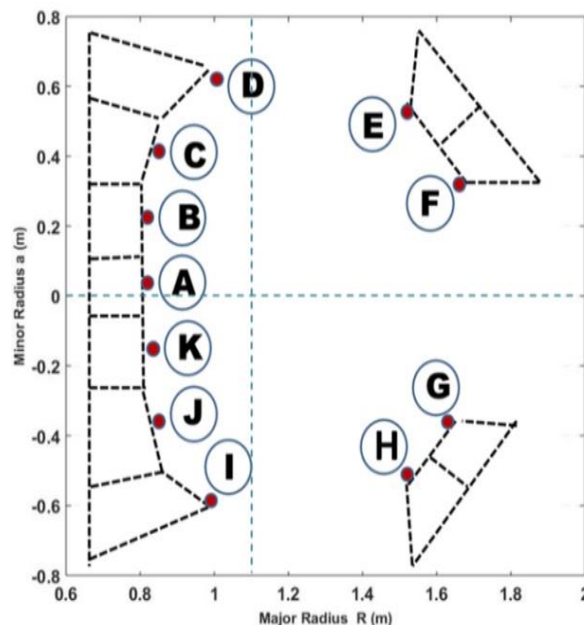


Figure 2. 2 The orientation of flux loops (Red Dot) and SST-1 vacuum vessel.

2.3.1 Model

The electrical circuit model employed to carry out eddy current evolution has been described in this section. The model adopted in the following analysis is general in nature and is similar to what was earlier published in the context of eddy current computations carried out by Gates et al. [2.12] for NSTX tokamak. However, this general model has been adapted to the context of SST-1. As stated earlier, the array of installed internal flux loops become the coupled secondary to the flux generated by the central solenoid magnets. We first break up the SST-1 vacuum vessel into several segments similar to a filament model, as shown in Figure 2. 2. In this figure, the

locations of the installed flux loops have also been shown along with their positions (R, Z). The internal RCC coil, the primary sides of the electrical circuits (VF, OT & PF) are also shown. In order to determine the eddy currents, the line average electric field around each segment needs to be measured. For these purposes, simple circular shaped flux loops have been used. In this case, we have considered eleven axisymmetric flux loops with a nomenclature from A till K as shown in [Figure 2.3](#). The electric field measured on the surface of the vessel segment has been used to approximate the average electric field inside the conductor. The approximation is valid under the assumptions of $(dE/dl) \Delta l \ll E$ and $(dE/dr) \Delta r \ll E$, where, Δl and Δr are the tangential and normal dimensions of the segments. These assumptions are justified when the measurement loops are installed in the vicinity of the surface of the vessel and the dimensions of the vessel segments are small compared to the segment's radius. A single vessel segment and corresponding flux loop used for calculation purpose are shown schematically in [Figure 2.4](#).



[Figure 2.3](#) The several segments of SST-1 vacuum vessel used for Calculation purpose.

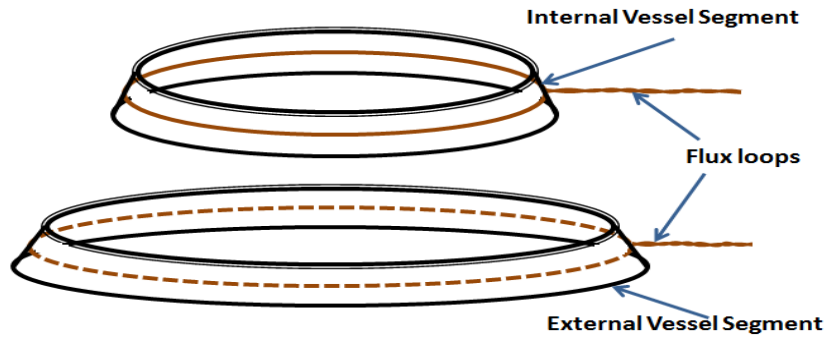


Figure 2.4 The schematic representation of single vessel segments and corresponding flux loop used for Calculation purpose

2.3.2 Circuit Equations

The equivalent circuit for two concentric conducting loops such as the vessel segments and voltage measurement loop is described in Figure 2.5. The Kirchhoff's Voltage equations are then

$$L_0 \frac{dI_e}{dt} + I_e R_0 + M_{01} \frac{dI_1}{dt} + \sum_{i=2}^{\infty} M_{0i} \frac{dI_i}{dt} = 0 \quad (2.1)$$

$$V_{loop} + L_1 \frac{dI_1}{dt} + I_1 R_1 + M_{10} \frac{dI_e}{dt} + \sum_{i=2}^{\infty} M_{1i} \frac{dI_i}{dt} = 0 \quad (2.2)$$

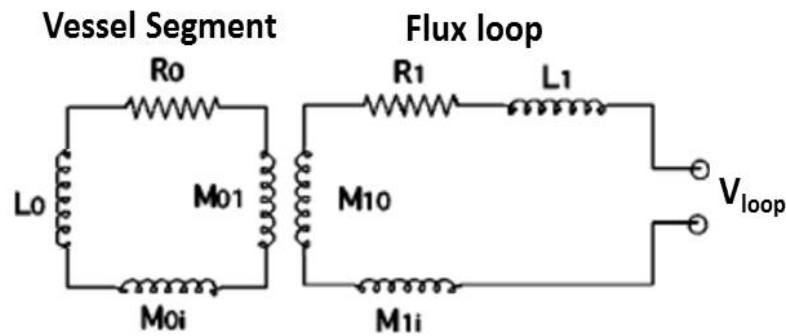


Figure 2.5 The Circuit Model between flux loops and SST-1 vacuum vessel Segments.

Here circuit elements are,

R_0 - effective vessel segments resistance

L_0 - effective vessel segments inductance

R_1 - Flux loop resistance

L_1 - Flux loop inductance

I_e - The sectional eddy current

α - No of vessel segments

$M(0,1)_i$ - The mutual inductance between the vessel segment/measurement loop and i^{th} current carrying circuit element.

Suitable termination resistors together with the low resistance of the measurement coil have enabled to make $I_1 \approx 0$ (approximately) which eliminates term that depends on it. V_{loop} , the flux loop voltage can be written as

$$V_{\text{loop}} = I_e R_0 + (L_0 - M_{10}) \frac{dI_e}{dt} + \sum_{i=2}^{\infty} (M_{0i} - M_{1i}) \frac{dI_i}{dt} \quad (2.3)$$

Table 2.1: Computed Parameters of SST-1 Vessel.

Loop Name	R (mm)	Z (mm)	A (mm ²)	R0 (Ω)	L0 (μH)
A	700.0	20.0	1400.0	0.002166	0.09651
B	755.0	170	1550.0	0.0021108	0.10685
C	755.0	330	1764.0	0.0018463	0.12160
D	792.4	518	2572.4	0.0013430	0.17710
E	1593.8	638	1234.1	0.0055861	0.08200
F	1669.3	562	2115.0	0.0034200	0.14580
G	1686.0	-462	1451.2	0.0050341	0.10004
H	1612.0	-635	1241.6	0.0056280	0.08555
I	805.0	-484	2779.0	0.0012550	0.19157
J	762.0	-280	1873.9	0.0017620	0.12057
K	755.00	-110	1500.0	0.0021810	0.10180

The other approximation is to equate the self -inductance of vessel segment with the mutual inductance between the measurement loops. The sectional inductance (L_0) and mutual inductances have also been calculated. Each segment's resistance (R_0) value is

necessarily towards the computation of the sectional eddy current computed in Table 2.1. With R as the radius of corresponding segments, the resistance Ro becomes,

$$R_o = \rho \frac{l}{A} = \rho_{ss} \frac{2\pi R}{\text{Sectional Area}} \quad (2.4)$$

2.3.3 Reconstruction of the B-field

The circuit model has been extended to the reconstruction of the overall B- field contours of SST-1 vessel. The individual segments have been considered as a current carrying conductor. The individual normal(B_{zi}) and radial (B_{ri}) components are computed using the off-axis formulation (2.5,2.6) by time varying the segmental current and other vessel parameters mentioned in Table 1 for each section.

$$B_{zi} = B_0 \frac{1}{\pi\sqrt{Q}} \left[E(k) \frac{1-\alpha^2-\beta^2}{Q-4\alpha} + K(k) \right] \quad (2.5)$$

$$B_{ri} = B_0 \frac{\gamma}{\pi\sqrt{Q}} \left[E(k) \frac{1+\alpha^2+\beta^2}{Q-4\alpha} - K(k) \right] \quad (2.6)$$

Where, $\alpha = \frac{r}{R}$, $\beta = \frac{z}{R}$, $\gamma = \frac{z}{r}$, $Q = [(1 + \alpha^2) + \beta^2]$ and

$k = \sqrt{4\alpha/Q}$, $B_0 = \mu_0 I_e / 2R$, I_e is the segmental current, $K(k)$ & $E(k)$ are the complete elliptic integral functions of the first kind and second kind. The contribution of all the segments are summed up to produce the effective vessel magnetic field described in [Figure 2.11](#). The appropriate simulation model has been developed using MATLAB to learn the influences of the induced field inside the vessel.

$$B_T = \sum_{i=1}^{11} B_{\text{sec_eddy}} = \sum_{i=1}^{11} \sqrt{[B_{ri}^2 + B_{zi}^2]} \quad (2.7)$$

A comparison of the field lines with and without the plasma column in identical conditions has also been carried out.

2.3.4 Computational procedure

To reconstruct the magnetic field patterns of SST-1 vessel using this principle, we follow underneath steps:

Step-1 Initialization of vessel segmental parameters as mentioned in Table 2.1.

Step-2 Computation of segmental eddy current from circuit model equation (2.3) and flux loop experimental data.

Step-3 Computation of magnetic field from segmental eddy current and formulation (2.5, 2.6)

Step-4 Calculation of total eddy current and reconstruction of the field by summing up the impacts of all the segments using equation (2.7).

The flow chart of the eddy current calculation and the subsequent computation of B-field evolution has been carried out as shown in Figure 2.6.

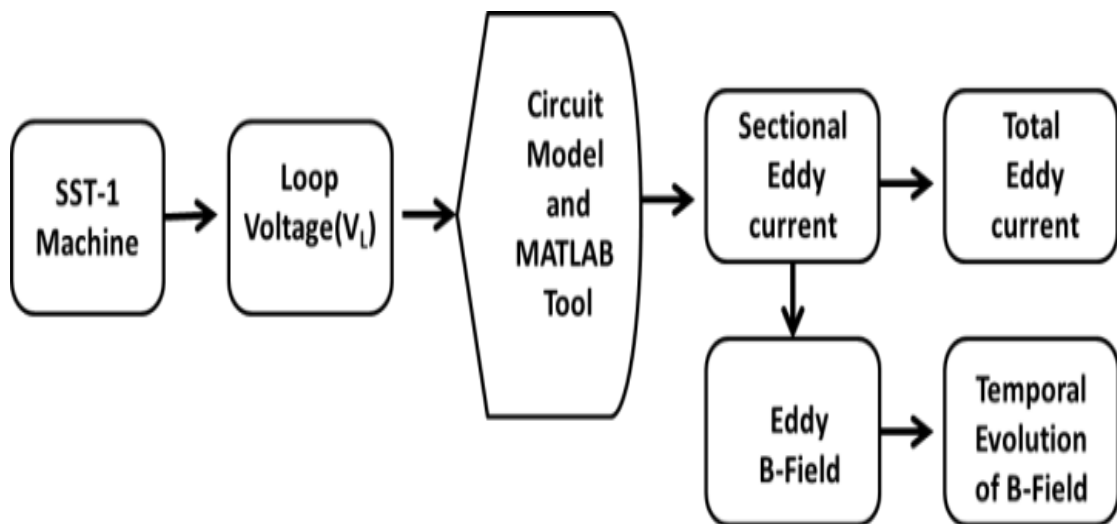


Figure 2.6 The Flowchart of Eddy Current Measurements.

2.4 Results

The experimental results computed from the above-described model have been elaborated in this section. The primary objective has been the estimation of the magnitude and contour patterns of the net axisymmetric eddy current flowing in the vessel. Sectional eddy currents have been determined by the above circuital model. The total eddy current of the vessel has been computed from the weighted sums of sectional eddy currents. The computed maximum eddy current in SST-1 in the present operating scenarios is about 17 kA. The vessel currents could be described better with a larger number of sections or filaments. However, we have limited our analysis to sections which can be adequately represented with the installed flux loops. A typical shot 6059 in SST-1 has been studied with the input flux loop signals (as shown in [Figure 2.7a](#)) being used to determine the corresponding sectional eddy currents (shown in [Figure 2.7b](#)). The net eddy currents flowing in the vessel in response to the central solenoid (OT) and equilibrium field coil (VF) for the same shot 6059 have been shown in [Figure 2.8](#). In this shot, there was no plasma and hence only the eddy currents in the vacuum vessel have been generated. Next, the eddy current pattern in the SST-1 vacuum vessel is determined in an identical manner but with plasma current $I_p \sim 60$ kA lasting for ~ 450 ms as shown in [Figure 2.9](#) and [Figure 2.10](#). A close observation reveals that, as expected, the eddy currents (in magnitude and in time) do get influenced by the plasma current.

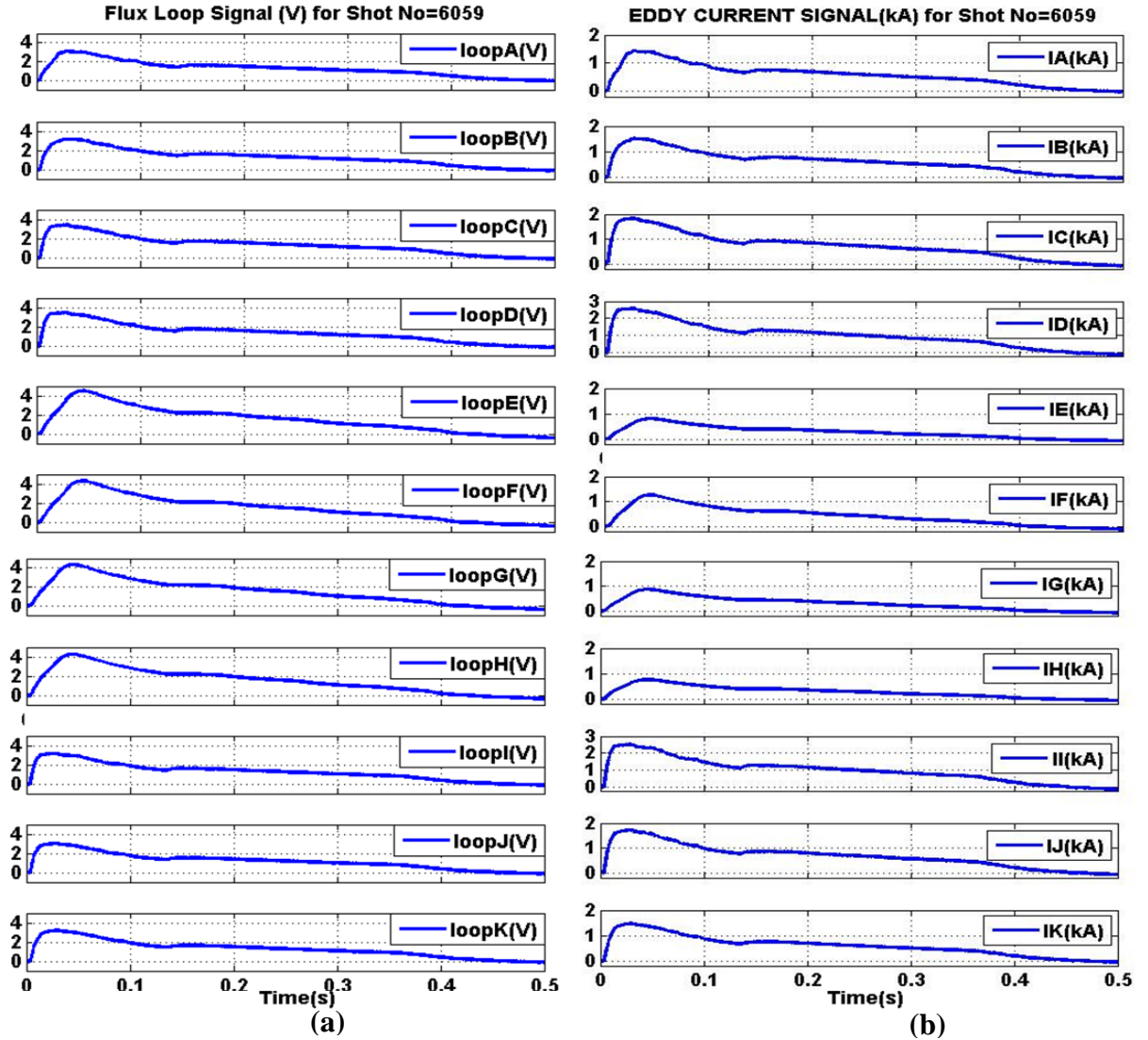


Figure 2.7 The actual flux loop (a) signals and the corresponding segmental eddy current (b) calculated from flux loop signals for vacuum shot no 6059.

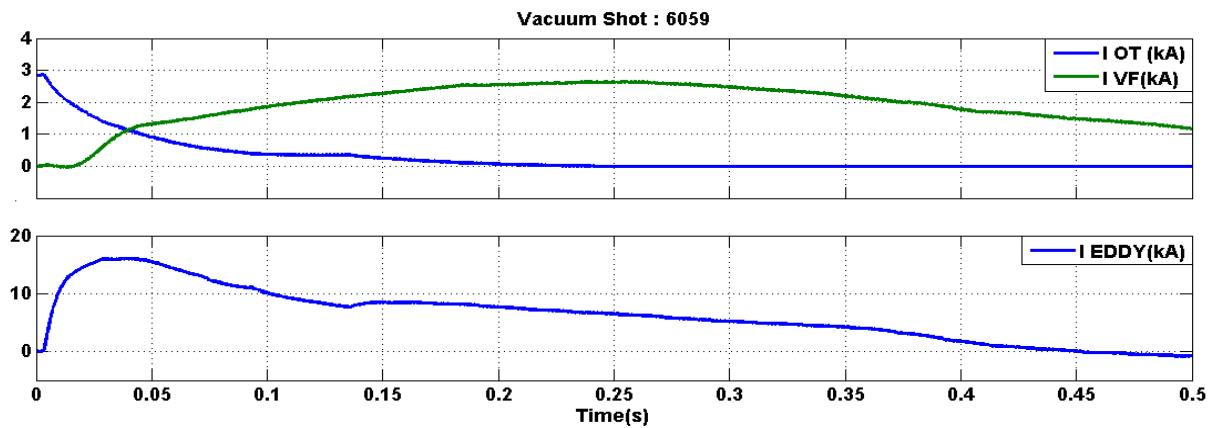


Figure 2.8 The total eddy current with $I_p = 0$ and Central solenoid current (I_{OT}), Vertical field current (I_{VF}) (green) for vacuum shot no 6059.

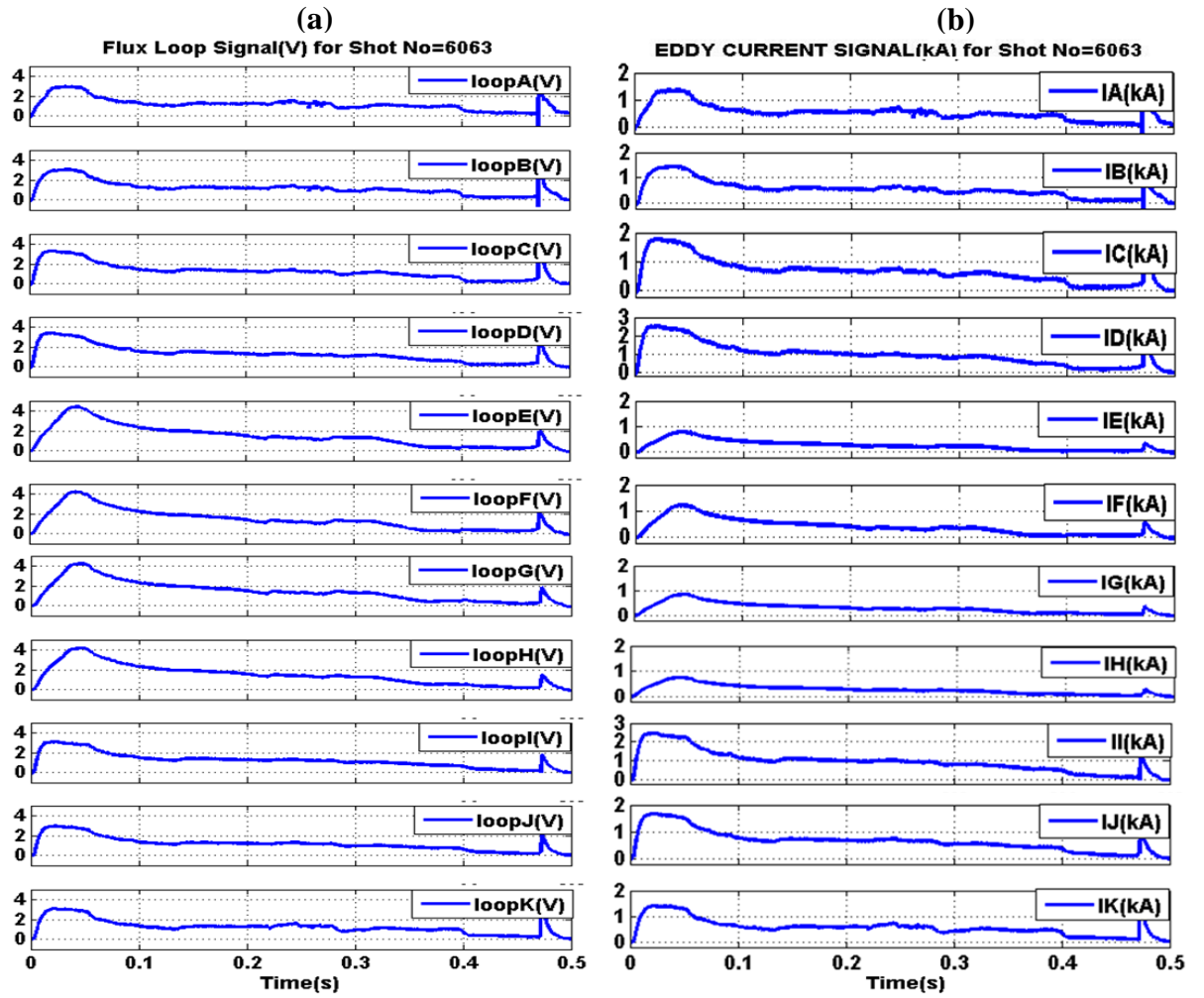


Figure 2.9 (a) The actual flux loops signal and (b) The segmental eddy current of SST-1 vacuum vessel for plasma shot no 6063.

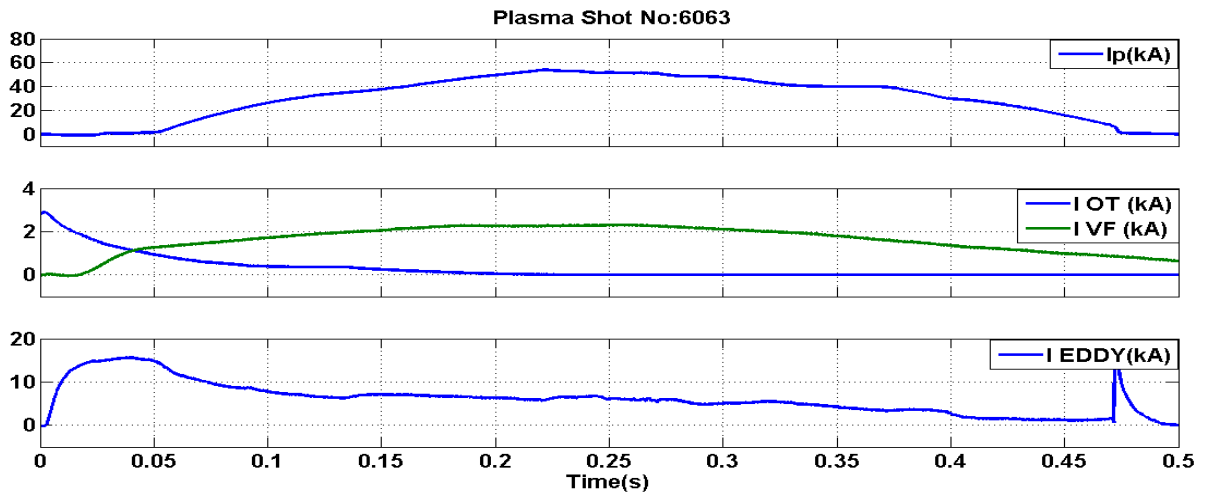


Figure 2.10 The total eddy current with plasma current (I_p), Central solenoid current (I_{OT}) and Vertical field current (I_{VF})(green) for plasma shot no 6063

A secondary objective has been towards the determination of the vessel current distribution and its influence on the overall null and equilibrium characteristics. There is evidence that an unfavorable eddy current can affect the null position significantly and hence the initial plasma break down characteristics can be altered in a significant fashion. This has motivated us to investigate some of these aspects.

In order to compute the eddy current induced field distribution inside the vacuum chamber, it is necessary to plot the B-field contours inside the vacuum vessel resulting from the eddy currents as a function of time. An eddy current induced magnetic field (B-field) reconstruction has been performed through a MATLAB code using computed data calculated from each vessel sectional current and location of the segment and cryostat positional details.

A comparison has been carried out between the temporal evolutions of the field line between vacuum shot (6059) and plasma shot (6063) and has been shown in [Figure 2.11](#). In this comparison, the differences have been observed for vacuum and plasma shot during break-down (30ms), plasma flat top (220ms) and plasma disruption region (475ms). The eddy current effect is larger during break-down region and the minimum B-field contours centre has been formed near to inboard region. ($R=0.95\text{m}$). The significant existence of eddy magnetic field is observed because of rapid flux swings of the central solenoid coil, compensating coils and equilibrium field coils. Whereas, the minimum B-field contours centre during flat top region (220ms) has been changed during vacuum and plasma shot from $R=0.95\text{m}$ to $R=1.05\text{m}$ respectively and size of minimum B-field contours has been increased also. During the disruption region (475ms), due to the non-availability of plasma discharge rate the eddy current B-field contours is missing in left hand side whereas significant existence of eddy magnetic field is observed due to sharp discharge of plasma current in right hand side. The

minimum B-field contours position is varied as per the location of plasma disruption region.

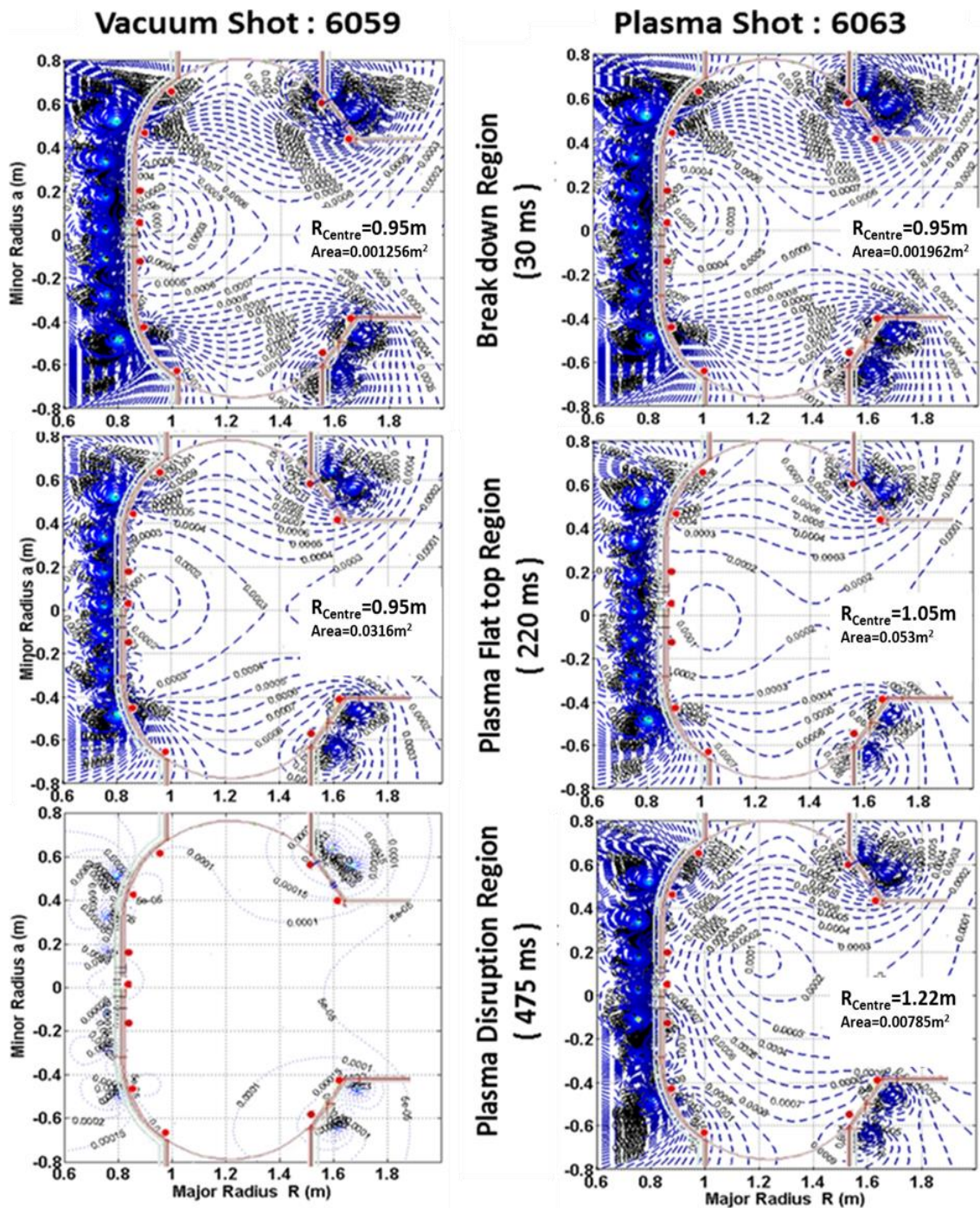


Figure 2.11 The comparison of the eddy field line between vacuum shot (6059) and plasma Shot (6063) at 30ms, 220ms, and 475ms.

2.5 Experiment for Validation using RCC coil

An experiment with the Radial control coil (RCC) has been carried out to validate our model prior to the actual experiments for calibration and benchmarking purposes. In this experiment, a predefined current profile was applied to the RCC coil and the eddy current was determined using flux loop model. The first validation test was that the output behaves correctly as predicted. Experiments have also been carried out with identical predefined RCC profile (i.e. same rise time and fall time of the current in the RCC coil) prior to plasma-facing components installations in SST-1 with installed plasma facing components. The motivation has been to experimentally determine the contribution of the eddy current characteristics on SST-1 plasma facing components. These results have been shown in [Figure 2. 12\(a\)](#). It is evident that both the magnitude and the rate of increasing of the eddy currents have been influenced by the plasma facing components of SST-1.

Alternately, the computed eddy currents have been compared with the difference of the Rogowski coil placed around the cryostat and the vacuum vessel, while placing another Rogowski coil inside the vacuum vessel. The external Rogowski encircles the current passing in the in-vessel RCC coil as well as the eddy currents formed in the cryostat and vacuum vessel whereas the internal Rogowski encloses the current passing through the radial control coil only. Thus, the difference of these two Rogowski actually measures the integrated eddy currents. These integrated eddy current responses in case of the SST-1 vacuum vessel with PFC and without PFC have been shown in [Figure 2. 12 \(b\)](#) and [Figure 2.12 \(c\)](#). It is evident from these graphs that the shielding of the signals have occurred with plasma facing components indicating that the vessel penetration (L/R) time constant has become larger.

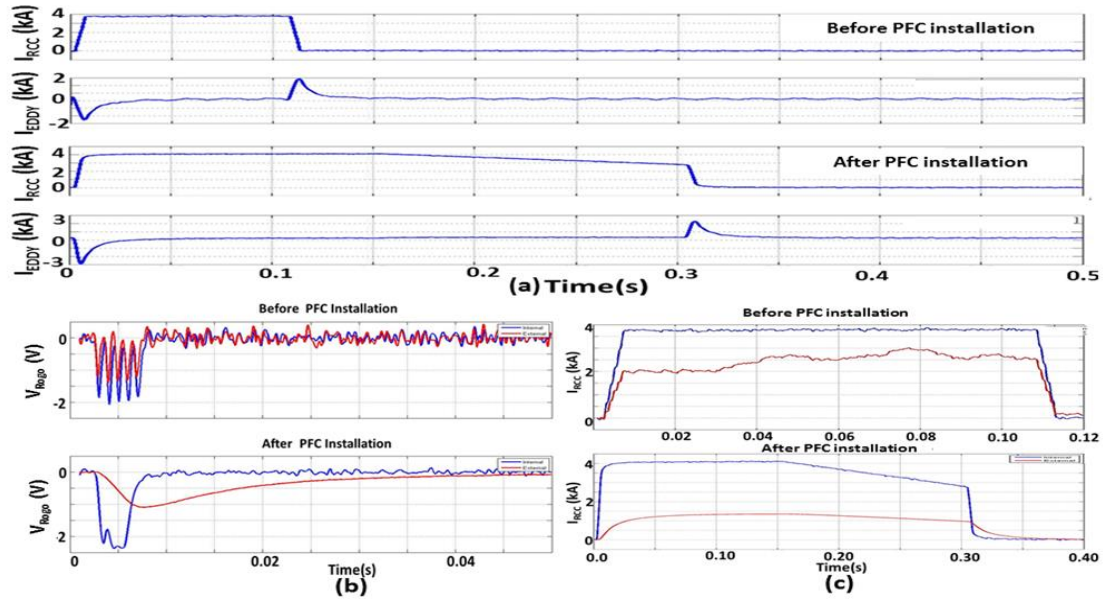


Figure 2. 12 (a) The Predefined RCC current pulse and measured eddy current for before and after PFC installation. (b) The Comparison of Internal (blue) and External (red) Rogowski voltage signal and their comparison for before and after PFC installation. (c) The Comparison of Internal (blue) and External (red) Rogowski signal Current and their comparisons for before and after PFC installation.

2.6 Summary and Conclusion

In this chapter, we have computed eddy currents using a simple circuit model. This model is able to calculate eddy current that flows in the electrically continuous and conducting SST-1 vacuum vessel and cryostat. The typical flux swings of the central solenoid and equilibrium field coils current are the main reason of generation of eddy current. This model uses the experimental data from the in-vessel installed flux loops. The eddy current evolutions have been observed both in the presence of plasma and in the case of a vacuum experiment with an identical central solenoid and equilibrium fields current pulse. The computed results from our model have been benchmarked against a large amount of data obtained from a number of SST-1 plasma shots and have shown good agreement repeatably. The maximum eddy current computed from this

method ($I_{\text{EDDY max}}$) is about 20kA in the present operating scenarios. The rate of change of current in the central solenoid ($(dI_{\text{OT}})/dt$) and the sudden disappearance of plasma current during disruptions are main reason for the production of eddy currents. The eddy current patterns seriously influence the field null and hence the plasma breakdown characteristics. These findings are extremely useful towards magnetic null evolution control as well as for the plasma break down in SST-1.

The computed eddy current distributions will be useful information for plasma equilibrium modeling as well as plasma discharge process. The eddy current characteristics with and without plasma facing components in SST-1 have also been determined. The additional shielding effects of the plasma facing components have been determined. Presently, the up gradation work of plasma facing components (PFC) installation for SST-1 has been completed. Thus eddy current contribution after the up gradation will be carried further in near future.

CHAPTER - III

Electromagnetic Modeling of SST-1 Plasma start-up

- Motivation and literature survey
- Type of plasma start- up
- SST-1 magnet System
- Description of ANSYS Model
- Validation using VF Coil.
- Different SST-1 Start- up scenario
- Contribution of Radial control coil during start-up.
- Observations & Conclusions

3.1 Motivation and Literature Survey

Plasma break-down and start-up followed by its confinement with the imposed external magnetic field is essential to the tokamak plasma experiments. A superconducting tokamak is a complex thermo-mechanical structure with complicated active and passive electromagnetic circuits. Traditional plasma start-up and subsequent plasma start-up from RF are both therefore still subjects of active research. Detailed studies of electromagnetic fields including field errors influencing tokamak operation especially towards plasma break down, start-up and plasma controls are additionally important for plasma control operations during the early stages of plasma formation in a tokamak. Plasma current ramp-up and feedback control depend critically on the electromagnetic fields created by both active currents carrying coils and circulating currents in the passive elements in a tokamak. The initial stages of a tokamak discharge are generally divided into three phases: breakdown, plasma formation and current ramp up. Thereafter, the plasma flat-top is achieved using optimized current feedback control. Plasma initiation in a tokamak is most commonly achieved [3.1] with a Townsend avalanche. The gas inside the vacuum vessel is maintained at a certain pressure (P) and is ionized by applying a toroidal electric field (E_ϕ). This toroidal electric field is induced by the variation of the current in the central solenoid. Alternative methods, [3.2-3.5] such as Electron Cyclotron (EC) assisted pre-ionizations have also been adapted for tokamak plasma break down, especially where the devices are superconducting or in cases where the vacuum vessel and the cryostats are electrically continuous. In any successful plasma breakdown, the connection length (L_C) should be much greater than the ionization length (λ_i). The connection length is defined as the distance an electron travels prior to its escape from the helical magnetic field of the tokamak. The ionization

length denotes the distance an electron travels to gain sufficient kinetic energy from the toroidal electric field in order to ionize a neutral atom.

Ohmic or pre-ionization assisted break down and subsequently start-up of tokamak plasma has remained a very keenly investigated subject. These issues have attracted significant attention in recent years. A number of review articles have listed various formulations as well as methods of calculations. A two-dimensional FEM electromagnetic model has been employed to predict the stray field configuration to explain the breakdown of tokamak JET [3.6]. In this paper specific experiments and corresponding modeling work has been carried out to optimize the magnetic field null during the breakdown at JET. An investigation of the field null for the HL-2M tokamak start-up has been performed by J. Liu [3.7] et al. using the finite element method. This paper presents dynamic modeling of the inductive plasma start-up using an ohmic solenoid (CS) coil and some of the shaping (PF) coils currents. An ECRH assisted ITER start-up model has been described by B. Lloyd et al. [3.8]. In this work, it has predicted that in ITER, the electric field applied for ionization and towards ramping up of the plasma currents may be feasible at a field value of 0.3 V m^{-1} . A zero-dimensional (0-D) code has been developed to analyze burn through in ITER. A similar type of analysis had been performed for SST-1 by Aveg Kumar et al. [3.9], explaining successful plasma start-up under low loop voltage conditions. SST-1 has successfully achieved plasma break down and start-up assisted with EC in both the second harmonic mode as well in the fundamental mode of operation [3.10]. In all SST-1 experiments, successful plasma breakdown has been achieved at loop voltages of $\sim 3.0\text{V}$ that corresponds to $\sim 0.35\text{--}0.4 \text{ V/m}$ of the toroidal electric field in SST-1. Efficient ECH-assisted plasma start-up with a low loop voltage and low volt-second consumption utilizing the trapped particles have been previously demonstrated by Young Hwa An [3.11] et al. in spherical

torus experiments. The operational scenario involving plasma breakdown and current ramp-up phases in JT-60SA tokamak has been developed by H. Urano et al. [3.12]. In that work, it was shown that the operational scenarios for plasma breakdown and current ramp-up phase can be optimized considering the large eddy current induced by the current ramp-up. Electron cyclotron heating (ECH)-assisted start-up experiments have been successfully performed by K. Kajiwara et al. [3.13] in JT-60U following model predictions. The breakdown loop voltage was successfully reduced from 25 to 4V ($E=0.26 \text{ V m}^{-1}$) by 200kW ECH assisted pre-ionization. Plasma start-up designs for fully Superconducting tokamaks like EAST and KSTAR with implications for ITER has been described by J. A. Leuer et al. [3.14-3.15]. The COMPASS magnetic field originating from the poloidal field coils was computed using numerical integration of Biot-Savart law by J. Havlicek et al. [3.16]. Finally, an attractive solenoid-free start-up scenario exploiting economic issues involving a tokamak based power plant has been performed by Wonho Choe [3.17] et al. Thus, in this context, such a study involving electromagnetic modeling holds adequate importance in the case of the Indian Superconducting Tokamak, SST-1.

In this chapter, we have described a model that has captured the electromagnetic details of the SST-1 device during its EC assisted plasma break-down and subsequent ohmic plasma start-up. A 3D simulation platform has been developed to compute iso-field lines in different phases of SST-1 plasma break down and start-up. These off-axis electromagnetic fields for SST-1 have been investigated employing a finite element modeling tool, ANSYS Maxwell. The model includes all the actively driven coils, both outside the cryostat and inside the vacuum vessel as well as the contributions of the passive structures such as the electrically continuous and conducting vacuum vessel and cryostat and the discrete in-vessel support structures. Pre-ionization in SST-1 is

assisted with a 42 GHz Electron Cyclotron source. The magnetic null and subsequent current ramp-up indices during SST-1 plasma evolutions are typically supported by a set of resistive ohmic coils and vertical field coils outside the cryostat and a pair of in-vessel radial control coil, whenever necessary. In this work, we have analyzed and benchmarked some of the experimentally observed start-up scenarios to be in conformity with the computed poloidal field null configurations. In the beginning, the static field null calculation has been performed employing the vacuum fields for the initial magnetization stage. Subsequently, the dynamic null region is influenced by the eddy currents distribution in the vacuum vessel, in-vessel support structures and in the cryostat. In this work, a detailed electromagnetic model has been proposed that accounts all the above characteristics. The model predicts individual electromagnetic field contours (iso-field) for active electromagnets such as the central solenoid (CS), vertical field coil (VF), radial control coil (RCC) and other passive current carrying entities during plasma break-down and start-up in SST-1. These simulated field results have been validated with experimental data obtained from the in-vessel magnetic diagnostics.

3.2 Type of plasma start-up

The standard procedure to start a tokamak plasma (ohmic startup) relies on plasma breakdown in the presence of a toroidal electrical field E_ϕ . According to Townsend's theory, this is facilitated by the optimization of neutral gas pressure (usually called pre-fill pressure) and maximum connection length which is achieved by optimizing different start-up parameters. Additionally, toroidal electrical field (E_ϕ) drives a toroidal ohmic current in the initial plasma. This current is an important constituent of the evolving magnetohydrodynamic (MHD) equilibrium of the tokamak. The formation of this equilibrium increases thermal insulation such that ohmic heating is sufficient to

generate a fully ionized plasma of several hundred eV electron temperatures. In present day superconducting tokamaks, the use of superconducting magnets in the central solenoid, toroidal field (TF) coil and the thick vessel walls limit the toroidal electrical field available for plasma breakdown well below the values used in most of the previously operated tokamaks. There are several plasma start-up scenarios which have been investigated as per the requirements of up-gradation and for the different real-time constraints. Some commonly adopted tokamak start-up procedures are explained below.

3.2.1 Central solenoid based inductive (Ohmic) start-up

A conventional ohmic solenoid is placed on the inboard side of the toroidal plasma such as the one shown in Figure 3.1. It produces average large vertical field (i.e. poloidal magnetic flux) during its discharge inside the coil and significantly lower fields outside the solenoid or inside the plasma region. This property makes it well suited to initiate a toroidal plasma current by magnetic induction since the plasma initiation usually requires a very small transverse stray field.

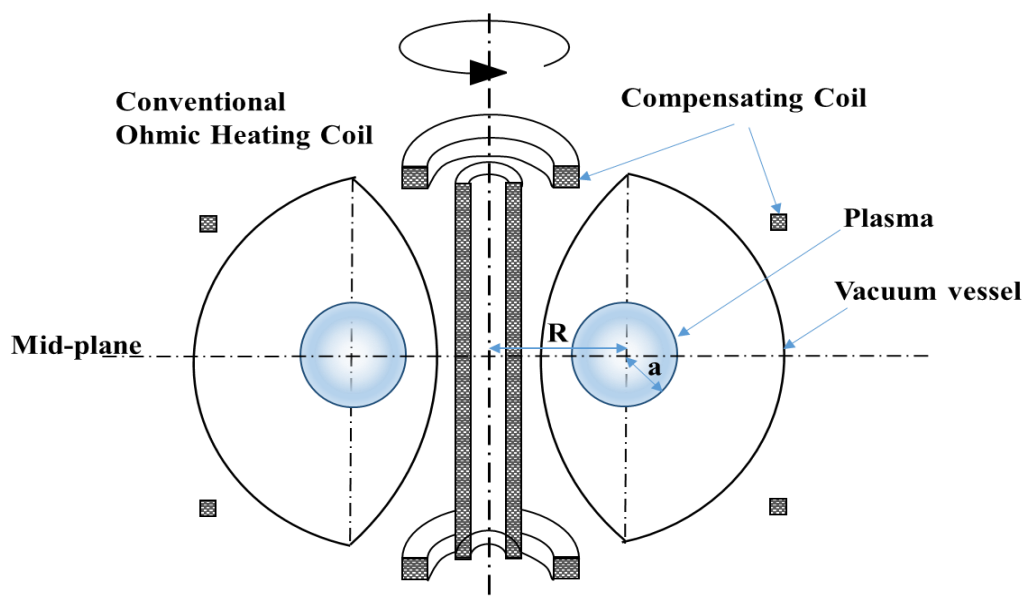


Figure 3.1 Schematic block diagram up ohmic start-up using a central solenoid.

3.2.2 Ohmic with ECRH pre-ionization start-up.

In addition to the central solenoid, the electron cyclotron source (ECH) has been used effectively for pre-ionization in most presently operated tokamaks to enable robust and reliable plasma start-up and to avoid the constraints of the toroidal electrical field in a superconducting tokamak. The formation of a trapped particle configuration before the initiation of the loop voltage allows the plasma to start up with a lower loop voltage and lower volt-second consumption as well as a wider operation range in terms of ECH pre-ionization power and pre-filling pressure. These concepts have been explained in detail in different experimental and simulation models as they are extended to different tokamak. These are best utilized in advanced superconducting tokamaks requiring a low loop voltage start-up with the available limited volt-seconds, such as ITER, or in spherical tori of future.

3.2.3 Radio frequency (RF) driven start-up or Solenoid free startup

The inductive variances of plasma start-up without ohmic central solenoid (shown in [Figure 3.2](#)) and RF sources are also studied in various tokamak experiments successfully. The MAST tokamak experiment [\[3.18\]](#) routinely uses in-vessel poloidal field (PF) coils at larger major radii than plasma for solenoid-free plasma initiation and current ramp-up by means of merging and compression. Non-inductive start-up and current ramp-up methods utilizing radio frequency (RF) and neutral beam injection (NBI) current drive have been successfully demonstrated on various devices, but at a lower plasma current level [\[3.19-3.20\]](#). Bootstrap current drive based ramp-up [\[3.21\]](#) is also identified as a promising current ramp-up technique in a reactor design where the long ramp-up time requirement is not an inherent issue for a steady-state reactor system.

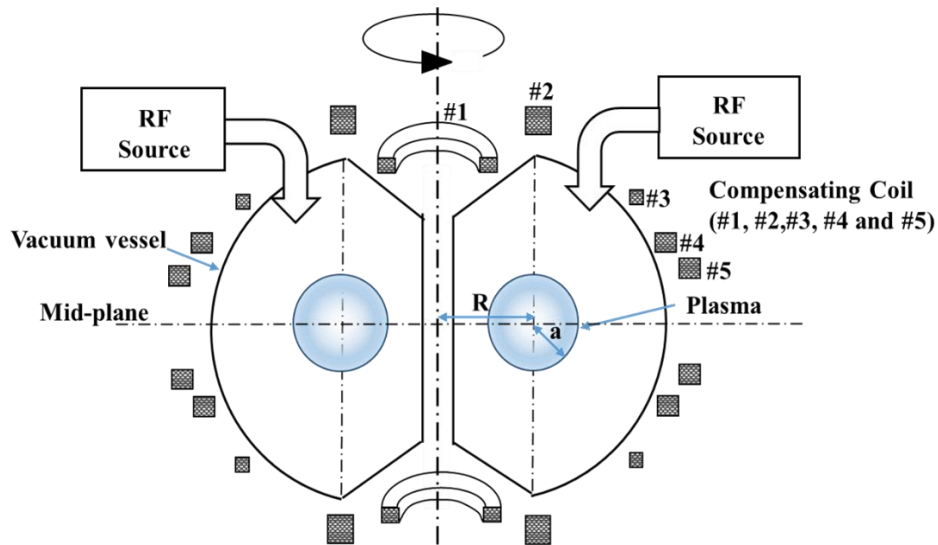


Figure 3.2 Schematic block diagram of solenoid free inductive start-up with RF source.

A method based on coaxial helicity injection (CHI) [3.22-3.23] has been successfully demonstrated on the Spheromak and smaller Spherical tokamak devices. However, application of these methods in next generation devices are generally plasma physics intensive so that considerable physics R&D effort is necessarily required to extend these techniques toward multi-MA regimes.

3.3 SST-1 Magnet System

The Ohmic Transformer in SST-1 consists [3.24-3.25] of seven coils aligned with top-down symmetry. The orientation and dimensions of these coils are given below in Table 3.1 and Figure 3.3. The ohmic transformer is used for plasma start-up and initial current ramp up. The TR1 coil has been made from continuously transposed conductors whereas all other coils have been made from hollow copper conductors as described below in Figure 3.4. The equilibrium of the plasma column is supported by a pair of resistive vertical field coils placed outside cryostat. In these experiments, the Poloidal Field (PF) magnets of SST-1 were not charged and were allowed to carry some circulating currents. SST-1 is also equipped with a pair of up-down symmetric in-vessel

single turn coils known as Radial Control Coils (RCC) for fast radial position & future feedback control.

In the [Figure 3.4a](#)) shows the actual drawing of the SST-1 current carrying coil with b) side view with the actual dimension of each coil. This [Figure 3.4](#) also explains the actual copper-based TR1 coils of SST-1, a cross-sectional view of individual rectangular single turn copper coil and its dimension.

Table 3.1: SST-1 Magnet parameter (TRs and VFs)

Coil Name	No of Turns	Cross-sectional shape of single turn	L (mm)	R _{IN} (mm)	R _{CEN} (mm)	R _{OUT} (mm)	Z _{IN} (mm)	Z _{OUT} (mm)	dR (mm)	dZ (mm)
TR1	112×6 =672	Rectangular 19×22.7	2680	200	262	324	-	-	124	2680
TR2	40	Rectangular 19×22.7	2890	487	591	694	1397	1493	207	96
TR3	3	Rectangular 19×22.7	2744	2421	2450	2479	2732.6	2755.4	58	22.8
TR4	1	Rectangular 19×22.7	1221	2459	2469	2478	1209.6	1232.4	19	22.8
VF	20	Rectangular 19×22.7	2890	2513	2564	2615	1394	1496	102.54	102.54
RCC	1	Circular 16×16	350	1324	1330	1338	342	358	16	16

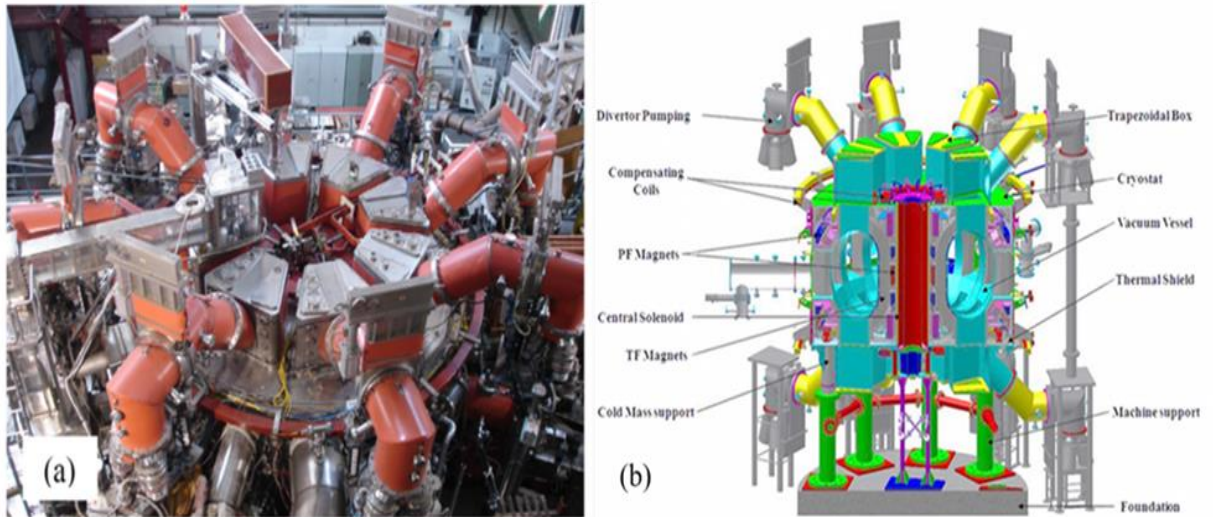


Figure 3.3 a) Top View of SST-1 Tokamak b) The Cross-sectional View of SST-1 Machine.

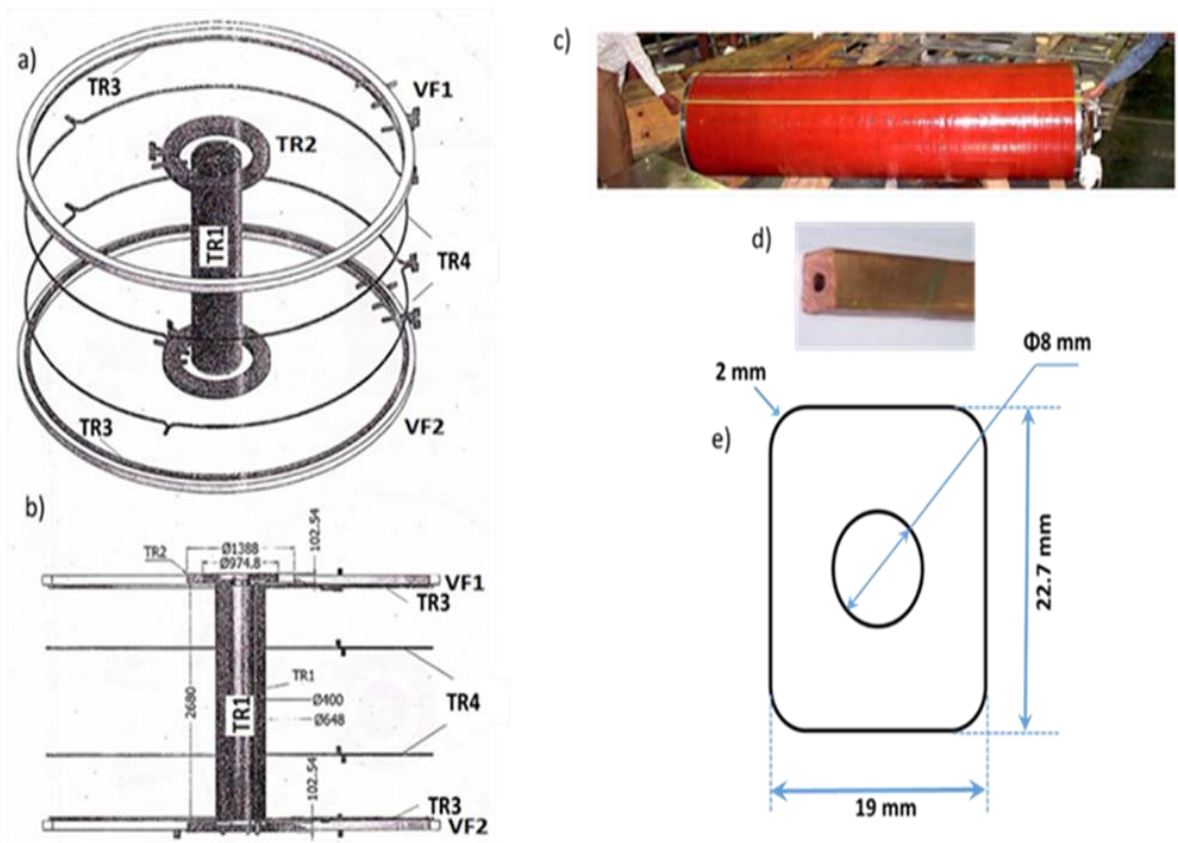


Figure 3.4 a) The actual drawing of SST-1 current carrying coil b) Side view with actual dimension, c) The actual TR1 coils, d) The cross-sectional view of individual rectangular single turn copper coil and e) The dimension of rectangular single turn coil.

3.4 Description of ANSYS Model

The finite element electromagnetic modeling of a complicated structure like a tokamak is based on the widely used Finite Element Analysis tool, ANSYS Maxwell [3.26]. ANSYS Maxwell incorporates finite element method solvers to solve static, frequency-domain, and time-varying electromagnetic and electric fields. Here, in this model, actual orientations and parameters of the coils have been given as inputs. The model also takes into account the detailed geometric and constructional features of the SST-1 vacuum vessel and cryostat. The necessary material properties have also been appropriately provided in the modeling. Figure 3.5 shows a flowchart of the FEM modeling. A few structural constraints such as the viewports of SST-1 are not considered for this analysis.

The dynamical null region is influenced by time-varying eddy current distributions in the vacuum vessel, in-vessel support structures, and cryostat. The eddy current distributions in the vacuum vessel have been computed by a circuit model [3.26] using the data obtained from an array of internal voltage loops (flux loops) installed inside the vacuum vessel. A 3-D transient model has been chosen to incorporate time-dependent calculations accounting for vacuum vessel eddy currents, induced by the changes in various external coils currents.

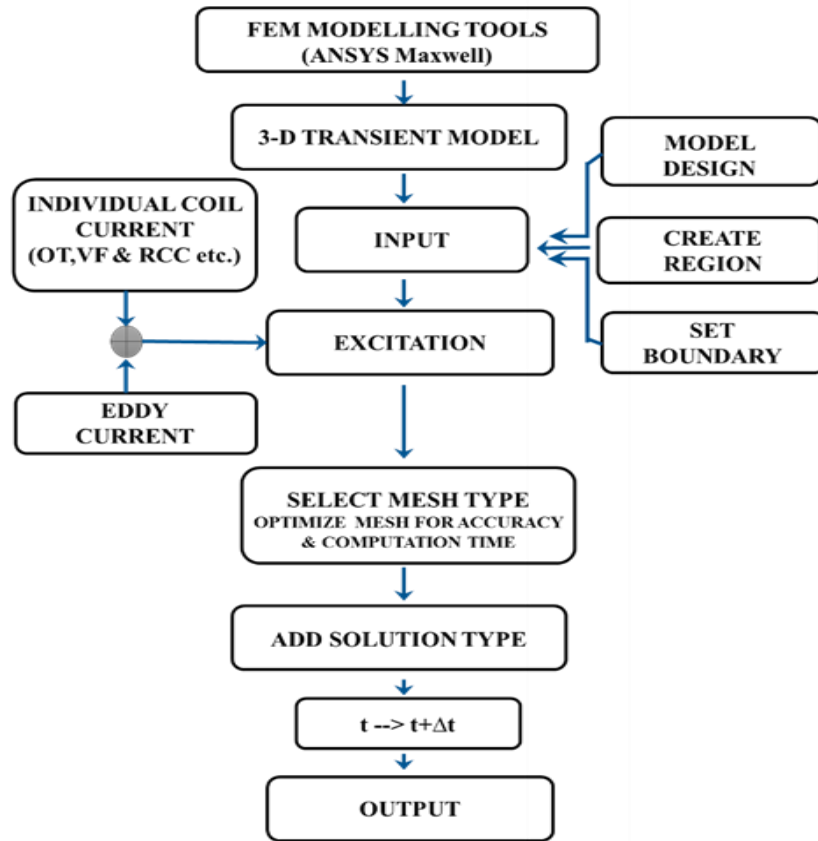


Figure 3.5 The Flowchart of FEM Modelling.

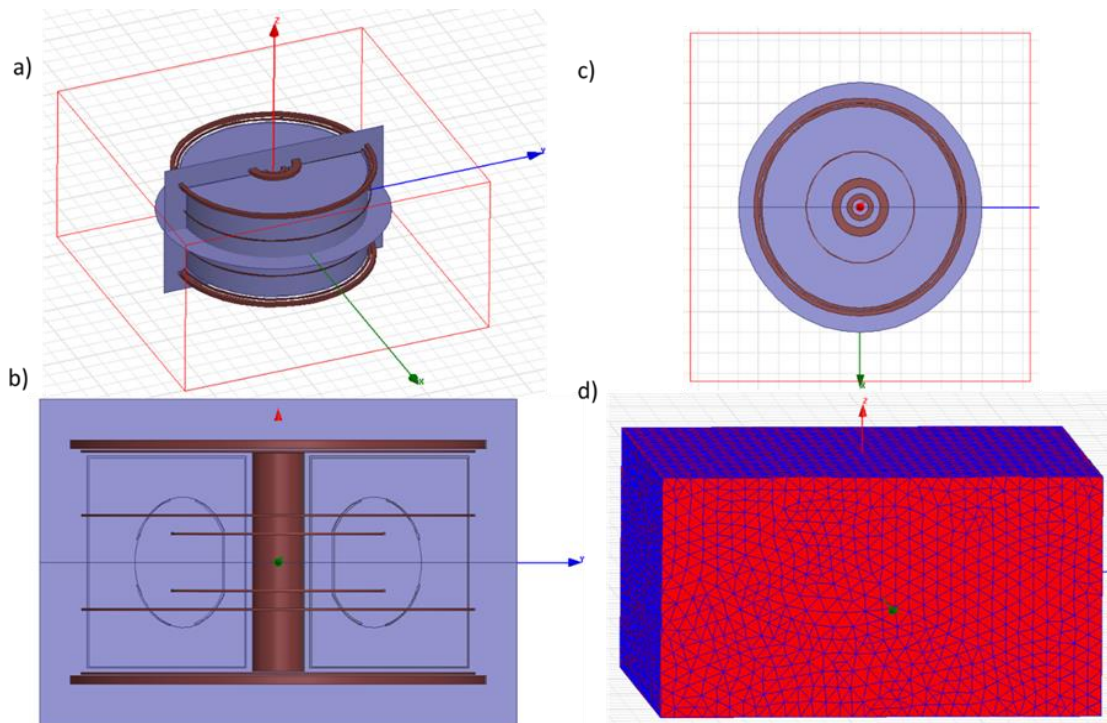


Figure 3.6 The ANSYS model a) Overall 3D transient model with selected boundary region b) Cross-Sectional view c) Top view d) The Mesh structure.

Our 3-D transient models with selected boundary region have been shown in [Figure 3.6\(a\)](#). The main design parameters such active coils, vessel structure have been shown in both cross-sectional and top views in [Figure 3.6\(b\)](#) and [3.6\(c\)](#). Appropriate mesh sizes (shown in [Figure 3.6. \(d\)](#)) have been chosen to ensuring computational accuracy.

3.5 Result and Analysis

The results of the electromagnetic analysis and their validation with experimental data, wherever applicable during the plasma break-down and start-up have been detailed in this section. In section 3.5.1 the magnetic field generated by the vertical field coil computationally has been shown in comparison with the experimental signals obtained during the vacuum shots. In section 3.5.2, the various experimental situations present have been elaborated considering operational combinations such as OH, OH+VF, OH+VF+EDDY, and OH+VF+EDDY+RCC etc. In section 3.5.3, the dynamic null has been computed by considering eddy currents in a transient model. The evolution of the dynamic null has also been presented. These results have been subsequently validated against experimental results obtained from the magnetic diagnostics of SST-1. Finally, in section 3.5.4, the contribution of the radial control coil has been added, where it is demonstrated to be favorable to plasma startup scenarios.

3.5.1 Validation of simulation model using known vertical field (VF) coil current

The Vertical Field (VF) Coil in SST-1 is a pair of electromagnets, located outside the cryostat and placed symmetrically around the midplane. In most of our experiments, vertical field coil is used to support initial magnetic field scenarios during plasma formation, ramp up and later it also provides the equilibrium conditions [\[3.28\]](#). Thus, the regions of interest are divided into two parts. Firstly, in $I_{VF} < 1\text{kA}$ range, the VF

contributes to support initial plasma formation and secondly in the range of $1\text{kA} < I_{VF} < 3.5\text{kA}$. In this later range, the vertical field coil is solely used to support plasma equilibrium, which is achieved by balancing the outward hoop force against the radial force. The comparison between the measured magnetic field from probe diagnostics and simulated magnetic field using finite element modeling for Pure VF Shot # 8573 simulated results have been presented in Figure 3.7. The iso -B field line and the B vector field line at maximum VF current (3.2kA) has been shown in Figure 3.8(a) and (b). This is the methodology used for the benchmarking of our electromagnetic model.

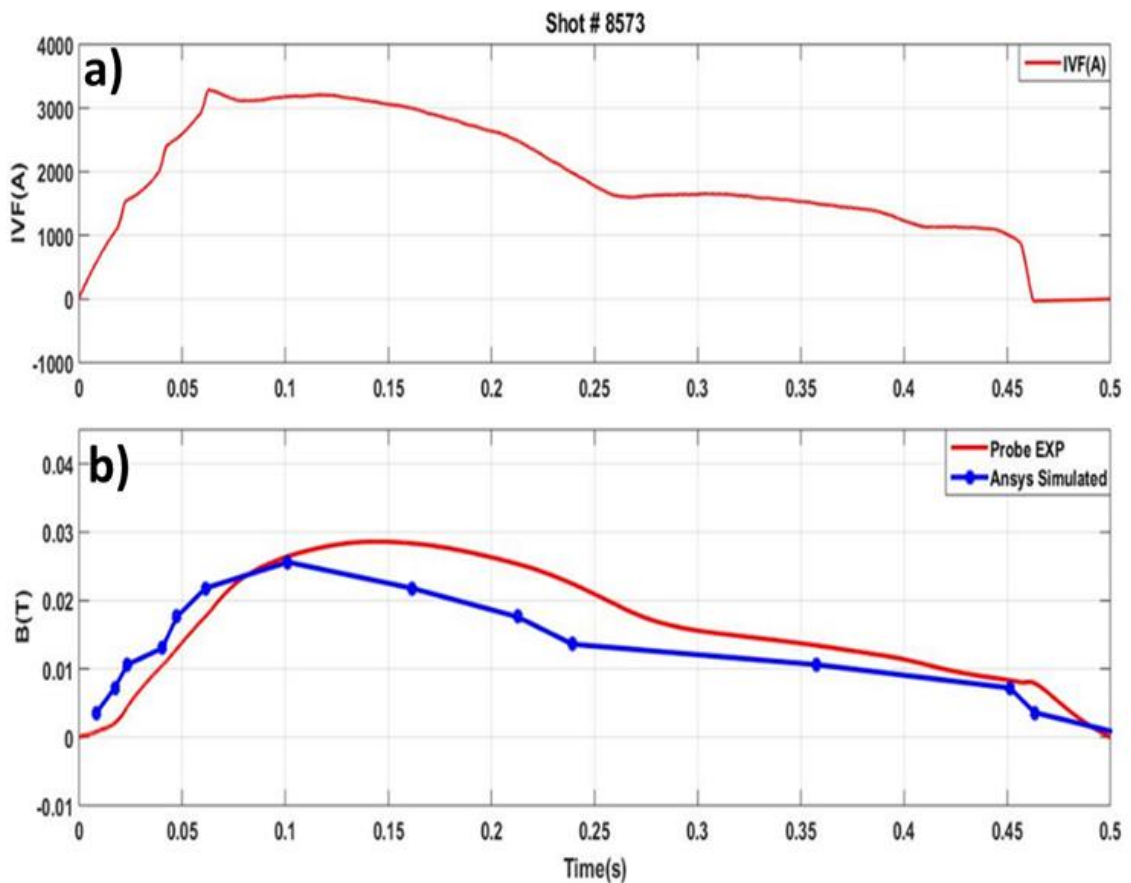


Figure 3.7 (a) The evolution of vertical field current for Pure VF Shot # 8573.(b)The comparison between measured magnetic field from probe diagnostics and simulated magnetic field using finite element modeling for Pure VF Shot # 8573.

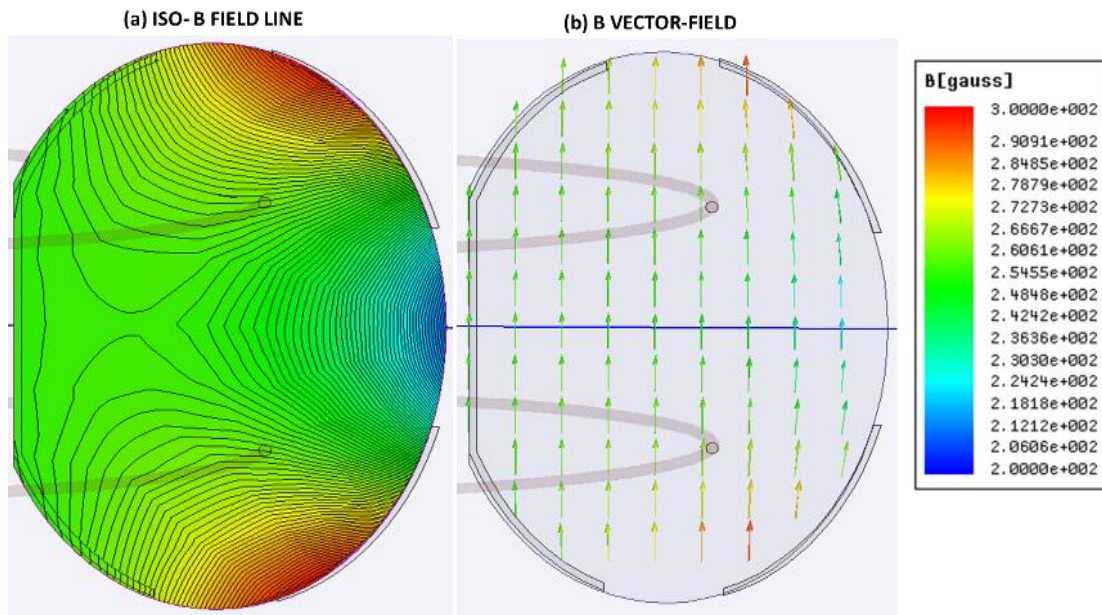


Figure 3.8 (a) The Iso – B field line and (b) The B vector field line for Pure VF Shot # 8573 at 3.2kA.

3.5.2 Different scenarios for SST-1 Start-up

Various experimental scenarios and sequences have been discussed in this section, which have been generally adopted in SST-1. The combinations are; OH, OH+VF, OH+VF+EDDY, OH+VF+EDDY+RCC etc. An accurate computation of the vacuum field contributed by (a) ohmic coils alone (b) the equilibrium coils alone (c) in combinations influencing the iso-field contours during scenarios of start-up have been carried out. At the same time, there is a pair of in-vessel single turn radial control coils, which may be used to support the initial configuration. Different startup scenarios have been studied extensively and shown in Figure 3.9. A static field null calculation was performed for the initial magnetization stage by taking the contributions of only ohmic coils (OH) assembly, which has been shown in Figure 3.9(a). Studies have revealed that the ohmic coil assembly alone (TR1, TR2, TR3, and TR4) in SST-1 would not be able to provide a sufficient null region of its own with the prevailing constraints. The vertical

field is necessary for plasma formation. The static null is only formed by the contribution of ohmic and vertical field coil (OH+VF) (shown in Figure 3.9(b)). The calculation of the dynamic null has been computed (shown in Figure 3.9(c)) by taking into consideration the vessel eddy current contribution. The radial movement has been observed by charging up the radial control coil. If we increase the rating of the vertical field coil currents, the null position moves towards the inboard side and would vanish subsequently. It has been shown that under the prevailing constraints, vertical field coil currents of more than 1.5 kA (shown in Figure 3.9(d)) fail to maintain the successful initial configuration indicating that the field errors dominate and breaks the iso-flux contours. Figure 3.10 shows some important experimental parameters such as I_P , I_{OT} , I_{VF} , ECRH power rating, vessel pressure and produced H_{Alpha} level during the corresponding instances.

It is always desirable for the Tokamak operator to obtain a NULL region around the defined major axis of the device. In the case of SST-1, the plasma major axis is at $R=1.1$ m. Thereafter, as a result of the $J \times B = \text{Grad } P$ force balance and from the increasing equilibrium field profile, the plasma may move either inward or outward. The longer the formed plasma column stays around the major radius without getting crushed either inboard or outboard, the better is the control and confinement of the plasma column. In SST-1, The scenario Figure. 3.9(c) is a representative preferable scenario towards ease plasma start up and plasma sustainability.

Different Experimental scenario for SST-1 Start -up

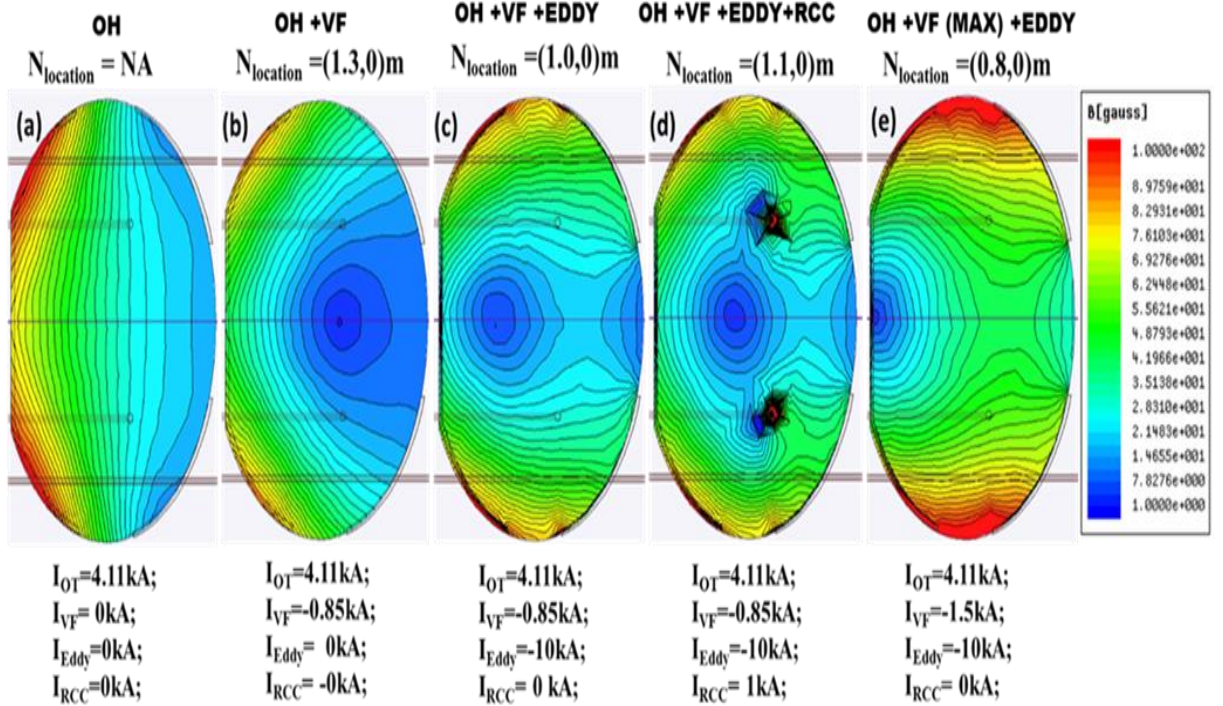


Figure 3.9 The evolution of the simulated magnetic field in the different experimental scenario for SST-1.

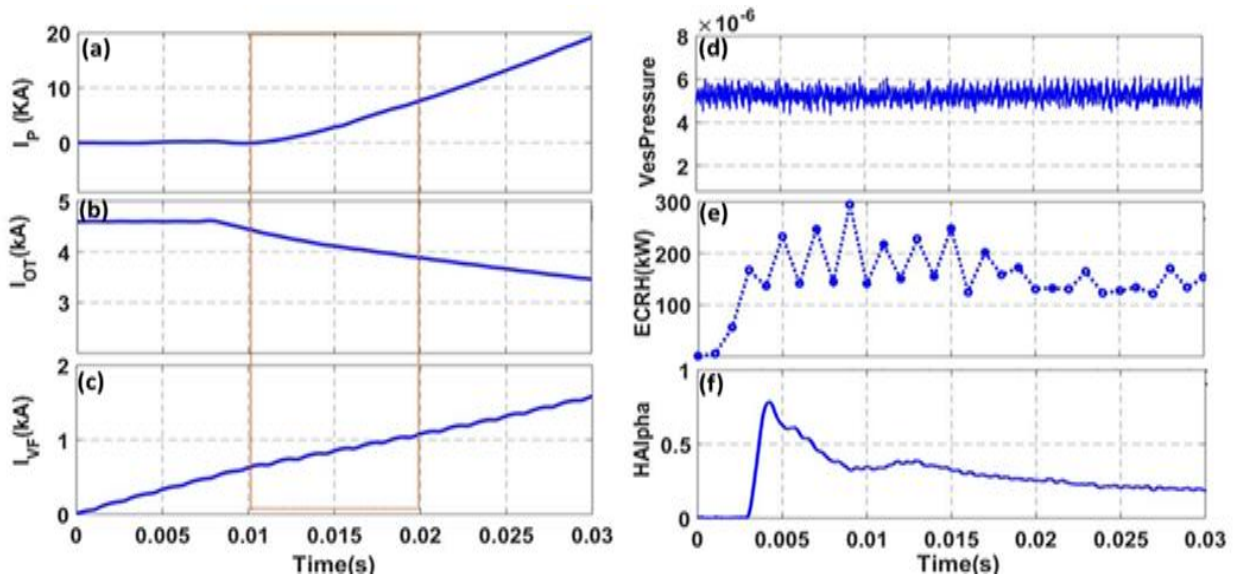


Figure 3.10 (a) Plasma current (I_P), (b) Central solenoid current (I_{OT}) (c) Vertical field current (I_{VF}) (d) Vessel pressure (e) ECRH Power (f) H_{α} signal for SST-1 shot # 8707 during startup. (Magnified part is used for simulation).

3.5.3 Computation of Dynamic Null

Generally, the ‘dynamic null’ refers to the ‘null characteristics at different instances of the time evolution’ as the pulse progresses. The static null configuration is usually influenced by time-varying vessel eddy currents. An important objective of our work has been to determine vessel current distributions and their influence on overall null characteristics. There is considerable evidence that an unfavorable eddy current can affect null position significantly and thus initial plasma breakdown characteristics [3.29] can be altered significantly. The current contribution of eddy currents is opposite to that of the central solenoid contributions.

A simple circuit model [3.27] to compute eddy current distribution in the vacuum vessel has been employed. The computed maximum eddy current in SST-1 in present operating scenarios is about 15-20 kA (shown in Fig. 3.12(b)). The vessel currents could be described even better with more sectional elements or more filaments. The plasma facing component support structures may also contribute more induced effects. However, we have limited our analysis to sections which can be adequately represented with the installed flux loops, since the model predictions need validation against experimentally observed signals.

As a representative case, simulated results of the dynamic evolution of magnetic null due to vessel eddy currents for a typical shot #8707 have been presented in this section. The study also reveals that for successful plasma formation, appropriate synchronization of OT +VF assembly currents and ECRH pulse are extremely important. For the specimen shot # 8707, it is shown that the poloidal null usually gets formed in the outboard region. This null gradually moves inward as a result of an increase of vertical field coil current. Figure 3.11 shows the evolution of the poloidal null field at an interval of 10ms. We have found identical trends for successful plasma

shots. The average magnetic field has been measured experimentally (shown in Figure 3.12(a)) during that phase. The magnetic field has been found to be in the range 20 to 50G. This is a necessary threshold for SST-1 that leads to a successful plasma start-up and subsequent formation.

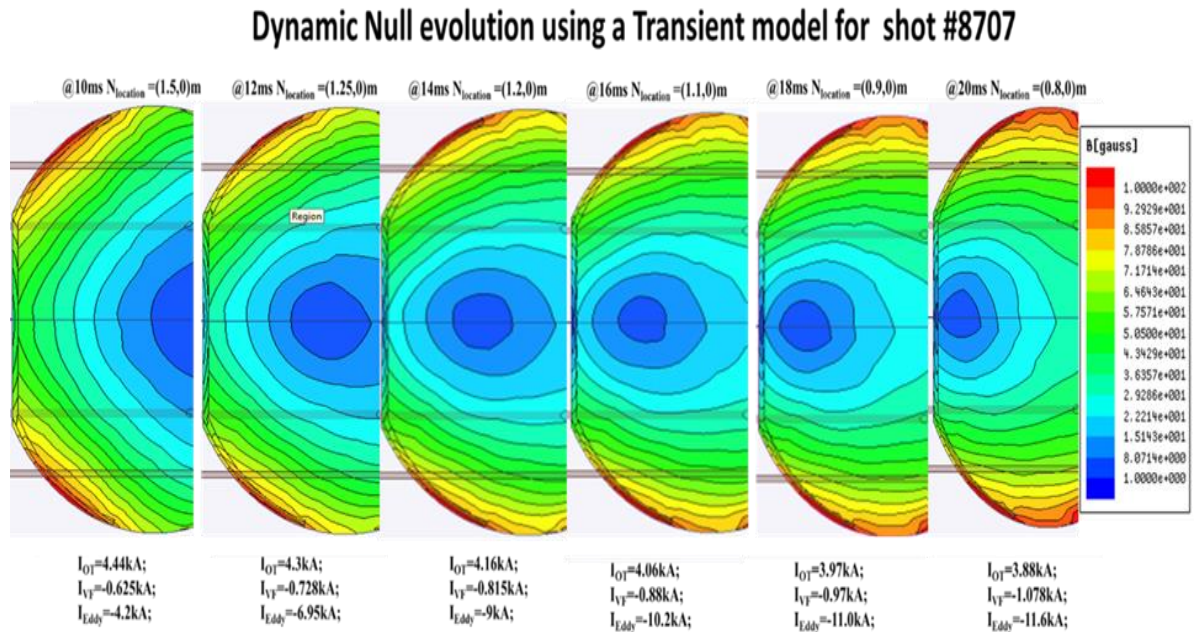


Figure 3.11 The evolution of Dynamic null region simulated using FEM modeling tools for specimen shot # 8707.

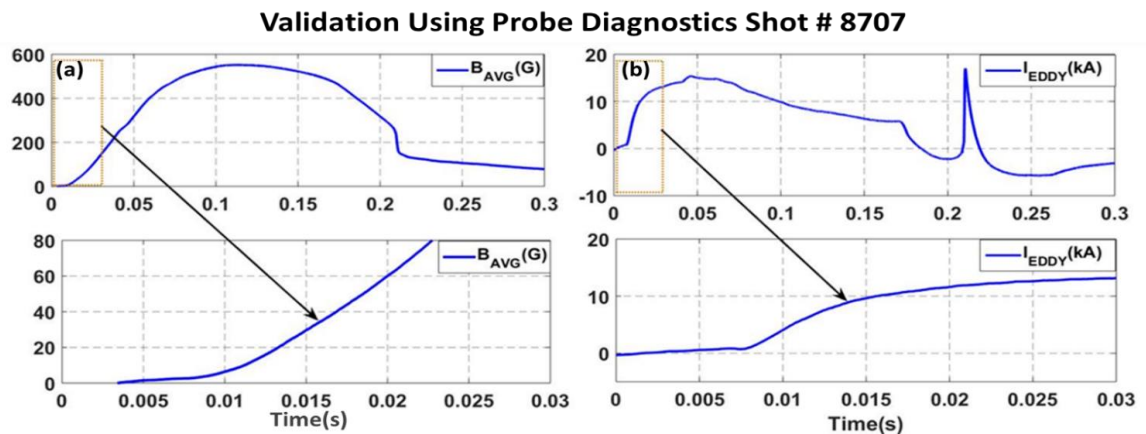


Figure 3.12 (a) The magnetic field measured using magnetic probe diagnostics and its magnified representation shown below. (b) The profile of vessel eddy current field measured using flux loop diagnostics and its magnified representation has been shown below.

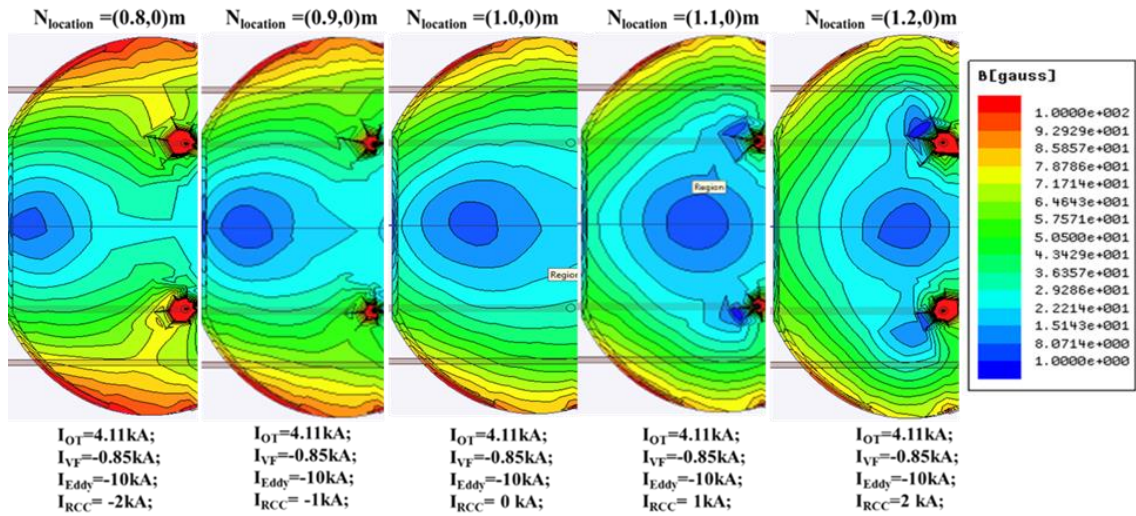


Figure 3.13 The evolution of simulated magnetic field with the contribution of the RCC coil.

3.5.4 Effects of Radial Control Coil (RCC)

The contribution of in-vessel radial control coil (RCC) has been analyzed for the case of a successful plasma formation, which has been studied earlier using FEM simulation. It is found that this particular coil could make significant effects on the existing null due to its proximity to plasma region. Figure 3.13 shows an evolution with the RCC contribution being included.

3.7 Summary and Conclusion

In this chapter, an electromagnetic model for SST-1 tokamak has been elaborately described. The electromagnetic fields for different current carrying coils for the SST-1 tokamak have been investigated using the finite element method. The simulation results have been validated using the known vertical field (VF) coil current pulse. The results on comparison are found to be in good agreement.

The magnetic field status for each active coil during start-up has been studied. An accurate computation of the vacuum field contributed by the 1) ohmic coils alone, 2) the ohmic coils with combinations of equilibrium coils, and 3) the vessel influenced by eddy currents during start-up have also been carried out. We have discovered the necessity of using vertical field current in addition to the central solenoid assembly for successful plasma start-up in the present operating situation under the prevailing constraints of the machine. Various conditions and investigations of null regions during low voltage EC assisted breakdown have also been studied. For a successful plasma start-up and current ramp-up stage the in-vessel magnetic field has been found to be in the range 20 to 50G. This is a necessary threshold for SST-1.

The role of the eddy current has been interpreted by means of dynamic modeling of the SST-1 startup scenario. All the simulated results from the electromagnetic modeling have been validated using experimental data obtained from the in-vessel magnetic diagnostics. The contribution of the in-vessel Radial Control Coil (RCC) has been analyzed successfully for the case of a successful plasma formation. It is found that this particular coil could make significant effects on the existing null and can contribute positively towards the plasma formation in SST-1.

The time evolution study of eddy current characteristics and the observations from this electromagnetic modeling has contributed to optimizing the initial start-up condition which significantly helps increase the plasma current from 60kA to 100kA in recent campaigns.

C_{CHAPTER} **–IV**

Electromagnetic Diagnostics for SST-1

- **Motivation and literature survey**
- **Principle: Radial Shafranov shifts Calculation**
- **Results and Discussion**
- **Comparison with imaging diagnostics**
- **Observations & Conclusions**

4.1 Motivation and literature survey

Diagnostics are essential towards the characterization of the plasma column in a tokamak configuration. In general, based on standard physics, plasma diagnostics are instrumental set-ups and associated experimental techniques employed to measure various properties and characteristics of plasma; such as plasma density, energy distribution function, temperature spatial profiles and dynamics etc. Among them, plasma magnetic diagnostics enable researchers to derive equilibrium plasma parameters in terms of magnetic fields and fluxes. In tokamak research, there exist fundamental interests in the subjects of plasma equilibrium conditions, axisymmetric stability, and disruptions scenarios. The involvement and inference of magnetic diagnostics in these measurements are immense because of their simplicity, cost, and upgradability etc. A primary use of the magnetic diagnostic system is to estimate the plasma equilibrium for the purposes of feedback control of the plasma current, its position inside the vacuum vessel and the shape of its boundary.

The plasma diagnostic system is also influenced by the structural detail of the tokamaks and physics-based objectives of the machine. There are several research articles and books available regarding the descriptions of plasma diagnostics specifically in the topics of magnetic diagnostics. P. E. Stott, G. Gorini and E. Sindoni [4.1] have explained complete details of plasma diagnostics in their book on the ‘Diagnostics for Experimental Thermonuclear Fusion Reactors’.

Ian H. Hutchinson [4.2] in his book ‘Principles of Plasma Diagnostics’ has provided a detailed derivation and discussion of the principles of plasma physics upon which the diagnostics are based. In addition to this discussion, some of the details in the research literature about the plasma diagnostics studies are also mentioned there with important highlights.

In a review article of tokamak plasma diagnostics, the EQUIPE TFR [4.3] team has emphasized the trends of tokamak plasma diagnostics with their limitations and needs for future large tokamaks. The design, development, instrumental techniques and theoretical considerations of magnetic diagnostics have been elaborated.

D. V. Orlinskij [4.4] et al. has described different diagnostic methods according to the physical quantities. The diagnostics involved with the electric and magnetic diagnostics, measurements of electron density, electron temperature, and the ion components of the plasma, radiation loss measurements, and spectroscopy of impurities, edge diagnostics and study of plasma stability have been outlined. The main parameters of the various diagnostic systems used in various tokamaks have also been summarized.

In a review, G. F. Matthews [4.5] has explained the principles and applications of electrical probes for the diagnosis of tokamak edge plasmas. The progress in the application of advanced electrical probes such as field analyzers and mass spectrometers to the tokamak boundary are reviewed in this context. T.R. Hodapp [4.6] has investigated the development of magnetic field measuring diagnostics for future long pulse tokamaks like ITER. Usually, an integrator is used to compensate the integrating drift in magnetic diagnostic instrumentation. In a specific study of analog integrator design for KSTAR advanced magnetics diagnostic system J. G. Bak [4.7] et al. has investigated the characteristics of those integrators experimentally. They explained that the noise pick up in the integrated signal due to a long signal path may be reduced under certain conditions. They also demonstrated the effectiveness of the sensor and cable resistances on the actual signal also reduce by adding two differential amplifiers to the signal path between the sensor and the integrators. E.J Strait et al. [4.8-4.9] have described various magnetic diagnostics system of the DIII-D tokamak. Various

magnetic diagnostics such as axisymmetric poloidal flux loop, diamagnetic loop, magnetic probes and saddle loop have been explained for the measurements of plasma shape and position control with the real-time digital control system, post-discharge equilibrium reconstruction, spectrum analysis in time and space of plasma instabilities. G. Vayakis [4.10] et al. have described the development of ITER magnetic diagnostics setup with highlights of specific design progresses. In this work, specific design processes for in-vessel coils, steady-state sensors, saddle loops and diverter sensor with their working concept, software, and electronics specification have been outlined. P. Moreau et al. [4.11] has covered some aspects of manufacturing constraints and positioning requirements for all the important magnetic diagnostics one finds in tokamaks. Their use and expected accuracy and precision have been assessed in terms of magnetic equilibrium reconstruction and plasma current measurements. D. Testa [4.12] et al. have presented multiple sets of requirements for the ITER magnetic diagnostics system and their current status in various R&D activities.

This section briefly reviews the basic principles of magnetic measurements with reference to plasma position measurements particularly in the context of the SST-1 tokamak [4.13]. Initially we have considered the form of the magnetic field external to the plasma and its dependence on the presence of the plasma. Its implications for magnetic diagnostics have been discussed, including the measurements that are needed to completely characterize the external field and, the information about the plasma that can be obtained from such measurements. Lastly, studies about the installation of some new magnetic diagnostics have been shown with their orientation details, the results of which have been used for subsequent equilibrium reconstruction and possible feedback control in the future.

4.2 Importance of magnetic diagnostics and their challenges in tokamak study.

The main purpose of the magnetic diagnostic system [4.1-4.13] is to estimate plasma equilibrium criteria by computing plasma, shape and boundary and then its use for the purpose of feedback control. Usually, the data from magnetic sensors are combined and fed through in an online real-time code which computes and adjust by solving the standard form Grad-Shafranov equation's solution. Some of the main purposes of the magnetic diagnostics are as follows

- Study the transient electromagnetic phenomena in various spatial locations.
- Determination of plasma equilibrium configuration.
- The use of magnetic diagnostics for real-time plasma position control.
- To study the magneto-hydrodynamics (MHD) phenomena.

There are a number of challenges during the design phase of magnetic diagnostics such as requirements of long pulse operation, the need to integrate voltage provided by the sensors and development of high-quality integrators. Thus, appropriate precautionary techniques have to be obtained during the designing of the instruments and subsystems.

Some of the basic criteria for tokamak magnetic diagnostics design are as follows:

- The magnetic diagnostics system must have a high degree of reliability and redundancy for continuous operation of tokamak environment measuring precise values in a fast response timescale.
- The magnetic sensors must withstand disruption transients. Criteria such as plasma interactions, heat, and eddy current effects need to be considered and must be considered both in the design as well as in the analysis of the data.

- The dimension of the magnetic diagnostics may be restricted by space availability specifically on the inboard side.
- The sensor size, shape, and position are required to be chosen in such a way that best accuracies are obtained with reliable and repeatable measurements, especially during control operations.

4.3 Brief description of various magnetic diagnostics

The sources of the magnetic field in tokamaks are of various kinds. Usually, different profiles of currents need to be generated by power supplies for active current carrying coils towards initial magnetization and plasma control scenarios. The vessel eddy currents generated by induced voltages and the plasma current give rise to magnetic fields in the poloidal and toroidal directions. The accurate measurements of these currents and their fields employing magnetic diagnostics are simple, cost-effective and reasonably accurate. Various plasma parameters such as total plasma current, plasma position, plasma shape, plasma conductivity, total energy content and MHD instabilities could be measured using specific magnetic diagnostics. In this section, some of these basic studies related to these magnetic diagnostics, which have been used in the course of our investigation have been outlined. Table 4.1 shows some important diagnostics with plasma parameters meant to be measured by these diagnostics. The schematic diagrams [Figure 4.1](#) have explained basic techniques for measuring basic plasma parameters.

Table 4.1: Summary of Plasma Diagnostics	
Diagnostics	Function
Rogowski coils	Plasma current, Individual coil current
Flux loop	Poloidal flux for plasma control, Plasma start-up study.
Br and Bz coils	Plasma position and shape measurements
Mirnov coils	Plasma MHD instability
Diamagnetic loop	Stored energy and poloidal beta
Multichannel bolometer	Radiated power profile
Microwave interferometer	Plasma density
Survey spectrometer	Plasma impurities
Soft X-ray imaging	Plasma instability and fluctuations
Thermocouple	vessel wall and cryostat temperature
Charge-exchange recombination spectroscopy	Ion temperature and toroidal rotation
H α detectors	Hydrogen emission
Visible Bremsstrahlung array	Zeff
Langmuir probe	electron temperature, electron density and electric potential of a plasma
Visible spectrometer	Edge/ diverter region spectroscopy
Neural particle analyser	Core ion temperature and fast ions

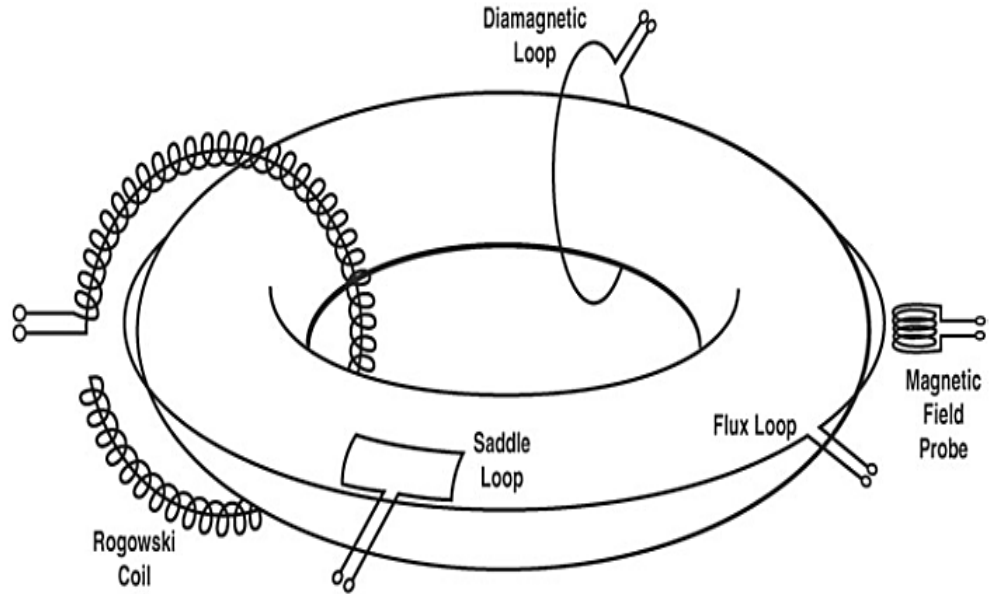


Figure 4.1 Schematic figure of a plasma-magnetic diagnostics; Poloidal flux loop, magnetic field probe, saddle loop, diamagnetic loop and Rogowski coil.

4.3.1 Rogowski coil

A Rogowski coil [4.15], named after Walter Rogowski, is an electrical device for measuring alternating current (AC) or high-speed current pulses. These coils measure a time-changing current (typically the toroidal current in a tokamak), when wound around a current carrying conductor typically plasma or coils. It consists of a helical coil of wire with the lead from one end returning through the center of the coil to the other end, so that both terminals are at the same end of the coil (shown in Figure 4.2). The coil is usually a helically wound solenoid, with a return center conductor so that the coil has no net loop around the plasma, and is usually encased in a Faraday shield to avoid electrostatic pickup. The whole assembly is then wrapped around the straight conductor whose current is to be measured. The winding density, the diameter of the coil and the rigidity of the winding are the critical parameters of the Rogowski coil and can be adjusted so as to preserve its immunity to external fields and low sensitivity to the positioning of the measured conductor.

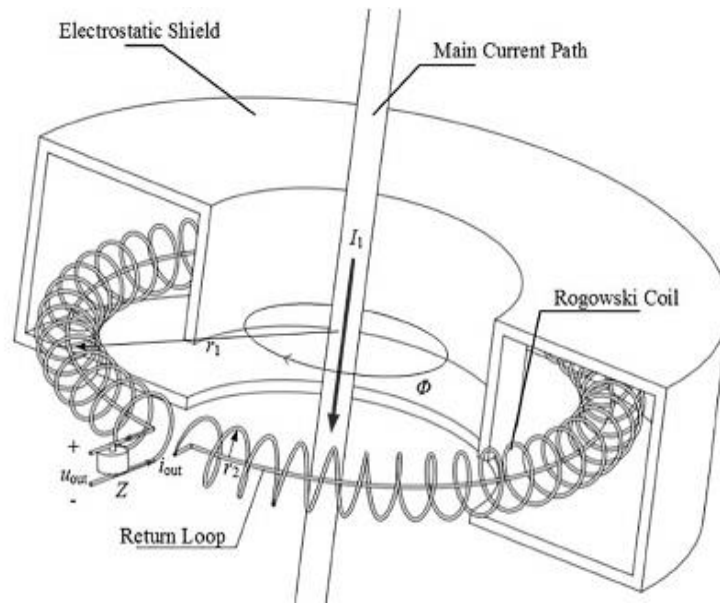


Figure 4.2 Structure of Rogowski coil [Image Credit: Ruo-Yu Han].

Since the voltage that is induced in the coil is proportional to the rate of change (derivative) of current in the straight conductor, the output of the Rogowski coil is usually connected to an electrical (or numerical) integrator circuit to provide an output signal that is proportional to the current. The voltage produced by a Rogowski coil is

$$v(t) = \frac{-AN\mu_0}{l} \frac{di(t)}{dt} \quad (4.1)$$

Where,

A is the area of one of the small loops,

N is the number of turns,

l is the length of the winding,

$\frac{di(t)}{dt}$ is the rate of change of the current threading the loop and

μ_0 is the magnetic constant

To achieve better accuracy and precision, the turns of the Rogowski coil need to be evenly spaced and small relative to the radius of the coil.

In SST-1, redundant Rogowski coils have been installed to measure plasma current (I_p).

Two full Rogowski coils and two pairs of half Rogowski coils have been used to

measure the SST-1 plasma current in the present operating scenario. Different sets of Rogowski coils have been used to measure the transport current in different TR coils, vertical field (VF) coil and radial control coil (RCC). The Rogowski coil outputs have been calibrated with a known source and known current profiles first. Once calibrated with sources like that of a RCC current profile, the SST-1 plasma currents have been measured in actual plasma shots.

4.3.2. Diamagnetic Loop

Plasma diamagnetic loop [4.16-4.21] measurements are carried out to measure the plasma poloidal beta (β_p), plasma kinetic pressure (p), the stored energy (W_d) and the energy confinement time (τ) in the tokamak. These parameters are very important for the stable operation of the tokamak. The diamagnetic loop is a poloidal loop placed inside the vacuum vessel enclosing the plasma column to measure diamagnetic flux changes in the plasma discharge in a tokamak.

The simplest way to measure diamagnetic flux change is to measure the small voltage drops across the TF coil itself during the plasma discharge in the vessel caused by plasma diamagnetism. The other method for diamagnetic flux measurement is done by proper analysis of circuit model and to determine the different self and mutual inductances of diamagnetic and compensating loops that are obtained from the analysis of vacuum shot.

The compensating method uses a one-turn diamagnetic loop enclosing the plasma column to measure the total toroidal flux and a multi-turn compensating loop that excludes the plasma column and thus measures the vacuum toroidal flux. The diamagnetic flux is obtained from the difference of these two signals after proper calibration. These loops can be installed either inside or outside the vacuum vessel. The

loops are preferably placed inside the SST-1 vacuum vessel to minimize the time delay and the effect of conducting vacuum vessel.

In the diamagnetic flux measurement we use an inner diamagnetic loop and a concentric compensating loop during a plasma discharge; the flux in the inner concentric loop Φ_D and that in the compensation loop Φ_C are given as follows:

$$\Phi_D = (\Phi_D)_{TF} + (\Phi_D)_{OH} + (\Phi_D)_{VF} + (\Phi_D)_{ED} + \Delta\Phi_D \quad (4.2)$$

$$\Phi_{DV} = (\Phi_D)_{TF} + (\Phi_D)_{OH} + (\Phi_D)_{VF} + (\Phi_D)_{ED} \quad (4.3)$$

$$\Phi_C = (\Phi_C)_{TF} + (\Phi_C)_{OH} + (\Phi_C)_{VF} + (\Phi_C)_{ED} \quad (4.4)$$

Φ_D and Φ_C are the fluxes picked up by the diamagnetic loop and the compensating loop in a plasma shot respectively, Φ_{DV} is the vacuum contribution to the flux linked to the diamagnetic loop by the toroidal coils, ohmic central solenoid, vertical field coils and eddy fields in the vacuum vessel. $(\Phi_C)_{TF}$, $(\Phi_C)_{OH}$, $(\Phi_C)_{VF}$ and $(\Phi_C)_{ED}$ are the vacuum fluxes picked up by the compensating loop due the toroidal coils, ohmic central solenoid, vertical field, and eddy field in both the vacuum shot and plasma shot respectively. This is due to the non-enclosing structure of the compensating loop. $\Delta\Phi_D$ is the plasma diamagnetic flux change linked to the inner diamagnetic loop. Due to the larger area of the diamagnetic loop in comparison with the compensating loop, the vacuum flux pickups in the compensating loop are smaller than the diamagnetic loop. In order to get comparable signals in these two loops, we have to use multiple turns in the compensating loops. Further, in order to get the diamagnetic flux, one needs to subtract the vacuum flux in the inner coil by using the balance coefficients, which can be determined from the vacuum shot. We can write the diamagnetic flux change in the plasma shot as:

$$k = \Phi_{DV}/\Phi_C \quad (4.5)$$

$$\Delta\Phi_D = \Phi_D - k \Phi_C \quad (4.6)$$

In these measurements, the compensation for the toroidal, ohmic, vertical and eddy field has been performed with the help of the vacuum shot. In these shots the toroidal field, vertical field, loop voltage etc. have nearly same value and a similar type of variation but without plasma in the vacuum vessel. The voltage signals picked by the diamagnetic (V_D) and the compensating loop (V_C) in this scenario is contributed by the changes in the current in all the active coils and eddy currents. The voltage signals are time integrated to get flux changes $\Phi_{DV} = -\int_0^t V_D dt$ and $\Phi_C = -\int_0^t V_C dt$ in the diamagnetic and the compensating loops respectively. Using the Φ_D and Φ_C equations, the balance coefficient k is determined. The difference of the flux passing through the diamagnetic loop in the plasma shot and in the vacuum shot gives the diamagnetic flux change due to plasma diamagnetism. The voltage signal picked up by these two loops in the plasma shot are again time integrated like the above mentioned method to get Φ_D and Φ_C and using the equations (4.5) and (4.6) we can obtain the $\Delta\Phi_D$.

The diamagnetic flux change ($\delta\Phi_D$) is a much smaller quantity than the toroidal flux (Φ_T); nearly $\sim 10^{-3}$ times. Therefore, the diamagnetic flux measurement is severely affected by several factors, such as changes in the toroidal field (TF), vertical field (VF), central solenoid ohmic transformer (OT) field; vibration of the diamagnetic loop and its flux linkage with various external currents, such as the currents in active magnetic field coils, eddy current in the vacuum vessel etc. The mechanical vibration of the diamagnetic loop in a space varying toroidal field produces high frequency noise in a diamagnetic loop signal during the plasma discharges. The misalignment of the diamagnetic loop in the poloidal plane causes the loop to have pick-ups of currents in various field coils and the flux due to the eddy current induced in the vessel. The pick-ups of voltages due to changes in current of the external coils and the eddy current in the vessel need to be compensated from the diamagnetic loop signal accurately for a

reliable measurement. Compensation for the vacuum flux has been performed using a non-enclosing coplanar coil or the compensating coil. Due to the greater area of the diamagnetic loop the signal in the diamagnetic loop is greater than the compensating loop. In order to have the same signal strength in these two loops in the vacuum shots, generally multiple numbers of turns are used in the compensating loops.

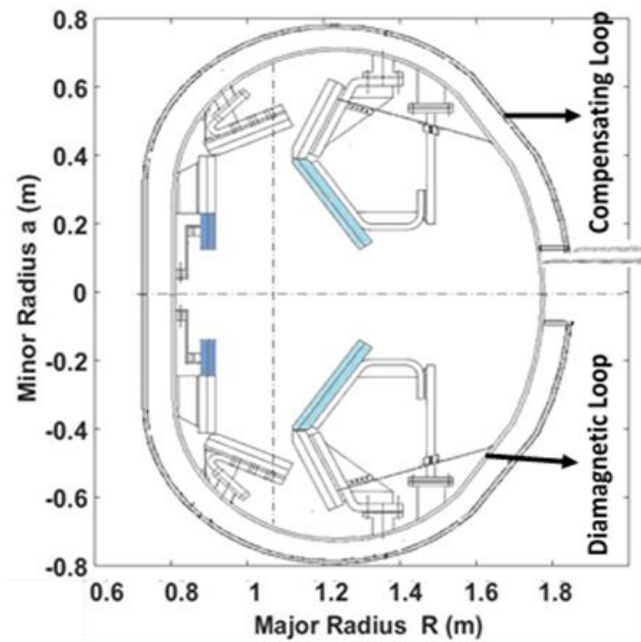


Figure 4.3 Diamagnetic and compensating loop positioning in the SST-1 poloidal plane.

In SST-1, the diamagnetic flux change has been measured by taking the difference of the diamagnetic loop and compensating loop signals (schematic of the diamagnetic loop has been shown in Figure 4.3). The diamagnetic loop consists of a single turn loop of polyimide-coated wire of diameter 0.2 mm which encloses a circular plasma column of diameter 0.4 m, the diamagnetic loop has an elliptical cross-section of radius 0.44m, ellipticity 1.5; the approximate area of the diamagnetic loop is 0.95 m². The compensating loop consists of 20 turns of elliptical cross-section, which are mounted on an I-beam having a radial width of 1 cm, supported on the same hoop as on the diamagnetic loop. The diamagnetic loop and the outer turns of the compensating loop have same diameters.

4.3.3 Flux loops

A flux loop [4.22] is a loop of wire. If a varying magnetic field passes through that loop, a voltage is generated. The induced voltage is determined using the standard Faraday law and the magnetic flux could be measured using this induced voltage. In case of the tokamak, these coils are typically single-turn loops which measure the time-rate of changes of the poloidal flux, from which one can infer the toroidal loop voltage. In a typical tokamak, there is at least one inner and outer loop or a multiply-redundant set of these coils for various applications.

The loop voltage can be written as

$$V_{\text{Loop}} = I_P R_P + L_p \frac{\partial I_P}{\partial t} + I_P \frac{\partial L_P}{\partial t} \quad (4.7)$$

Where, L_p is the plasma inductance and I_P is the plasma current. The plasma inductance for toroidal plasma is in the form of major radius (R), plasma internal inductance (l_i) and elongation (k) is

$$L_p = \mu_0 R \left[\frac{1}{4} + \ln \left(\frac{8R}{3\sqrt{k}} - 2 \right) + \frac{l_i}{2} \right] \quad (4.8)$$

The toroidally induced voltage combined with the plasma current is a measure of the ohmic power input to the plasma. Therefore, it is of great importance to measure the loop voltage. Induced loop voltage for plasma shot could be written in another form as

$$V_{\text{loop}_{i(R,Z)}} = M_{iOH} \frac{\partial I_{OH}}{\partial t} + M_{iBV} \frac{\partial I_{BV}}{\partial t} + I_P \frac{\partial M_{iP}}{\partial t} \quad (4.9)$$

Where, $\frac{\partial I_{OH}}{\partial t}$ and $\frac{\partial I_{BV}}{\partial t}$ are the rate of change of currents in the ohmic coils and vertical field coils respectively. The M_{iOH} is the total mutual inductance between the i^{th} flux loop and the ohmic coil whereas M_{iBV} is the total mutual inductance between the i^{th} flux

loop and the vertical field coil. The last term is the contribution of the plasma current and its contribution towards the surrounding structures, and I_P is the plasma current.

SST-1 has eleven sets of in-vessel flux loops installed inside the vessel. A voltage is induced from the flux variation in the central solenoid and the vertical field. The plasma position and shape could then be computed from the magnetic probes and flux loop data, and subsequently validated with the analytical solution of Grad-Shafranov equation (GSE). We have used a set of particular in-vessel flux loops for the measurement of inboard (ϕ_{IN}) and outboard flux (ϕ_{OUT}) and hence the radial shift measurements in SST-1 plasma. An appropriate compensation technique has been used to estimate the plasma position information. The reference signal has been generated using a non-plasma shot but having exactly the same parameters such as an ohmic transformer (OT), vertical field (VF) and other active coils. The contribution of the plasma has been calculated from the difference between that reference signal and the signal from the plasma shot.

4.3.4 Magnetic Probes:

An electromagnetic coil or probe [4.23-4.26] is an electrical conductor such as a wire; in the shape of a coil, spiral or helix. Electromagnetic coils [4.1-4.2] are used in various applications where electric currents interact with magnetic fields [4.27], in devices such as inductors, electromagnets, transformers, and sensor coils. As an electric current is passed through the wire of a coil, a magnetic field gets generated; similarly, when an external time-varying magnetic field passes through the interior of the coil, an EMF (voltage) generates in the terminal of the coil.

According to Faraday's law, output of the magnetic probe is proportional to the derivatives of the magnetic flux passing through it ($V = -NA \frac{dB_i}{dt}$) where, NA is the

actual magnetic section and $i=R, N$ stands for radial and normal direction. In schematic [Figure 4.4](#), I. Hutchinson has presented the procedure of EMF generation. A schematic representation of the actual probes has been presented in [Figure 4.5](#). This type of orientation of magnetic probes is able to measure the radial (B_R) and vertical (B_N) magnetic field in the same point usually used in most tokamak devices for the measurement of spatial the magnetic field.

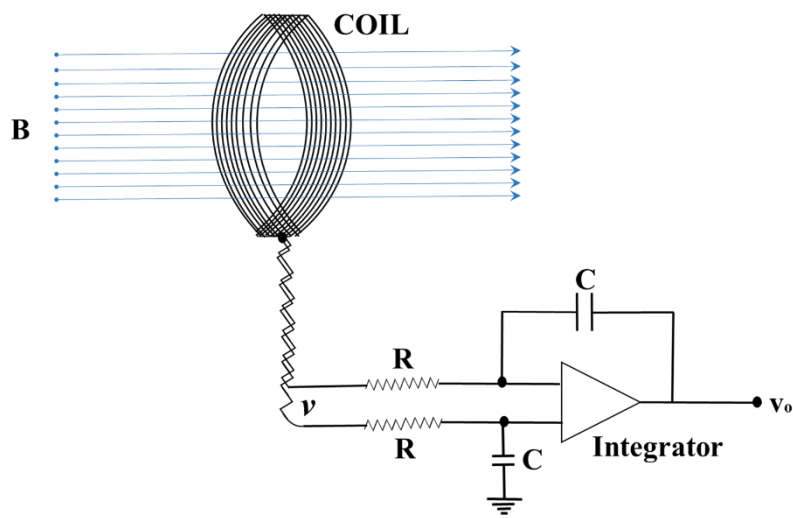


[Figure 4.4](#) Schematic of typical magnetic coil and integrators [4.1]

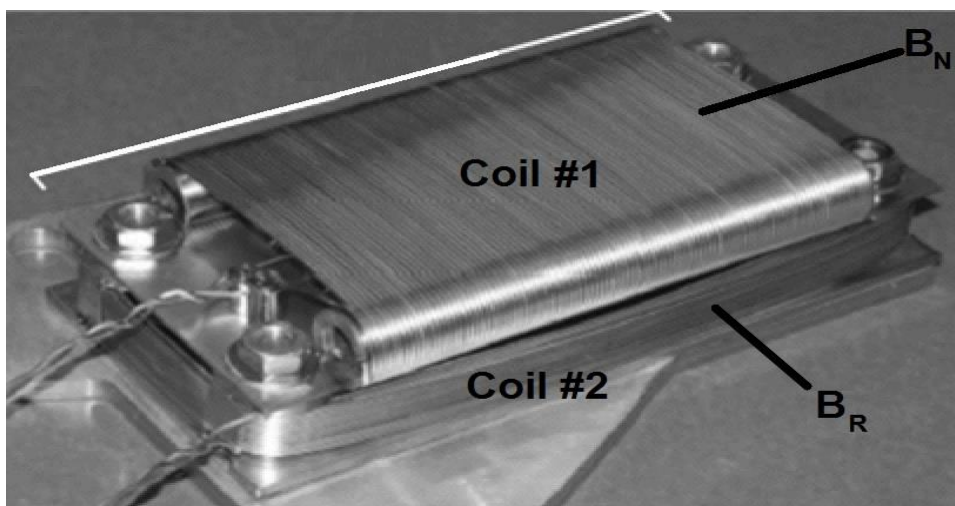


[Figure 4.5](#) Structure of Magnetic Probes

A current through any conductor creates a circular magnetic field around the conductor due to Ampere's law. The advantage of using the coil is that its output is solely

dependent on the number of turns and shape of winding. In the applied plasma experiments and in tokamaks, magnetic probes are preferred for measuring shape and plasma position from equilibrium criteria by the fitting method. The magnetic probes are the most used magnetic diagnostics for position control due to their fast response time and various other advantages.

4.4 Study and Installation of SST-1 Magnetic probe diagnostics

The SST-1 tokamak is equipped with eighteen pairs of identically designed magnetic probes (tangential and normal). It consists of multi-turn coils, oriented in a way that they intercept magnetic field lines and the resulting voltage is proportional to the rate of change of magnetic field. An ultra-high vacuum compatible single core copper conductor (silver electroplated $-1 \mu\text{m}$) (AWG24- of 0.65mm-Dia) is used in the winding. Necessary metallic shielding (SS-304L) is added to avoid unwanted noise pick up. Each probe has $N=140$ turns with an area, $A=2.28 \times 10^{-4} \text{m}^2$ and the nominal magnetic section is $NA=0.03192 \text{m}^2$. The basic design parameter and their dimensions are shown in [Figure 4.6](#). Each of these probes has been calibrated against a known field of a Helmholtz coil in a laboratory test setup. Once installed, all probes are calibrated using an in-vessel control coil (RCC) reference waveform and vertical field (VF) coil currents. An extensive study has been done and, it has been found that the probe's signals have a maximum deviation of less than 5% between the expected fitted signals and experimentally obtained signals for identical vacuum shots.

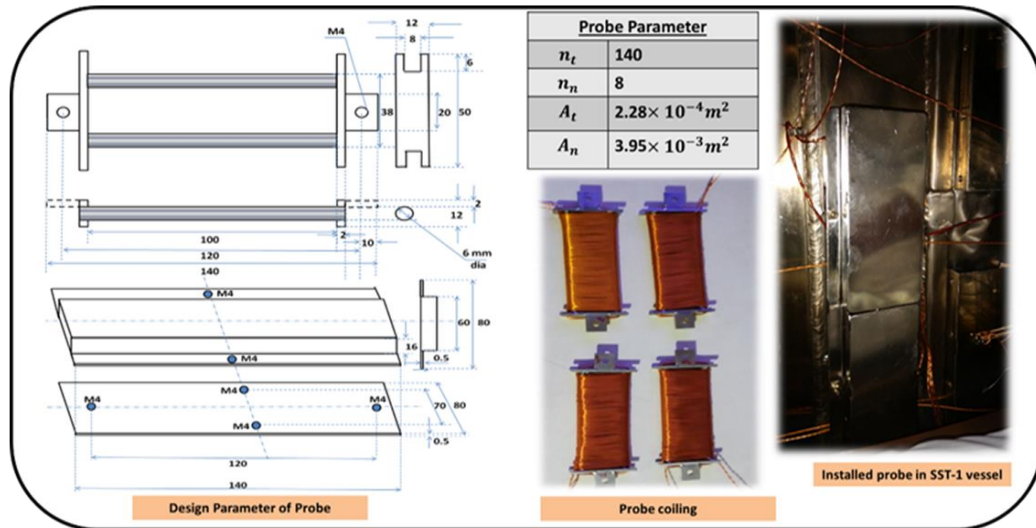


Figure 4.6 (In left) The design parameter of the magnetic diagnostics and (in right) a photograph of installed magnetic probe within the SST-1 vessel has been presented.

These are reproducible over a large number of vacuum shots as well as with plasma shots. The hardware comprises of multichannel signal conditioning with an isolation amplifier and a noise removal filter with a selectable gain controller (shown in Figure 4.7). In SST-1, a numerical integrator (with a DC offset and incorporating the drift correction is required after the integration) is used for integration purposes. For the experimental measurement of the radial Shafranov shift (ΔR) and vertical shift (ΔZ) in SST-1 plasma, the sets of magnetic probes installed inside SST-1 vacuum vessel has been used. Traditionally, these standard diagnostics installed at specific in-vessel locations have been used for accurate measurement of plasma positions in a tokamak. In SST-1, four sets of probes have been used for these purposes. With due compensations, these measurements have been used for the radial and vertical shifts of the present SST-1 plasma column. An ultra-high vacuum compatible single core copper conductor has been used in the winding of these probes. Necessary metallic shielding has been added to avoid unwanted noise pick up. A compensation technique has been used to compensate OT and VF current field contributions on probe diagnostics signals during plasma shift measurements.

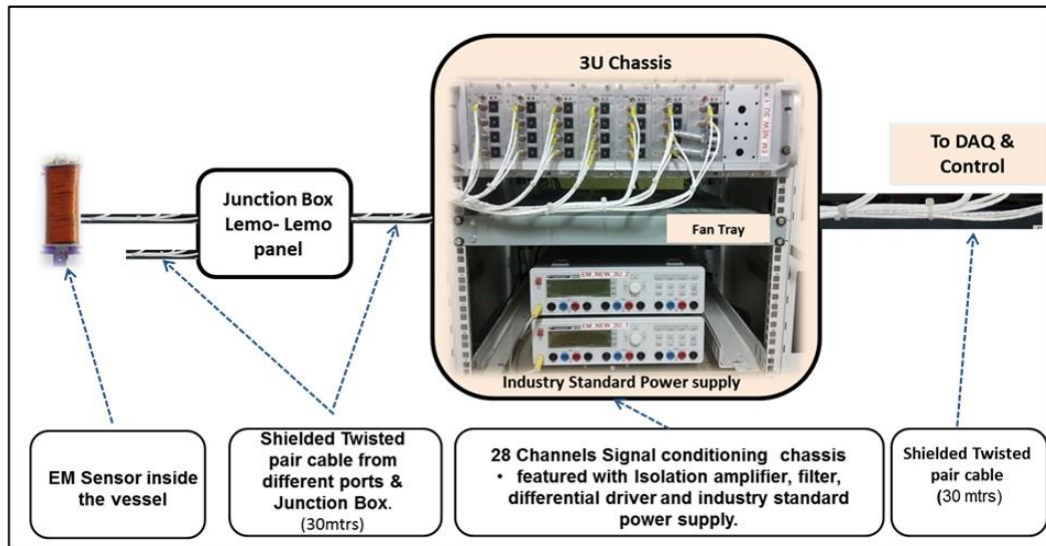


Figure 4.7 The basic blocks of magnetic diagnostics.

The relative positions of these newly installed magnetic probes inside the SST-1 vacuum vessel have been shown in Figure 4.8. For the radial shift measurements, probes at the horizontal $Z = 0$ plane near the inboard and outboard limiter (designated as P11, P12, PO1, and PO2) have been used.

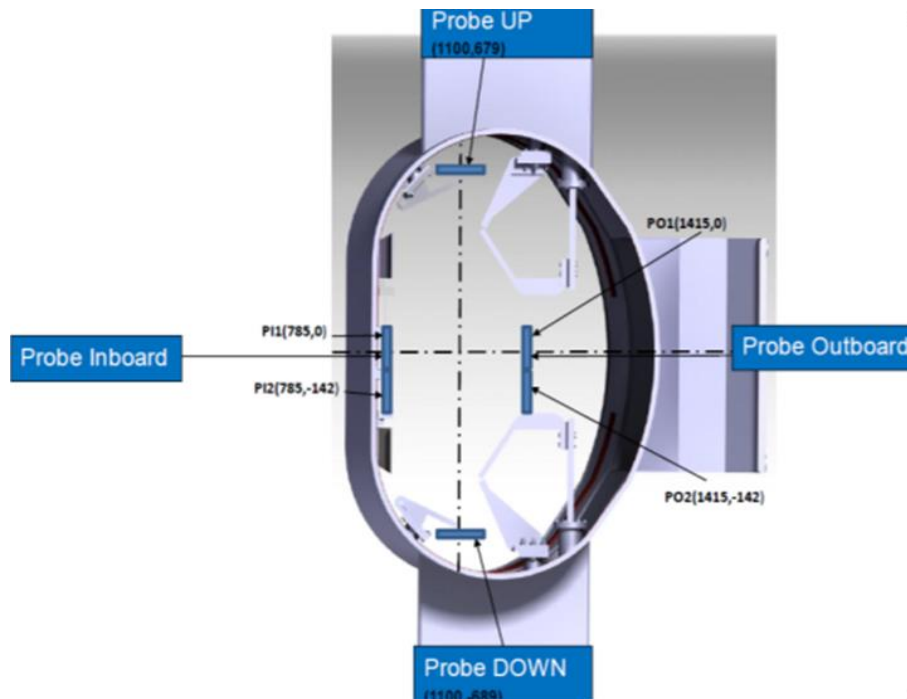


Figure 4.8 The schematic orientation of the installed magnetic probe diagnostics with (R, Z) location.

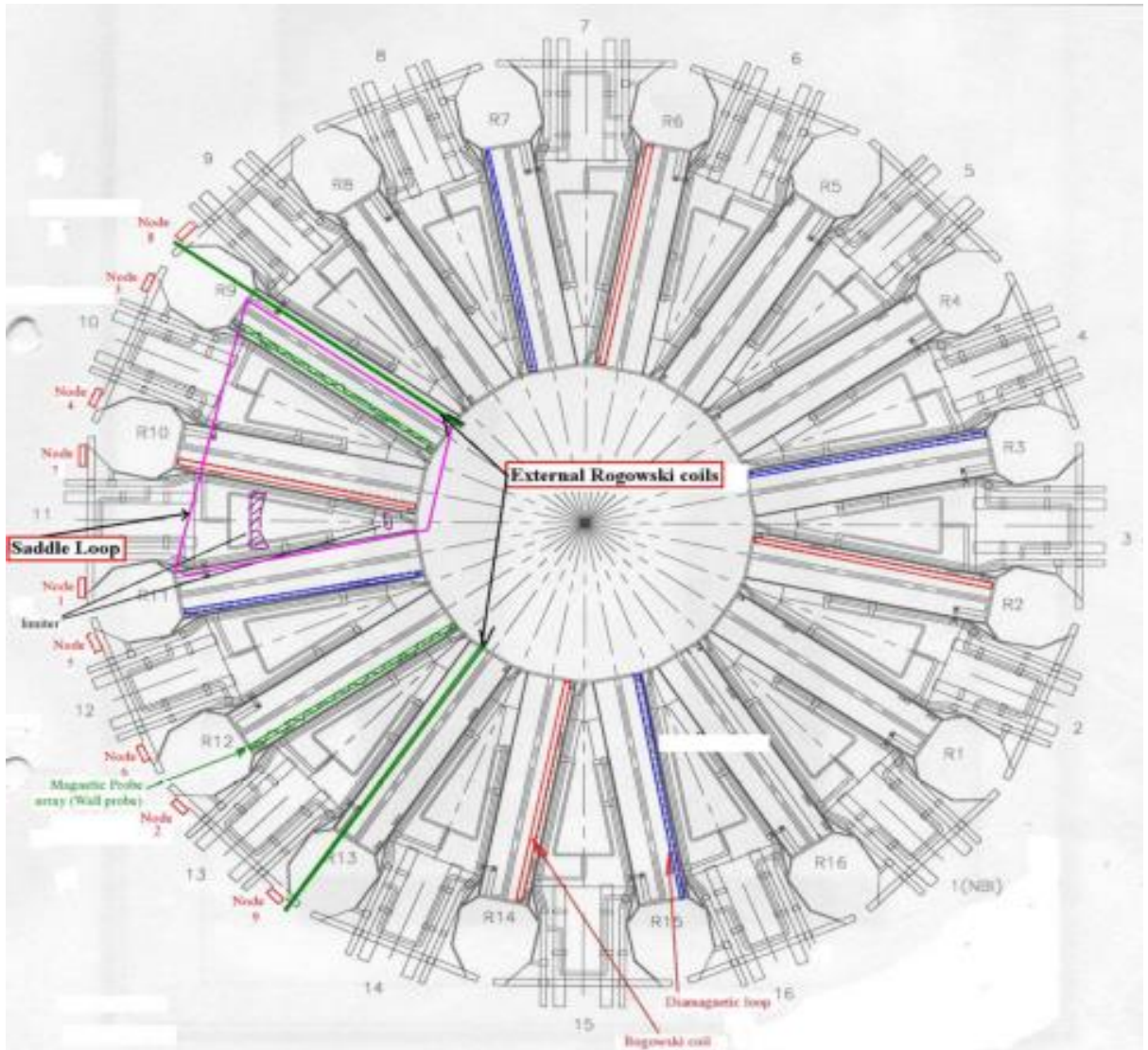


Figure 4.9 Layout of SST-1 existing magnetic diagnostics.

The overall layout of the magnetic diagnostics and their position port location in the SST-1 machine has been presented in Figure 4.9.

4.5 Results and Discussion

After successful installation of the magnetic probes, we have measured the contribution of the plasma using the installed magnetic probe diagnostics. In these measurements, a compensation technique has been used to compensate OT and VF current field contributions during plasma field computation. The comparisons between the expected theoretical signals and experimentally obtained signals have also been performed. The theoretical values have been computed from the off-axis formulation of the circular coil

in the elliptic integral form of the first and second kind. A maximum deviation is less than 5% has been observed between the expected probe signals and experimentally obtained probes signals. The Figure 4.10 has shown the flux and field profile for a representative plasma shot. These are reproducible over a large number of vacuum shots as well as with plasma shots.

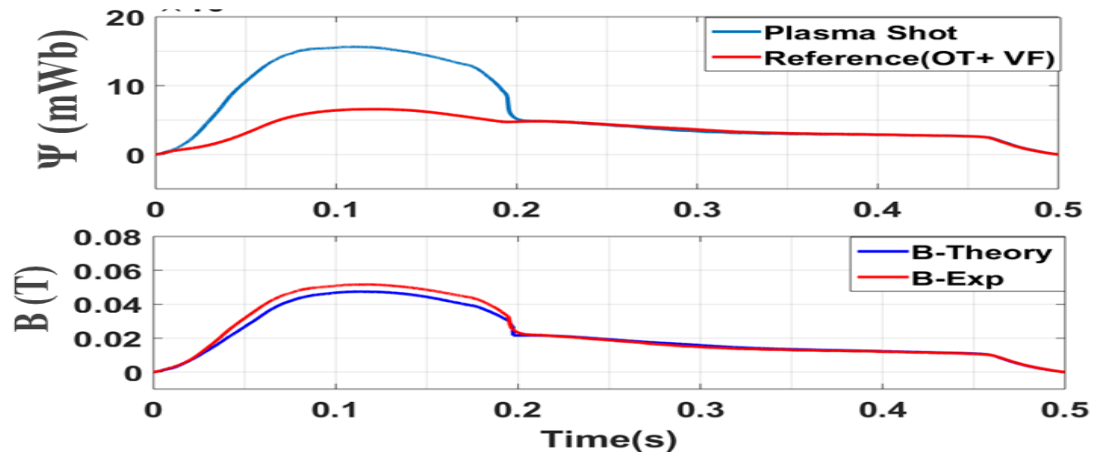


Figure 4.10 The comparison between expected theoretical signals and experimentally obtained signals.

4.6 Observations & Conclusions

In this chapter, the important SST-1 magnetic diagnostics such as Rogowski coil, diamagnetic coil, flux loop and magnetic probes diagnostics have been presented. Their position, orientation, challenge during precise application and accurate compensation technique have been explained. The basic principle of magnetic diagnostics have been described and the issues related to their practical implementation have been investigated. The importance of magnetic diagnostics during the operation of a magnetic fusion device has also discussed. The interpretations of magnetic measurements for equilibrium reconstruction have been outlined. However, the challenges presented by future steady-state burning plasma experiments may require the development of sophisticated techniques, particularly for the long-pulse magnetic measurements.

CHAPTER — V

Plasma Radial Shift in Steady State Superconducting Tokamak (SST-1)

- **Motivation and literature survey**
- **Principle: Radial shifts calculation**
- **Results and Discussion**
- **Comparison with imaging diagnostics**
- **Observations & Conclusions**

5.1 Motivation and literature survey

In a tokamak, plasma is formed into a vacuum chamber by maintaining the successful plasma start-up criteria as described in the earlier [chapter](#). In order to maintain the force balance condition, several magnetic fields have been applied which results in longer confinement of the plasma. The toroidal magnetic field in a tokamak, generated by the set of toroidal field (TF) coils which provide the basic confinement to the plasma column. However, such a plasma column is not in a forced balance equilibrium state. The gradient in the toroidal field (in the radial direction) results in the separation of charge species within the plasma column. This further gives rise to an electric field which traversed with the toroidal field and pushes the plasma column outward. Thus, toroidal magnetic field alone is not sufficient to keep the plasma column intact. In such circumstances, there can be a very rapid disruption of the whole plasma. For this reason, an additional magnetic field component in the vertical direction annulling the so-called charge separation must be added to confine the plasma. In the tokamak configuration, this difficulty is usually overcome by providing an external vertical component across the toroidal plasma column and more effectively by passing a toroidal current through the plasma itself. In such cases, the plasma acts as the secondary winding of a transformer whereas the central solenoid is the primary. The toroidally flowing plasma current, I_p generates a poloidal magnetic field. Thus, the combination of the toroidal field and plasma current flow induced poloidal magnetic field becomes helical. Normally in ohmically heated tokamaks, radial kinetic pressure (nKT) is balanced by the poloidal field, whereas the toroidal force balance is achieved by the interaction of the external vertical field with the toroidal current. The poloidal field is also externally generated using several poloidal field (PF) coils, which is additionally used to balance the plasma pressure component with magnetic field pressure. In this situation, inward

Lorentz force equals the outward forces. The outward forces are hoop force, the force due to pressure change and $1/R$ force typical to the toroidal configuration of the tokamak. However, in a force balance problem, the two opposing forces may be not equal. As a result, the plasma column shifts inward or outward depending on the relative magnitudes. Such a shift in the plasma column is detrimental towards maintaining the tokamak plasma equilibrium. In reality, the plasma undergoes a radial shift (ΔR) and vertical shift (ΔZ), even if this imbalance continues for a very short period (μs) of time span. These have been long considered as one of the fundamental problems of tokamak plasma control and equilibrium studies and are a prerequisite to being resolved effectively towards long-duration confinement of plasma in a tokamak configuration.

As evident from above, the measurement of accurate plasma position is extremely important, since it can be effectively used towards maintaining the plasma equilibrium conditions employing appropriate feedback control operations. There exist several prescriptions towards precise computation of plasma position for the tokamak configuration. Amongst them, magnetic measurements using magnetic probes are simpler and most effectively used. Such diagnostics are routinely used in most of the experiment. There are some alternative methods depending on magnetic momentum, fast imaging, and Fourier analysis transformations also available [5.1-5.2]. Studies aimed at developing newer diagnostics development are continuously going on.

The equilibrium conditions for axisymmetric toroidal plasmas had been obtained for the first time by H. Grad et al. and V. D. Shafranov et al. [5.3-5.5] in terms of aspect ratio a/R . 'a' and 'R' denotes the minor radius and major radius of the toroidal plasma column respectively. A probe method for measuring the displacement of the current channel in cylindrical and toroidal discharge vessel has also been explained by S.V Mirnov [5.6] et al. H. Ninomiya [5.7] et al. have estimated the plasma position using

magnetic measurement for high beta plasma condition. A. Salar Elahi et al. [5.8] has also explained the method to determine plasma position in IR-T1 tokamak using flux loops and magnetic probe diagnostics. A. Rahimi-Rad [5.9] has explained a special solution of Grad-Shafranov equation (GSE), $\beta + li/2$ and plasma position in a circular cross-sectional tokamak. Gergo Pokol [5.10] et al. have also explained a simple measurement technique to measure plasma position in GOLEM tokamak. The plasma current, position and shape control in tokamak have been explained by G. De. Tommasi [5.11] et al. using a plasma model for JET tokamak.

In this chapter, we have used both magnetic flux loop and magnetic probes for the determination of the plasma position of the SST-1 plasma column. The positions of the probes and flux loops in SST-1 machine used for this purpose have been shown in Figure 5.1 (a) and (b) in a poloidal cross section view. According to Faraday's law, outputs of all magnetic diagnostics are proportional to the derivatives of the magnetic flux that passes through them. Therefore, the output of flux loops and magnetic probes need to be integrated. Our primary aim of these measurements was to control the plasma position on the basis of several experimentally measured magnetic and electric signals and intrinsic physical parameters of the plasma column. These instantaneous parameters measured must necessarily be accurate with the due compensating techniques.

Plasma formation in SST-1 tokamak depends on the synchronization of many different systems and subsystems. Accurate control of the electromagnetic field created by central solenoid (CS) discharge, state of the toroidal field coil (TF), profiles of the vertical field currents (VF) and another poloidal field (PF) currents are critical to plasma formation and subsequent plasma current ramp-up. The particle density within the plasma chamber is maintained using gas puffing. These are the minimal requirements

towards plasma initiation and successful breakdown. Further, the ‘vacuum quality’ in the vacuum vessel must be very good and the impurity level residing in the vacuum chamber needs to be minimal for the burn-through. The auxiliary heating system such as ECRH and LHCD are used for pre-ionization, current ramp up and plasma heating for long pulse plasma tokamak machine. A typical parameter of SST-1 discharge is shown in Figure 5.1.

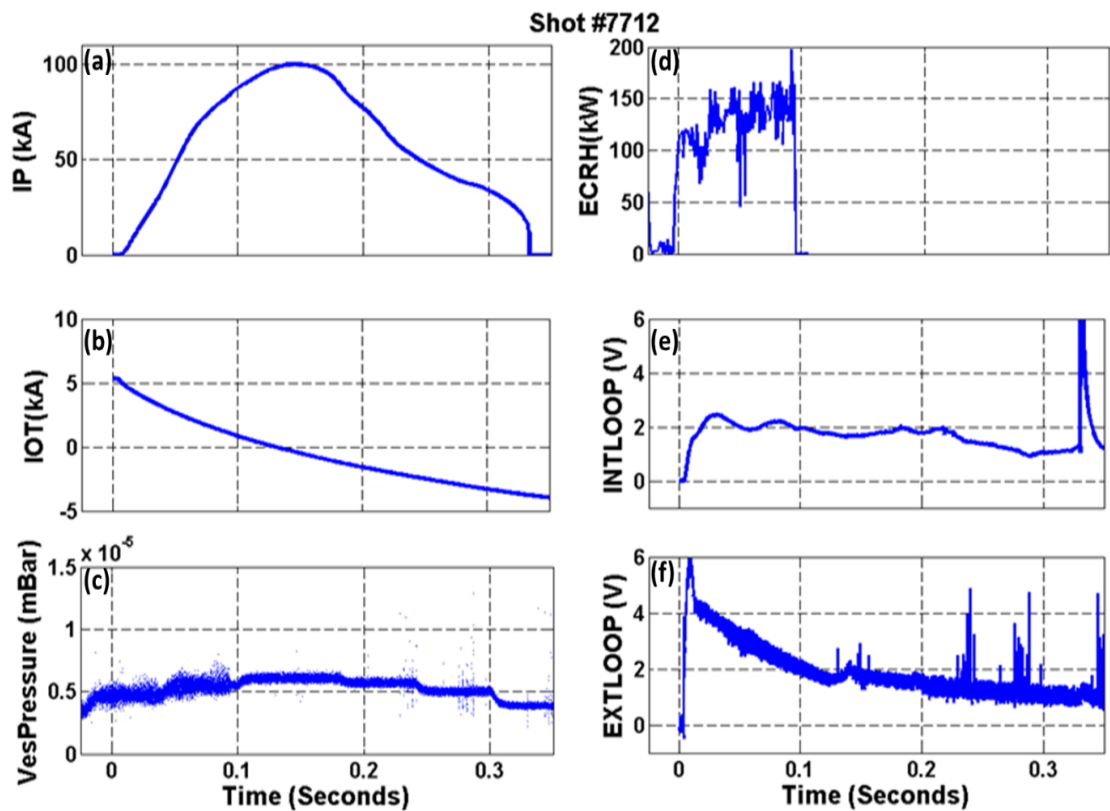


Figure 5.1 (a) Plasma current (I_P), (b) Central Solenoid current (I_{OT}), (c) Vessel Pressure, (d) ECRH Power, (e) Internal Loop Voltage, (f) Internal Loop Voltage for SST-1 Shot No: 7712.

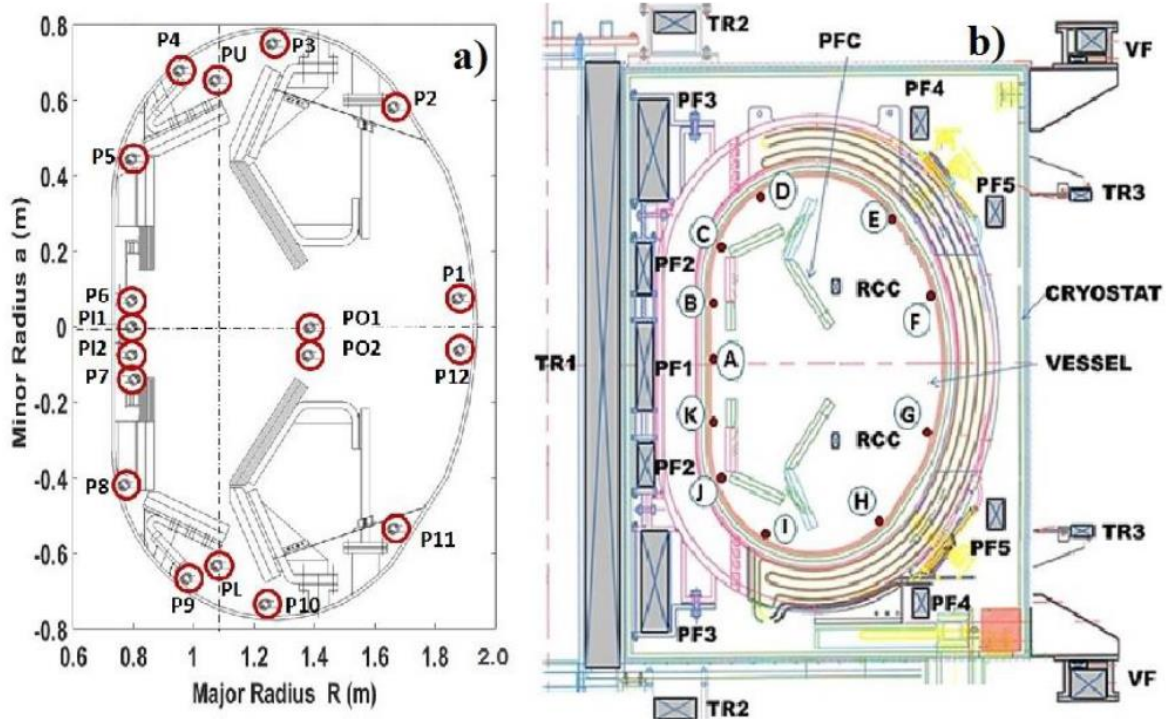


Figure 5.2 (a) The Schematic orientation of Magnetic Probe (Red Dot and Circle) is used for measurement. (b) The Actual orientation of flux loops (Red Dot).

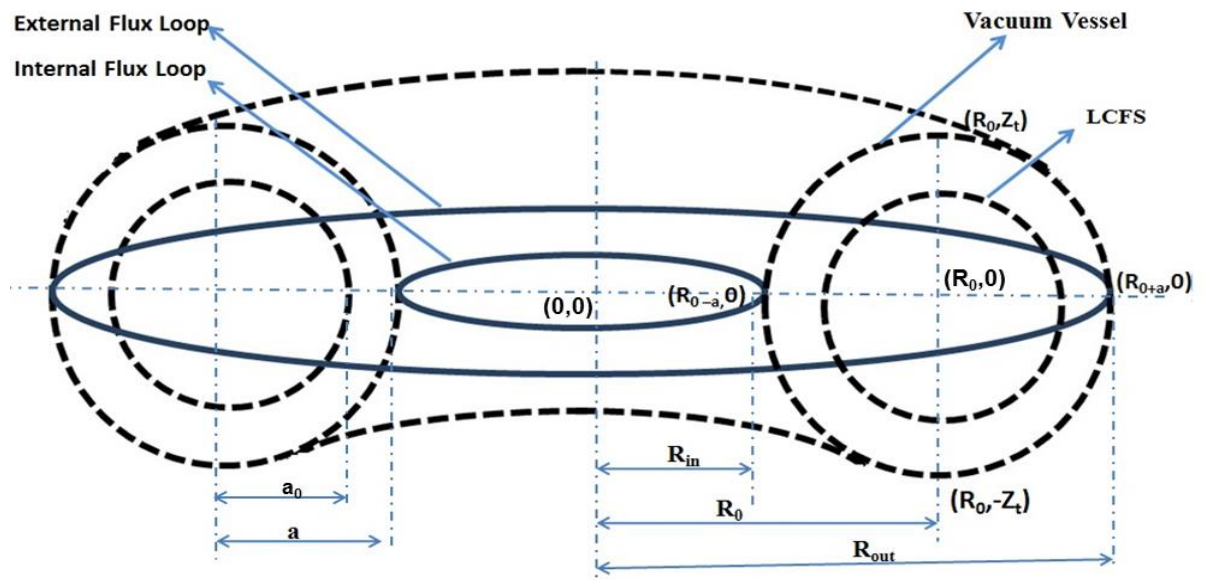


Figure 5.3 Schematic diagram of Flux loop orientation.

5.2 Principle

5.2.1 Radial shifts Calculation

The radial shift of the toroidal plasma column confined in a tokamak configuration is often referred as the ‘Shafranov Shift’ or the ‘Radial Shafranov Shift’. The radial Shafranov shift can be written as shown in the equation (5.1). It can be computed [5.7] from magnetic probe signals and from the poloidal and normal components of magnetic fields for circular cross-sectional plasma such as in SST-1.

$$\Delta R_p = \frac{a_0^2}{4R_0} \left\{ \left(\frac{a^2}{a_0^2} - 1 \right) - 2 \ln \frac{a_0}{a} \right\} + \frac{\pi a^2}{2\mu_0 I_P} \left\{ \Delta B_\theta \left(1 - \frac{a_0^2}{a^2} \right) + \Delta B_r \left(1 + \frac{a_0^2}{a^2} \right) \right\} \quad (5.1)$$

where, a_0 , a , R_0 , ΔR_p are the plasma minor radius (0.2m), chamber minor radius (0.35m), major radius (1.1 m) and the radial shift using magnetic probes. Here, $\Delta B_\theta = B_\theta(\theta = 0) - B_\theta(\theta = \pi)$ and $\Delta B_r = B_r\left(\theta = \frac{\pi}{2}\right) - B_r\left(\theta = \frac{3\pi}{2}\right)$.

For these estimations, we have installed four magnetic probes as shown in Figure 5.2(a).

The tangential component B_θ gets measured using the probe located at $\theta=0$ and $\theta=\pi$.

The normal component (B_r) gets measured using probes located at $\theta = \frac{\pi}{2}$ and $\theta = \frac{3\pi}{2}$.

Using the flux loops [5.8-5.9] method, we have calculated the plasma radial shift (ΔR_l)

as

$$\Delta R_l = \frac{a_0}{R_0 \mu_0 I_P \cos \theta} \Delta \psi \quad (5.2)$$

where,

$$\Delta \psi = \psi_{P_{out}} - \psi_{P_{in}} \text{ and } \psi_{P_{out}} = \psi_{out} + B_o \Delta S_o \text{ and } \psi_{P_{in}} = \psi_{in} + B_i \Delta S_i .$$

ψ_{out} and ψ_{in} represent the flux measured using the outer and inner flux loop respectively. The B_o and B_i are the average magnetic field between outer and inner

flux loops and plasma surface (LCFS) respectively obtained from magnetic probes, ΔS_i is the intervening area for internal loop and ΔS_o is the intervening area for external loop as shown in [Figure 5.3](#).

5.3 Results and Analysis

The plasma position in SST-1 has been calculated using the methodology described above has been analyzed in this section. In [Figure 5.4](#), two sets of flux loops (upper and lower) have been used towards radial shift measurement in the SST-1 machine for a typical reproducible shot# 7712. Flux loop ‘A’ at (R=0.75, Z=0) for ψ_{in} and for ψ_{out} at (R=1.45, Z=0) have been used (computed using the methodology mentioned in [Appendix II](#)) for the radial Shafranov shift in the SST-1 tokamak. These flux loops are shown in [Figure 5.2\(b\)](#).

The Plasma shot 7712 (in [Figure 5.4](#)) shows the plasma current and applied vertical field current (I_{VF}) being plotted as a function of time at top and bottom plots respectively. The Radial shift (ΔR) measured using flux loops and magnetic probes has been shown as a function of time in the middle plot. [Ref]. For this shot, a pre-profiled vertical field has been applied (without any feedback control). It is observed that initially plasma gets formed on the inboard side. It maintains a stable position thereafter satisfying the force balance condition. Subsequently, the plasma column moves outward due to mismatch of the vertical field leading to deterioration of the balance conditions of the plasma (as provided by vacuum fields against the plasma hoop forces). Finally, the plasma column crashes on the outboard side of the limiter. The characteristic vacuum vessel penetration time of the vertical field is ~12 to 13 ms. The position of the evolving plasma column is measured using the probe and flux loop method have been compared and are found to be in good agreement.

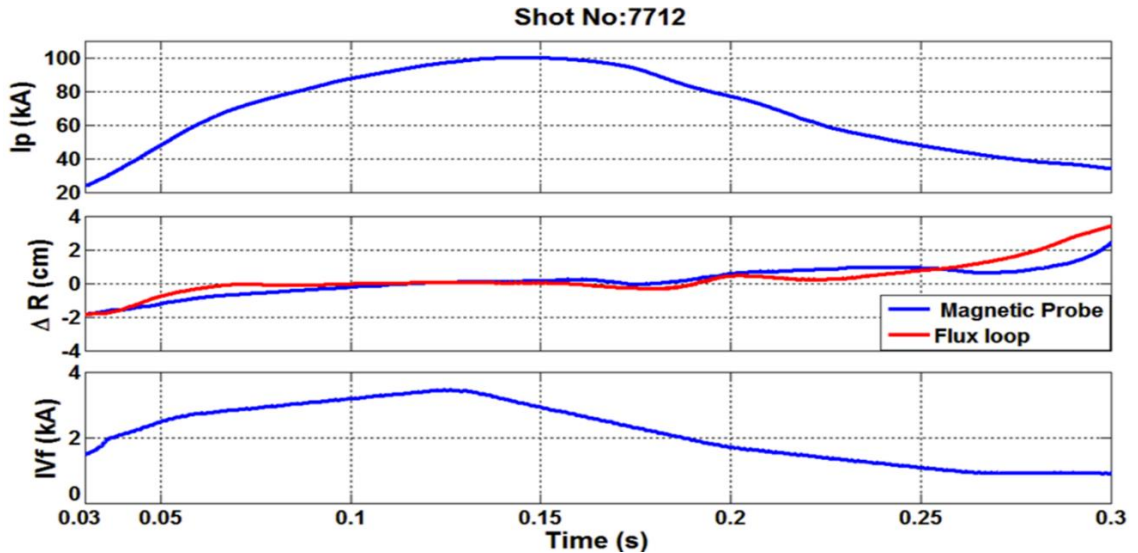


Figure 5.4 Plasma current [top], comparison of radial shift [middle] and applied vertical field current (I_{VF}) [lower] for SST-1 Shot no 7712.

5.5 Comparison with imaging diagnostics

In SST-1, visible imaging diagnostics are used for monitoring and visualizing of the plasma column in definite time intervals. The same diagnostics are also extended to analyzing the plasma edge boundary. The SST-1 plasma column emits visible radiations, primarily from a relatively thin emissive layer located in the edge region where the temperature is low. The interaction of neutral particles with plasma takes place in the central plasma column. It is relatively hotter and is invisible to optical detectors as it emits radiation of high energy. Visible light emitted by the edge plasma is detected by the camera. Each pixel of the two-dimensional camera images contains an integrated signal from the corresponding line of sight. The plasma emissive layer is assumed to be toroidally symmetric in this study. Generally, this assumption is valid if the exposure time of the camera is long enough such that fast edge plasma fluctuations smoothen out.

In SST-1, such a camera is located at the mid-plane viewing on the poloidal cross section inside the vessel. The pre-trigger pulse enables the camera at about 180ms

before the plasma experiment. The duration between each frame is 30ms. The optical plasma boundary shifts from such an imaging camera have been measured.

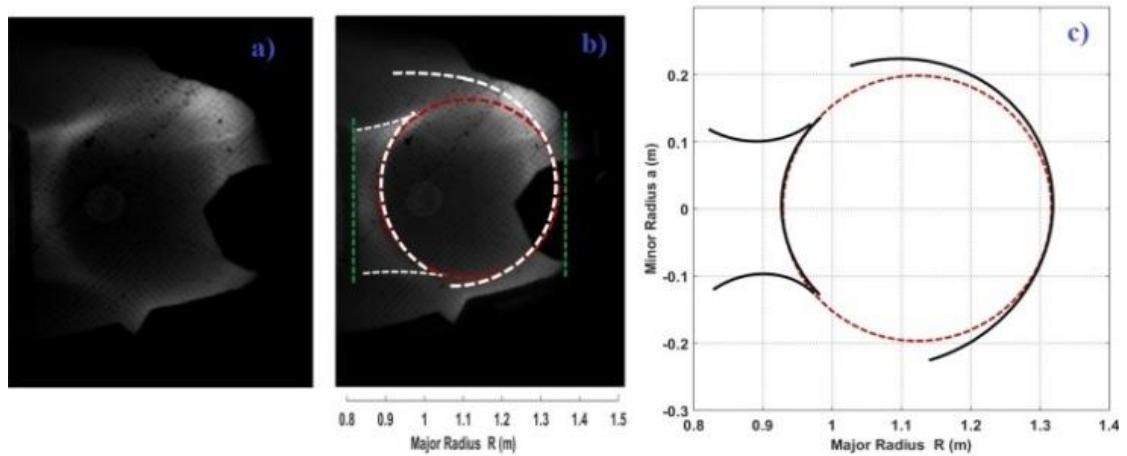


Figure 5.5 The boundary approximation of camera image.

In Figure 5.5 (a) camera image, (b) optical boundary (white dash) with limiter (green), (c) computed plasma location (red circle) are shown. The compensation of the angular misalignment has been rectified using the standard method. As explained earlier, each pixel on the camera image corresponds to a line integrated measurement of the light coming from the plasma emissive surface. The pixel that corresponds to a line of sight tangent to the emissive surface yields maximum intensity since the line of sight crosses the longest path through the surface. From the pixel information for a particular frame, the shift is calculated using the midline movement from the reference plasma center for that frame, and it is shown in Figure 5.6.

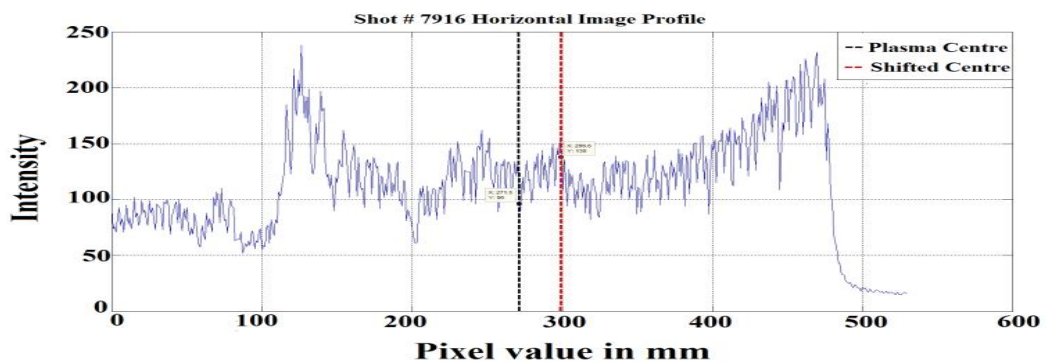


Figure 5.6 Horizontal image Profile (2.81 cm shift observed in this frame for shot # 7916) (Image Credit: Monaj Kumar)

The exact relation between the magnetic boundary, which is the Last Closed Flux Surface (LCFS), and the optical plasma boundary is unclear and is difficult to compare quantitatively with accuracy. The optical boundary reconstruction and its use in plasma position feedback control have been described by Hommen et al. [5.12-5.13]. Hacek et al. [5.14], has carried out a comparison between the optical plasma boundary reconstruction using camera images with a magnetic reconstruction technique. Adopting these techniques, a comparison between the shift computed from the magnetic diagnostics and the shift computed from a synchronized real-time imaging signal has been carried out in the same time domain. This is shown in Figure 5.7 where the comparison has been done for the shift of the plasma column after it is completely formed with maximum current in it. It has been observed that from a time of 120ms until 250ms, the trend and shifts calculated from both the techniques are in good agreement.

The plasma is initially generated at the outboard and is then shifted inward due to the increment of the vertical field (I_{VF}). Subsequently, it goes outward due to the decrement in the vertical field (I_{VF}). Finally, it crashes on the inboard side limiter at 250 ms. The maximum shift observed from the flux loops is 3.4 cm, flux surface contour is 3.5cm and imaging is 2.81cm for this particular shot.

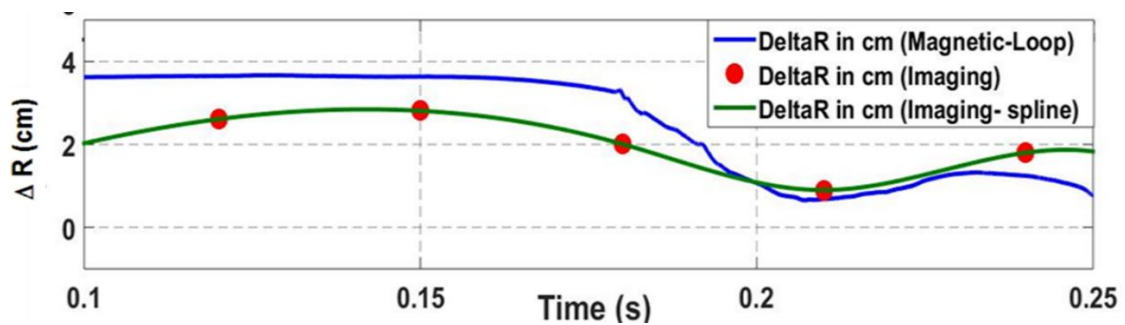


Figure 5.7 Comparison between the shifts of imaging with Magnetic.

5.6 Observations & Conclusions

In this chapter, the plasma position of the SST-1 tokamak has been measured from the magnetic probes and flux loops signal using a standard methodology. The shift computed from this methodology using the flux loops and magnetic probes are in good agreement, repeatable and reliable. The magnetic probes and flux loop are calibrated using a simple and reliable calibration technique. The main advantages of this technique is only dependent on the magnetic probes' measurement during the vacuum shot. The shift calculation employs the magnetic probes' signals obtained from the probes at four locations placed 90 degrees apart in the poloidal plane. The shift calculations based on the flux loops take into account the difference of the poloidal flux on high field side and low field side of the tokamak chamber. In the case of plasma position measurement using imaging signals, the midline movement from the reference plasma center has been calculated for each particular frame of imaging. Comparison and repeatability tests with imaging signals have been carried out. It has been observed that plasma movement trend from imaging is identical with the shift calculated from magnetic diagnostics.

These results are however susceptible to errors arising from approximations in measurements of the magnetic field distribution around the plasma as the number of probes is finite. There could also be some minimal errors from the lack of absolute compensation of the experimental signals.

CHAPTER-VI

Computation of magnetic flux surfaces using the magnetic diagnostics

- Motivation and literature survey
- Principle of Plasma Equilibrium
- Plasma flux surface
- Computational Procedure
- Flux surface computation for SST-1 Tokamak
- Results and Discussion
- Observations & Conclusions

6.1 Motivation and Literature Survey

Sustaining plasma equilibrium in a tokamak configuration is one of the most fundamental and essential elements of steady-state operation in tokamak. Thus, plasma equilibrium aspects need to be studied and understood comprehensively. In tokamak physics, plasma equilibrium is a fundamental and essential element to understand not only basic equilibrium properties but also various plasma phenomena such as MHD instabilities, transport, turbulence, flows, waves etc. Fundamental to all these is to calculate the magnetic field exactly at the equilibrium configuration and, to estimate control parameters to maintain the stability and equilibrium which would help the desired operation of the device. Recognizing the immense importance of these aspects, various analytical, numerical and experimental equilibrium studies have been conducted and tools have been developed.

The equilibrium conditions for axisymmetric toroidal plasmas had been obtained for the first time by H. Grad et al. and V. D. Shafranov et al. [6.1-6.4] in terms of the aspect ratio a/R . 'a' and 'R' denotes the minor radius and major radius of the toroidal plasma column respectively. In the Grad-Shafranov equations (GSE), the current and longitudinal magnetic fields over the plasma cross section are not explicitly included. Further, the formulations of plasma displacement in GSE formalisms are obtained by considering plasma as a conducting shell.

A general analytical solution of the Grad Shafranov equation (GSE) has been presented by Zheng et al. [6.5]. This work shows that if we possess a parametric description of a plasma, then an equilibrium can be computed with enough freedom to independently control pressure and plasma current. This is possible for arbitrary choices of plasma size, aspect ratio, elongation, and triangularity. This paper also explains scaling relations which

can be used to produce a new solution with identical shape and poloidal beta, but with a rescaled value of the plasma current. Their solution has limitations, however, in the form of fixed boundary conditions and poloidal beta.

In the works of Atanasiu et al. [6.6], two families of exact analytical solutions of the Grad-Shafranov equation have been presented by specifying the highest polynomial dependence of the plasma current density on the flux function. This solution uses pressure profile and poloidal current density parameterizations with four degrees of freedom. Thus, an independent choice of the plasma current, the poloidal beta, the internal inductance and the safety factor can be made. These solutions are applicable for both a D-shaped plasma and toroidally diverted plasma.

The study of poloidal beta and internal inductance by solving the GSE has been carried out for a circular cross-section tokamak by M. Asif et al. [6.7]. They have shown that the calculated poloidal beta and plasma internal inductance depend on the plasma current. Remi G. Lefrancois et al. [6.8] have presented a numerical solution for a three-dimensional nonlinear equilibrium equation for a single species plasma, confined on an equipotential boundary. An algorithm nearly identical to standard equilibrium techniques presented by J. R. Ferron et al. [6.9] could be used to identify tokamak equilibrium parameters for discharge control in real time scenarios. There are various other procedures to solve the Grad-Shafranov equation [6.10-6.11] and experimental methods to calculate plasma shift [6.12-6.14].

Here, we have chosen the Solov'ev [6.15] equilibrium solution with linear profiles of flux function and pressure, by considering a circular plasma cross-section. Since the Solov'ev solution does not require an explicit profile of the poloidal beta and plasma internal inductance, we have adopted the above family of solutions [6.16].

Nevertheless, the Solov'ev equilibrium solution has been used extensively to benchmark numerical equilibrium codes. It contains four unknowns; therefore, we need at least four boundary conditions. These boundary conditions have been provided by the data obtained from the in-vessel probes and the flux loops at four locations inside the SST-1 vacuum vessel. In this chapter, we have presented and discussed an experimental method to compute magnetic flux surface contours of the SST-1 tokamak from the data of the magnetic loops, the probes and an analytical solution of the Grad-Shafranov equation. Theoretical and experimental flux surfaces are thus computed for the present operating conditions. A quantitative comparison has been done between the two. It has been observed that the computed flux surfaces using experimental values agree well with those predicted by the theory.

6.2 Principle of Plasma Equilibrium

Magnetohydrodynamics describes the basic behavior of a magnetically confined plasma. The balance between plasma pressure and magnetic confinement forces can be studied with the aid of ideal magnetohydrodynamics (MHD) equations. There are two aspects of tokamak equilibrium. The first is the internal balance of the plasma pressure and the magnetic field forces on one hand and the second is the shape and position of plasma which is determined by magnetic diagnostics and controlled by currents flowing through the external coils (PFs ,VFs) on the other.

6.2.1 Plasma flux surface

In basic tokamak operational scenarios, an outward force across the minor radius is exerted by the plasma pressure and an inward force from the poloidal and vertical magnetic fields. The magnetic pressure of the toroidal magnetic field reflects the imbalance of these two forces. In a tokamak, the resulting magnetic field lines usually

follow a helical path due to the combination of poloidal and toroidal magnetic fields. These generate a set of infinitely nested magnetic field lines to squall the torus and, the magnetic field lines change their direction from surface to surface. For the stability of plasma, the shearing of the magnetic field has a very important implication. On each surface, the average twist of the magnetic field line is characterized by the safety factor (q) that gives the measurement of the pitch of a helical field line. The radial rate of change of the safety factor (q) contributes to the shear.

The basic condition for equilibrium in a tokamak is that the net force on the plasma should be zero at all points. And for this to happen, it is necessary that the magnetic forces should get balanced by the pressure. All these are simply expressed by $\mathbf{J} \times \mathbf{B} = \nabla p$. From this expression, $\mathbf{B} \cdot \nabla p = 0$ and $\mathbf{J} \cdot \nabla p = 0$ can be obtained. Thus, from the equation ($\mathbf{B} \cdot \nabla p = 0$), it is clear that along the magnetic field lines there is no pressure gradient and the magnetic surfaces are at constant pressure. Secondly, equation ($\mathbf{J} \cdot \nabla p = 0$) explains that the current also lies on the magnetic surfaces. Hence, the above explanation shows that the field lines of magnetic induction and the current density lie on isobaric surfaces or surfaces of constant pressure which are called magnetic flux surfaces. For most of the plasma equilibrium, the maximum pressure is observed near the center of the poloidal cross-section of plasma and the isobaric surfaces are toroidally nested as shown in [Figure 6.1](#). The limiting magnetic surface that approaches a single magnetic line or point, where pressure is maximum is called the magnetic axis.

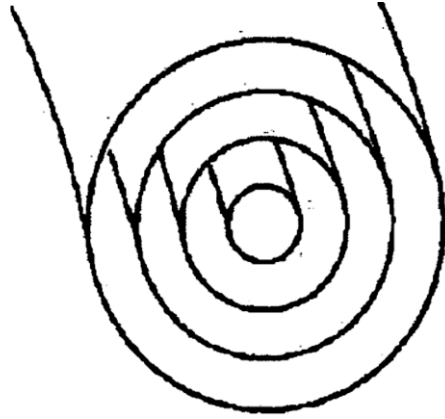


Figure 6.1 Magnetic flux surfaces forming a set of nested toroids.

For tokamak equilibrium, it is worth introducing the toroidal magnetic flux function. The poloidal magnetic flux function can be determined from the poloidal flux present in each magnetic surface. Therefore, these flux functions are constant on a surface that satisfies $\mathbf{B} \cdot \nabla \psi = 0$.

6.2.2 Flux surface Calculation

The solutions of the Grad-Shafranov equation (GSE) [6.1-6.15] are generally used for studies of plasma equilibrium, transport, and MHD stability. It is a nonlinear, elliptic partial differential equation, containing pressure and current gradients. One of the simplest analytical solutions to the inhomogeneous GSE is the well-known Solov'ev equation, which is also used to demonstrate the Shafranov shift. In an axisymmetric system, the magnetic field can be written in cylindrical coordinates (R, ϕ, z) as,

$$\mathbf{B} = F \nabla \phi + \nabla \psi \times \nabla \phi \quad (6.1)$$

F and ψ are axisymmetric scalar functions. F is the function associated with the poloidal current within the system. ψ is the poloidal flux divided by 2π . Here, ϕ is the ignorable angle in the cylindrical coordinate system (R, ϕ, z) . The Grad-Shafranov equation (GSE) [6.3-6.6] is as follows:

$$R \frac{\partial}{\partial R} \left(\frac{1}{R} \frac{\partial \psi}{\partial R} \right) + \frac{\partial^2 \psi}{\partial z^2} = -\mu_0 R J_{\phi} = -\mu_0 R^2 \frac{\partial P}{\partial \psi} - F \frac{\partial F}{\partial \psi} \quad (6.2)$$

Where, J_Φ is the toroidal plasma current density, P is thermal pressure and F is the flux function. Then, a simple solution of equation (6.2) is,

$$\mu_0 \frac{\partial P}{\partial \psi} = -A_1, F \frac{\partial F}{\partial \psi} = 0 \quad (6.3)$$

Where A_1 is a constant. If $\frac{\partial F}{\partial \psi}$ is set to zero, this has the inconvenient consequence of over-constraining the plasma current or the poloidal beta. The Grad-Shafranov equation can then be written as:

$$R \frac{\partial}{\partial R} \left(\frac{1}{R} \frac{\partial \psi}{\partial R} \right) + \frac{\partial^2 \psi}{\partial Z^2} = R^2 A_1 \quad (6.4)$$

Using the solution of the homogeneous equation (6.1),

We have,

$$\psi = \psi_0 + \frac{A_1}{8} R^4 \quad (6.5)$$

Here, ψ_0 is a solution of the homogeneous equation.

$$R \frac{\partial}{\partial R} \left(\frac{1}{R} \frac{\partial \psi_0}{\partial R} \right) + \frac{\partial^2 \psi_0}{\partial Z^2} = 0 \quad (6.6)$$

Assuming the plasma to be circular and up-down symmetric, its shape can be described by four parameters (c_1, c_2, c_3, c_4). The innermost and outermost equatorial points are R_{in} and R_{out} . The coordinates of the highest point are (R_t, Z_t) . The major radius of the vacuum chamber is $R_0 = (R_{in} + R_{out})/2$ and the minor radius of the vacuum chamber is $a = (R_{out} - R_{in})/2$, where the elongation is, $k = Z_t/a$ and triangularity is, $\delta = (R_0 - R_t)/2$. The corresponding schematic diagrams are shown in [Figure 6.2](#). Thus, the simplest solution by Solov'ev is given by,

$$\psi = c_1 + c_2 R^2 + c_3 (R^4 - 4R^2 Z^2) + c_4 (R^2 \ln(R) - Z^2) + \frac{A_1}{8} R^4 \quad (6.7)$$

In order to determine these five coefficients, it is necessary to have five equations. The boundary conditions are the magnetic flux measured at three poloidal positions of $0^\circ, 90^\circ$ and 180° and the magnetic field B_z found by a magnetic probe at an angle of 90° within the machine cross-section.

We assume that there is no pressure at the boundary, hence $\psi(R, Z)|_b = 0$ at the boundary of equation (4). The boundary condition that $R=R_0+a, Z=0, R=R_t, Z=Z_t$ leads to the equations (6.8), (6.9), (6.10), (6.11) and (6.12). Employing the following boundary conditions, the coefficients (c_1, c_2, c_3, c_4 and, A_1) have been calculated.

$$\psi(R_{in}, 0) = c_1 + c_2 R_i^2 + c_3 R_i^4 + c_4 (R_i^2 \ln(R_i)) + \frac{A_1}{8} R_i^4 = \psi_{180}. \quad (6.8)$$

$$\psi(R_{out}, 0) = c_1 + c_2 R_o^2 + c_3 R_o^4 + c_4 (R_o^2 \ln(R_o)) + \frac{A_1}{8} R_o^4 = \psi_0 \quad (6.9)$$

$$\psi(R_t, Z_t) = c_1 + c_2 R_t^2 + c_3 (R_t^4 - 4R_t^2 Z_t^2) + c_4 (R_t^2 \ln(R_t) - Z_t^2) + \frac{A_1}{8} R_t^4 = \psi_{90} \quad (6.10)$$

We also assume that the plasma is enclosed in a perfectly conducting toroidal boundary with a circular cross-section. Then, the normal component of magnetic field is,

$$\left(\frac{1}{R} \frac{\partial \psi(R_t, Z_t)}{\partial R} \right) = 2c_2 + 4c_3 (R_t^2 - 2Z_t^2) + c_4 (2\ln(R_t) + 1) + \frac{A_1}{2} R_t^2 = B_z(R_t, Z_t) \quad (6.11)$$

The coefficient A_1 can be obtained from

$$I_P = \int J_\phi dRdZ = \frac{1}{\mu_0} \int (RA_1) dRdZ \quad (6.12)$$

The plasma flux surfaces are then computed using these five known coefficients (c_1, c_2, c_3, c_4 , and A_1).

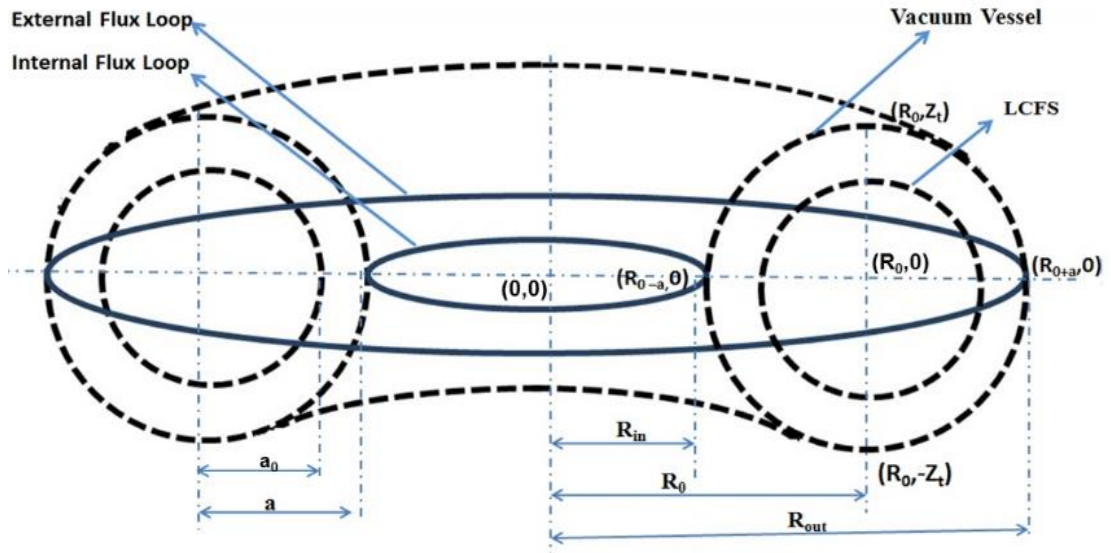


Figure 6.2 Schematic diagram of flux loop orientation.

Computational Procedure

Following the above prescription, the magnetic flux surfaces of the SST-1 plasma have been computed on a MATLAB platform. The procedure is listed below:

Step-1 Initialize the parameter R_{in} , R_{out} , R_t and Z_t etc.

Step-2 Next, the parameter A_1 is computed by solving the integration in the limits of R [R_{in} , R_{out}] & Z [$-Z_t$, Z_t] from equation (6.12).

Step-3 Next, we obtain four equations with four unknowns (c_1 , c_2 , c_3 , c_4) using the A_1 computed from step (2). In order to solve the final equations, the values of $\psi(R_{in},0)$, $\psi(R_{out},0)$, $\psi(R_t, Z_t)$ and $\{d\psi(R_t, Z_t)/dR\}$ obtained from the experimental magnetic probe and loop data are put. The parameter c_1 , c_2 , c_3 and c_4 are then calculated.

Step-4 Grid generation for R , Z (Limit of R goes from R_{in} to R_{out} and limit of Z goes from $-Z_t$ to Z_t).

Step-5 The flux (ψ) at each grid point is then calculated from LTI equation solver.

$$\psi = c_1 + c_2 R^2 + c_3 (R^4 - 4R^2 Z^2) + c_4 (R^2 \ln(R) - Z^2) + \frac{A_1}{8} R^4$$

Step-6 The center of the contours is computed and plotted with boundary conditions.

Figure 6.3 explains a simple position feedback loop for our device

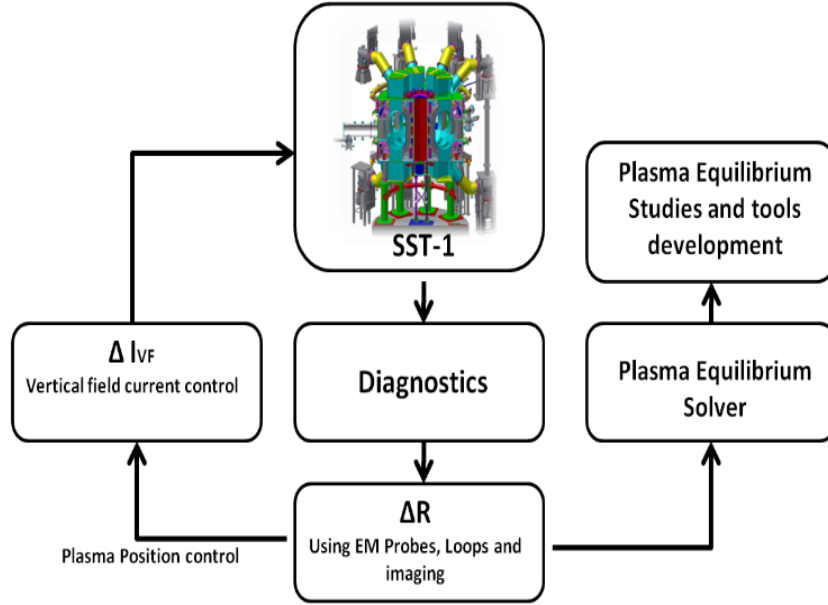


Figure 6.3 Plasma position control feedback loop.

6.3 Application for SST-1 Tokamak

The primary parameters of SST-1 have been used here as described in the earlier chapter. Now, the input parameters are $R_{in}=R_0-a=0.75\text{m}$, $R_{out}=R_0+a=1.45\text{ m}$, $R_t=1.1\text{m}$, $Z_t=0.35\text{m}$. From these five equations, we calculate

$$\psi(R_0 - a, 0) = c_1 + 0.5625 c_2 + 0.3164c_3 - 0.1618c_4 \quad (6.13)$$

$$\psi(R_0 + a, 0) = c_1 + 2.1025 c_2 + 4.4205c_3 + 0.7812c_4 \quad (6.14)$$

$$\psi(R_0, a) = c_1 + 1.21c_2 + 0.8712c_3 - 0.0072c_4 \quad (6.15)$$

$$\left(\frac{1}{R} \frac{\partial \psi(1.1, 0.35)}{\partial R} \right) = 2.0c_2 + 3.8606c_3 + 1.1906c_4 + 0.605A_1 \quad (6.16)$$

From the integral of the equation (6.12), we calculate A_1 in the form of I_P .

$$\mu_0 I_P = A_1 \int_{R_0-a}^{R_0+a} \int_{-\sqrt{a^2-(R-R_0)^2}}^{\sqrt{a^2-(R-R_0)^2}} R dR dZ \Rightarrow \mu_0 I_P = A_1 (\pi a^2 R_0 - 4 \frac{a^3}{3}) \quad (6.17)$$

For a typical SST-1 shot no- 7916, the coefficients are

$$A_1=0.8866, c_1= -0.03, c_2= -0.1432, c_3= -0.0525, c_4= -0.0158$$

The flux contours reconstructed at the time instant of 120ms have been shown in the results. The magnetic axis (R_{axis}) center has been found by equating the following derivative term to zero,

$$\begin{aligned} \left. \frac{d\psi(R, 0)}{dR} \right|_{R_{axis}} &= c_2 2R + 4c_3 2R^3 + 4c_4 R(2 \log(R) + 1) + \left(\frac{A_1}{2}\right)R^3 \\ &= 0 \end{aligned} \tag{6.18}$$

Finally, the shift of plasma column has been calculated using the difference of

$$\Delta R = (R_{axis} - R_0).$$

6.3 Results and Analysis

The theoretical and experimental flux surface of the SST-1 plasma has been shown in the present operating scenario. In Figure 6.4(a) magnetic flux surface at maximum plasma current has been shown for SST-1 shot #7916. The Figure 6.4(b) has shown the maximum flux value position from which we can determine the plasma shift at that instant. The magnetic flux surface as an ideal case and maximum flux value position at maximum plasma current has also been computed (shown in Figure 6.4(c) and Figure 6.4(d)) theoretically where flux (ψ) at the boundary is zero.

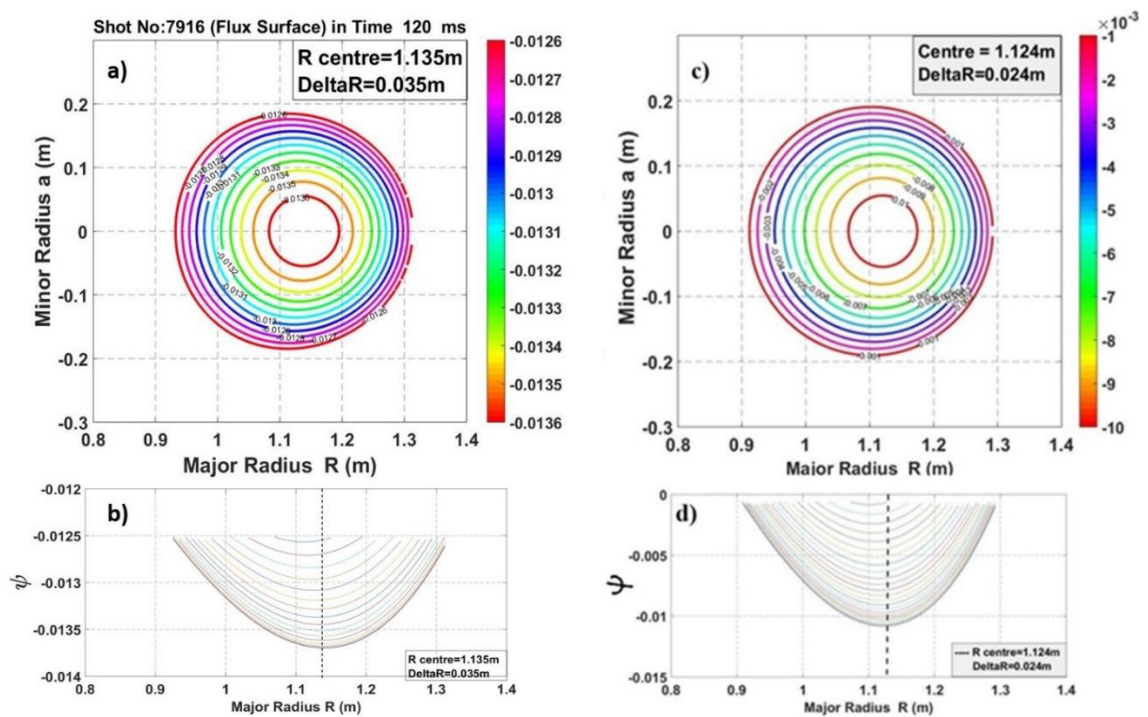


Figure 6.4 (a) Magnetic flux surface and (b) maximum flux value position for SST-1 shot #7916 ($I_p \approx 90\text{kA}$) (experimental) (c) Magnetic flux surface as an ideal case and (d) maximum flux value position at maximum plasma current ($I_p \approx 90\text{kA}$) (theoretical)

6.4 Summary and Conclusions

In this section, an experimental method has been presented to compute magnetic flux surface contours of the SST-1 tokamak plasma have been computed from the analytical solution of the Grad-Shafranov equation (GSE) by fitting experimental measurements obtained from magnetic probes and flux loops measurements. The Solov'ev equilibrium solution has been used with linear profiles of the flux function, pressure and circular plasma cross section criteria.

The flux surface contours computed from these methods have been benchmarked against a large amount of data obtained from a number of SST-1 plasma shots. The theoretical and experimental flux surfaces of the SST-1 plasma have also been computed in the present operating scenario. A quantitative comparison has been done between the two. It has been observed that the computed flux surfaces using experimental values agree well with those predicted by the theory. These findings would serve as useful inputs to upcoming plasma control aspects in the SST-1 plasma column.

C HAPTER- **VII**

Study on Plasma Feedback Control related issues in SST-1

- **Motivation and literature survey**
- **Basics of plasma position control**
- **Basics of plasma Shaping**
- **Initial implementation plasma radial position control in SST-1**
- **Results and Discussion**
- **Observations & Conclusions**

7.1 Motivation and literature survey

Tokamak operations involve several definitive sequences of operations. A complete plasma shot involves plasma initiation, start-up, shaping, heating, current drive, stabilization, and safe termination of discharges etc. These sequences need precise feedback and control mechanisms involving sensors, actuators, and model-based analyses. Operations and controls have been important on-going research topics in present-day tokamaks. Requirements towards more accurate physics models involving tokamak plasmas have been steadily increasing and increasingly sophisticated techniques are being incorporated into plasma controls in a tokamak. The confinement performance of a plasma within a tokamak greatly improves with optimized feedback control loop. There are several types of research related to plasma stability and control using feedback loops. In an experiment, D. C Robinson et al. [7.1] have confirmed theoretical predictions about plasma stability in tokamak TOSCA. However, vertically elongated plasma is known to be unstable. Hence, in order to stabilize the plasma, an active feedback system is required [7.2]. A circuit model has been used [7.3] to analyze a feedback system consisting of a single passive coil and an active feedback coil. It was proved that the proportional feedback of the plasma vertical position could stabilize the system. The circuit model has also been used to design sophisticated controllers for plasma vertical stabilization. However, this result is not quantitatively extendable to a massive structure of passive conductors. A modified linear-quadratic approach by Moriyama et al. [7.4], was extended to the stability region with standard PD controllers. Employing an H_∞ approach, Al-Husari et al. [7.5] has designed a vertical controller with low sensitivity to changes in the operating point. A low-order controller is also designed for a reduced-order plant model obtained from balanced truncation. A predictive control algorithm has been implemented by J. R Gossner et al. [7.6] for the

COMPASS-D tokamak. This algorithm stabilizes the plasma using only the flux sensors external to the vacuum vessel. A derivative controller [7.7] has been used to stabilize the plasma's vertical velocity. The derivative gain is adaptively changed with the growth time of the unstable mode. In particular, this model accounts for only the equilibrium field gradient at the chosen nominal location for the plasma filament. R. Albanese et al. [7.8] has presented a linearized, non-rigid model of the plasma vertical displacements. This is more accurate than multifilament models. It can be used for open-loop analysis and for designing stabilizing controllers. A modification of the linearization procedure has been proposed by D. A. Humphreys et al., [7.9] that includes the effect of the vessel on plasma stability. This model is obtained by approximating the plasma response to currents in the vacuum vessel in terms of equivalent poloidal field coil currents. P. Vyas et al. [7.10] have presented a model-based control design (H_∞ technique) approach towards controlling the vertical position of the plasma. A nonlinear, adaptive controller has been designed by L. Scibile et al. [7.11]. A fuzzy-logic-based controller has been designed and implemented by J E Morelli et al. [7.12] to control the position of the plasma column throughout an entire discharge. M.L Walker et al. [7.13] has exploited a full multivariable model of the vertical instability using a matrix analysis to provide for a rigorous demonstration of necessary conditions for stabilization of the plasma by PD feedback of vertical displacement.

The present study is a maiden attempt in SST-1 addressing some basic aspects of plasma control. A basic position control loop has been designed and implemented for initial radial position control for SST-1 plasma. In these studies, the factors and measures that would improve the performance, specifically the duration of SST-1 plasma have been studied and later attempted during experiments. This study is

essential for generating useful inputs towards the implementation of a robust and precise feedback control system that would contribute towards the long-duration confinement of SST-1 plasma column in future.

7.2 Basics of plasma position control

A control system is a system that regulates the behavior of specific devices to achieve desired output. In closed loop control, the feedback loop takes the system output into consideration, which enables the system to adjust its performance to meet the desired output response. Conceptually, positive feedback increases the gain of the amplifier; negative feedback reduces it. Some of the basic blocks of control system have been shown in [Figure 7.1](#).

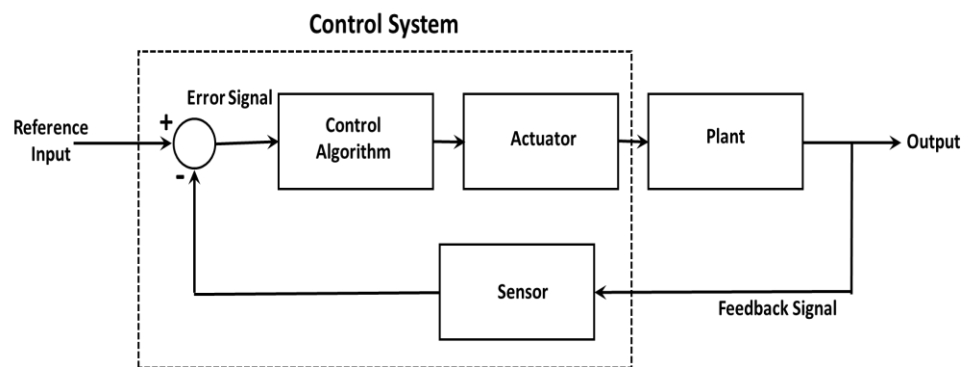


[Figure 7.1](#) Basic blocks of the control loop.

In case of the tokamak, the plasma is magnetically confined by magnetic fields generated by the set of conducting coils distributed around the vessel. Usually, active current carrying coils (TFs, VFs, and PFs) have been installed to produce a strong magnetic field surrounding the plasma vessel. The magnetic field interacts with the plasma to change its shape and position. This magnetic field also helps to balance the outward plasma force due to the pressure difference and the hoop force. This force balance problem (between the plasma field and the surrounding field for confinement), causes a radial shift of the plasma column. This phenomenon is very common and is

fundamental to maintaining plasma equilibrium in the tokamak. The appropriate use of feedback control loop can stabilize the plasma in its original or determined position. Thus, a plasma control system is both absolutely essential and necessary towards tokamak operation. The basic plasma control includes control of the plasma current, position and shape. In the schematic [Figure 7.2](#), the tokamak plasma radial position control is shown to be achieved by a pair of vertical field coils which stabilizes the plasma column by applying an inward radial force (F_{VF}). This is a standard practice in various tokamaks in maintaining the plasma position for circular plasmas.

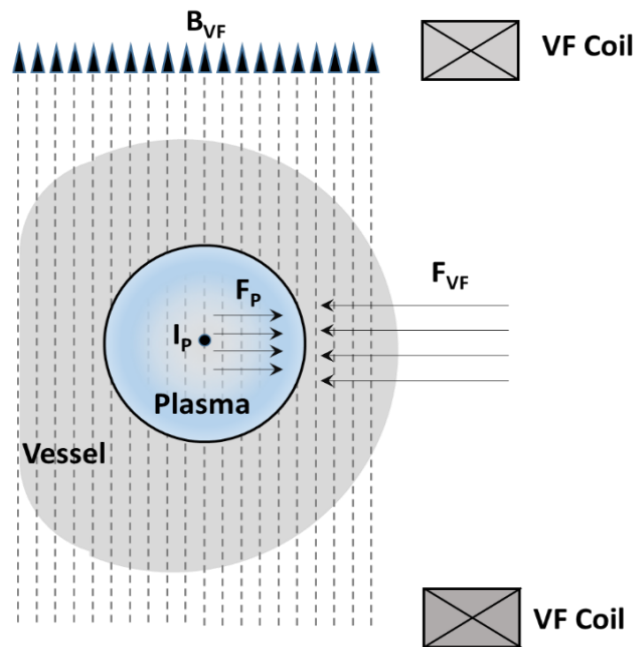


[Figure 7.2](#) Typical use of vertical field coil to maintain plasma position

Plasma position feedback control via the application of classical and modern control theory has been studied extensively. The magnetic control system is a feedback system, and is sometimes divided into separate sub-systems. It has the mandate of guaranteeing that the plasma equilibrium inside the tokamak is maintained with a prescribed position and shape of the plasma ring. The tokamak control problems can be separated into two major classes: electromagnetic control and plasma kinetic control. Electromagnetic control refers to controlling the magnetic and electric fields, which maintain or change

the plasma position, shape and current. As was previously explained, this task is performed by the poloidal coils, vertical field coils or in vessel radial control coils distributed around the vessel that contains the plasma. Predefined currents are flown through these coils which generate the magnetic fields to confine the plasma. The magnetic fields, regulated by feedback control; changes the plasma shape, and stabilizes the intrinsically unstable plasma horizontal/vertical position. The plasma regimes require production and regulation of extreme plasma shapes that allow operation at high plasma pressure. Magnetic control of shaped tokamaks depends on three challenges: identification of the existing equilibrium, stabilization of the unstable vertical position and regulation of the equilibrium to be as close as possible to the reference equilibrium. With an increase in the requirement of a number of variables such as computation and higher time scale in control application, advanced digital signal processors (DSP) with higher processing speeds have become more attractive for such control applications. Most tokamaks have adopted advanced fast response controllers precisely for these reasons. The confinement performances of a plasma within a tokamak have been greatly improved by the use of feedback control loop.

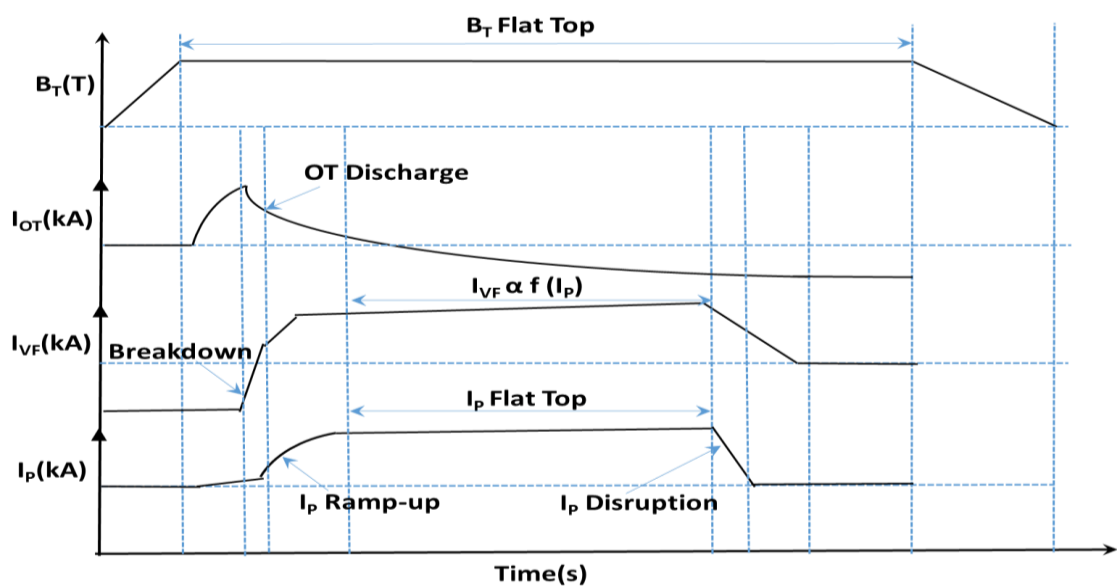


Figure 7.3 Typical sequences of the event in a plasma experiment in a tokamak.

The sequences of SST-1 plasma control are dependent on various subsystems. A timeline of control sequence has been shown in

[Figure 7.3](#), where plasma is created by the discharge of a central solenoid based ohmic transformer (OT). Then plasma ramp-up has been achieved by optimizing poloidal null and subsequent compensating start-up coil. Now the aim is to maintain and enhance plasma duration in the plasma flat-top state by appropriate control of external influencing parameters and intrinsic plasma parameters.

7.3 Basics of plasma shaping

In recent experiments of various tokamaks, plasma shaping has its own importance because of its influence on plasma stability, equilibrium, and various other characteristics. The particles in the plasma are charged; they conduct electricity and interact with magnetic fields. This characteristic helps create a shaped plasma within the tokamak. From the basic concept of a magnetic field, it is well known that the application of a quadrupole magnetic field in a confined plasma would elongate the circularly shaped plasma. The elongation could be in vertical or radial dimensions as per the polarity of the applied coil current. Similarly, the application of a hexapole magnetic field changes the plasma shape to more triangular shapes. A combination of these types of concepts are commonly used to achieve plasma shaping in a tokamak. This basic plasma shaping concept has been represented in the schematic [Figure 7.4](#).

There are different plasma shaping concepts which have been discussed in the context of plasma stability and equilibrium. Control algorithms for shape control are dominated by the multivariable, distributed nature of the problem. Often, a set of gaps (minimum distance between the LCFS and the wall) is defined yielding a discrete set of control variables. This shape control problem also related to the optimization of the required coil and sensor hardware in hostile plasma conditions. Shape control has been an active

area of research for many years and is usually integrated with plasma position and current control. The various tokamaks constructed to explore the effect of the shape on plasma performance. Some of the common plasma shapes are presented in [Figure 7.5](#).

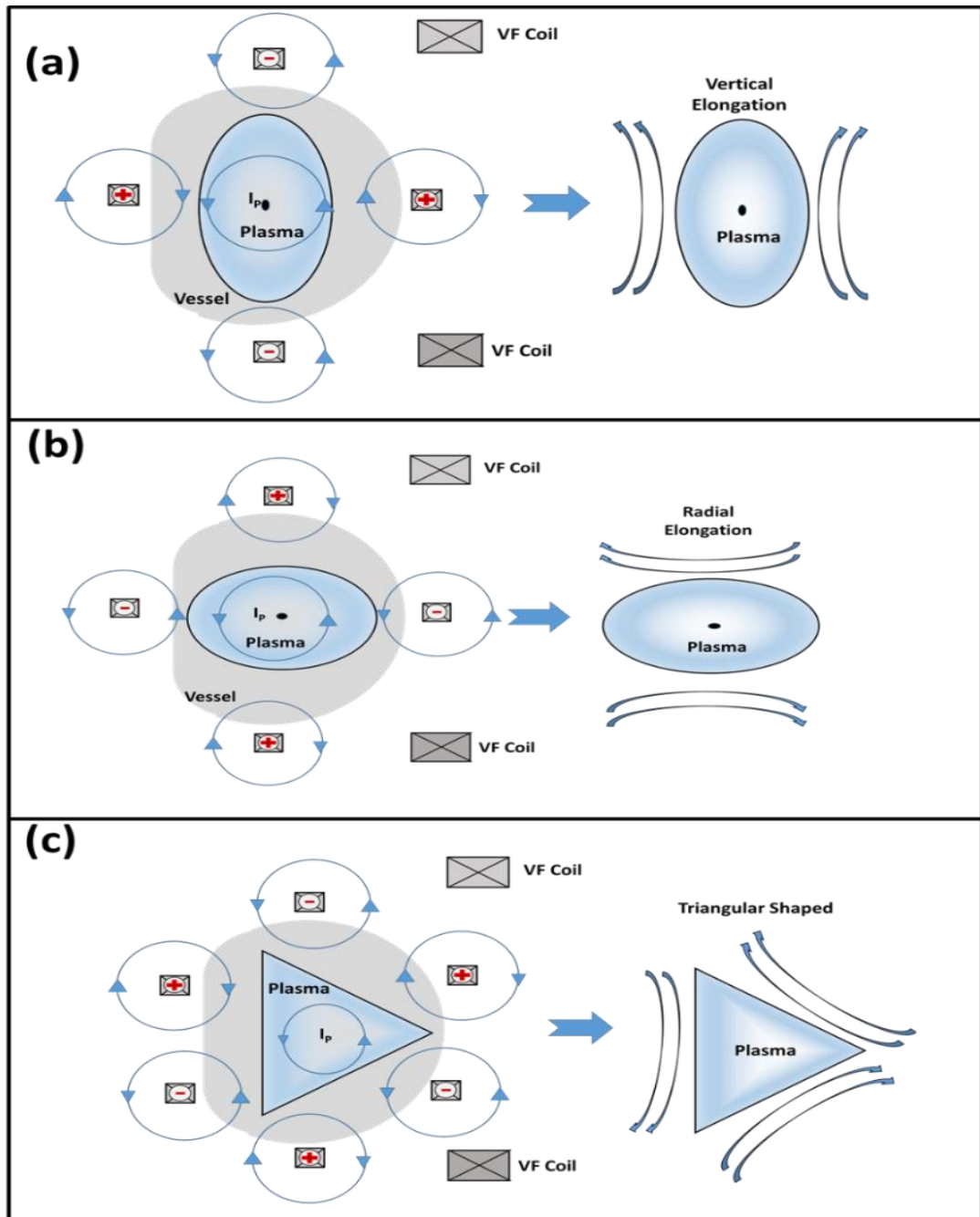


Figure 7.4 Magnetic field for basic plasma shaping

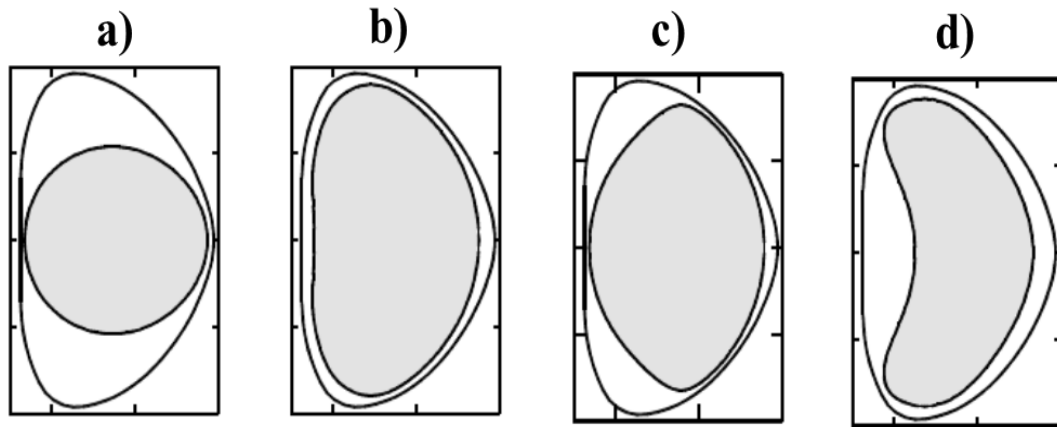


Figure 7.5 Some of the standard form of shaped plasma a) circular, b) D- shaped, c) Vertically elongated and d) modified D-shaped plasma

Shape control provides the means to produce plasma shapes that are required to achieve high β values. Operation at high β causes plasma instabilities that must be actively stabilized; optimization of the shape can reduce the effects of these instabilities. Energy confinement, stability properties and the fraction of plasma current provided by the bootstrap mechanism can be improved through control of internal pressure and current profiles. In addition, effective power exhaust, impurity, and particle control are required. All these controls must be performed simultaneously and continuously in a steady-state operation.

7.4 Initial implementation plasma radial position control in SST-1

7.4.1 Feedback methodology used in SST-1

In this maiden attempt, a simple feedback control loop has been designed and tested using vertical field coil. In the case of SST-1, resistive type vertical field magnets are located outside the cryostat and placed symmetrically around the midplane. The current applied to these symmetric coils results in inward/outward forces due to the vertical field. Thus, with appropriate vertical field current profile, the desired plasma outward

movement can be controlled. In SST-1 case, a basic principle has been adopted to control the plasma as follows:

- i) If plasma is moving inwards \rightarrow decrease VF field
- ii) If plasma is moving outwards \rightarrow increase VF field

In our present feedback loop design, we have generated a reference vertical field current as proportional to the profile of the plasma current. The real-time plasma position has been computed from magnetic diagnostics (i.e. flux loop and magnetic probes already described in [chapter IV](#) and [chapter V](#)) and used after applying appropriate compensation techniques. In the feedback loop, radial position direction is considered as +ve if plasma is moving outwards and -ve if plasma is moving inwards in reference to the initial plasma position. An error signal has been generated as proportional to plasma position and if that error signal's magnitude exceeds the defined threshold limit then the position controller output would adjust vertical field current (I_{VF}) by changing the actuator signal ($I_{VF} \pm \Delta I_{VF}$), where ΔI_{VF} is generated as proportional to the plasma position factor calculated from EM diagnostics. In this experiment, our efforts are towards maintaining the plasma position within the limit of ± 2 cm (One can adjust this parameter based on subsequent experiments) from the magnetic axis or the position where the maximum plasma current has been targeted.

At present, the SST-1 Control loop starts only when plasma is significantly formed. The $I_{P_{Max}}$ parameter defines the plasma current value after which the position feedback loop will start and $I_{P_{Min}}$ parameter defines the stop command of the control loop. The control loop is time-tested very 1ms i.e. every 1ms a control signal will be delivered to VF power supplies according to feedback algorithm. The control loop time can further be reduced up to $100\mu s$ as per the requirement the feedback loop.

The configurable parameters for the SST-1 feedback control loop are:

- Threshold ΔR (deviation of the plasma position from the reference position)
- $I_{P_{Max}}$ (plasma current value after which to start feedback)
- $I_{P_{Min}}$ (plasma current value after which to stop feedback)
- Control loop time (1ms)

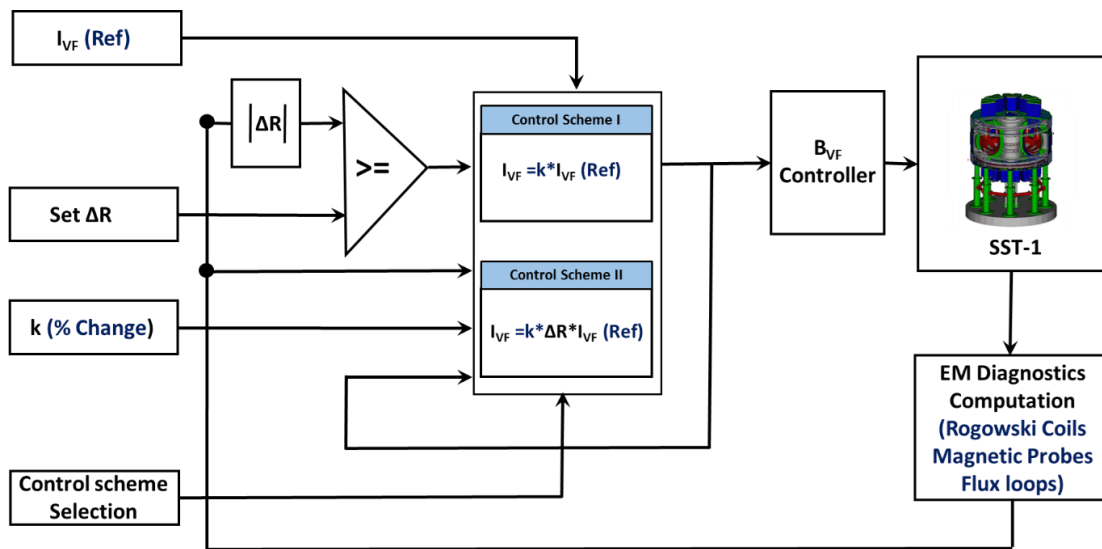
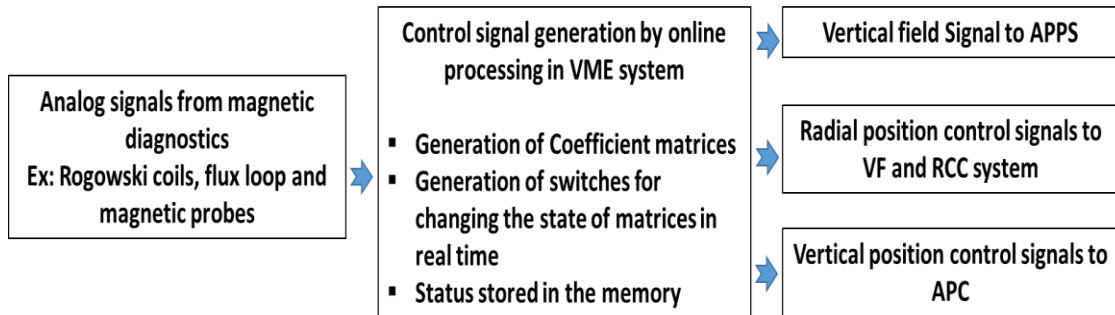


Figure 7.6 Schematic of B_V Feedback Control Loop

In a schematic Figure 7.6, the vertical Field (B_V) feedback control loop has been presented with its basic blocks. The plasma position control system usually generates various control signals in real time. Analog signals are generated from the magnetic diagnostics as per the change of plasma position. The real-time plasma current has been measured using the Rogowski coil encircling the plasma. This is fed into the control loop. The position is measured using magnetic diagnostics and fed into the control loop to generate the error signal. At present, B_V feedback control loop is only used for maintaining the radial plasma position. The use of RCC application can help the plasma

confinement scenario in a significant way as the RCC coil is within the SST-1 vacuum vessel and near to the plasma column.

The position feedback system is summarized as follows:



7.4.2 Hardware for feedback methodology

The magnetic diagnostics (magnetic probe or flux loop) detect the change in magnetic field and Rogowski coils measure the plasma current, Ohmic transformer current and VF coil current. The digital integration and normalization of EM signal have also been performed during that time. Magnetic probe signals are acquired by the PCS VME using a 6U sized VME ADC board, Pentek 6802. This 32-channel ADC board with FPDP interface is able to accept ± 5 V differential or single-ended analog input at a sampling rate of 10KSPS. During this time, sufficient precautions have also been taken to provide the networks with electromagnetic noise immunity.

The SST-1 central control system (CCS) is a distributed, modular and scalable system. [7.14-7.16] Fastest control loop time is achieved using VME based simultaneous sampling ADCs, PMC based quad-core DSP, Reflective Memory [RFM] based real-time network, VME based real-time trigger distribution network and an ethernet network system. The plasma control system VME acquires the Magnetic diagnostics data and runs the position and current control algorithm on a PMC based DSP. Coefficient matrices and switches for changing these matrices in a real time scenario are stored in the memory well ahead of actual experiment start-up. A PMC based DSP

board uses these data to perform plasma position control according to the algorithm and send the control signals to power supply over a real-time data network interface available on a PMC based RFM. Then it generates VF signals to the APPS. Radial position control signals to VF power supply system through the APPS power supply. In the present position control loop controlled by a proportional controller. This process is controlled in the automatic mode as the SST-1 power supply controller could be pre-programmed as per feedback value. During the experiment, the APPS controls the OT current, ramp-up delay, Input of I_P simulated waveform, I_P reference waveform, trigger pulse and emergency shutdown etc.

A client-server based software tool is used for control and monitoring purposes. This utility follows a state machine to complete the plasma discharge sequence, in which it passes experiment number along with the other parameter to the remote systems over TCP/IP communication. The timing system interface provides synchronization with the other SST-1 subsystem with the help of triggers and VME interrupts. APC interface of PCS node is used for sending the current reference signal over a dedicated fiber link to APC power supply. The RFM network is also used for real-time plotting of key parameter of plasma during the experiment. After the experiment, all the real-time raw data along with the control data are archived using the RFM network and the SCSI HDD. A MATLAB based utility is operated on a post-pulse analysis machine. This utility reads data from the central storage system and converts the data from binary to the physical quantity of the parameter.

The specific characteristics of the central control system (CCS) such as RTOS for deterministic control, FPGA for hardware implementation, fibre optics for network backbone, DSP for real-time computation and reflective memory for high-speed data transfer are an added advantage for fast feedback control system.

7.4.3 Simulation Scenarios in open loop

A vertical field simulation scenario has been developed to generate the reference plasma current and the corresponding signal for the vertical field coil ($I_{VF(Ref)}$) during the real-time experiment. This simulated ($I_{VF(Ref)}$) signal can be used as a control input.

This simulation scenario has been considered as per following criteria as follows:

- With experimental data of few shots, take I_p and ΔR as simulated input.
- The ohmic transformer power supply (APPS PS) run in control mode
- I_{VF} profile is adjusted as per the radial position data available from simulated data.(Tested on 1 ms and 10ms loop cycle)
- VF Simulation scenario is an open loop test.

7.5 Results and Discussion

In this section, some of the preliminary results obtained in SST-1 are presented. In an initial test experiment, plasma position control is applied by adjusting the output of the vertical field coil. The vertical field coil current is a function of the plasma current. A comparison has been performed between the plasma pulse with and without the feedback. In the comparison (shown in [Figure 7. 7](#)) of a representative plasma shot #7024 and shot #7026 (where the position control loop has been applied). We have observed that a plasma maintained its original position and the duration of plasma also increased. Both these shots have identical extrinsic parameters. The application of feedback loop has elongated the plasma duration.

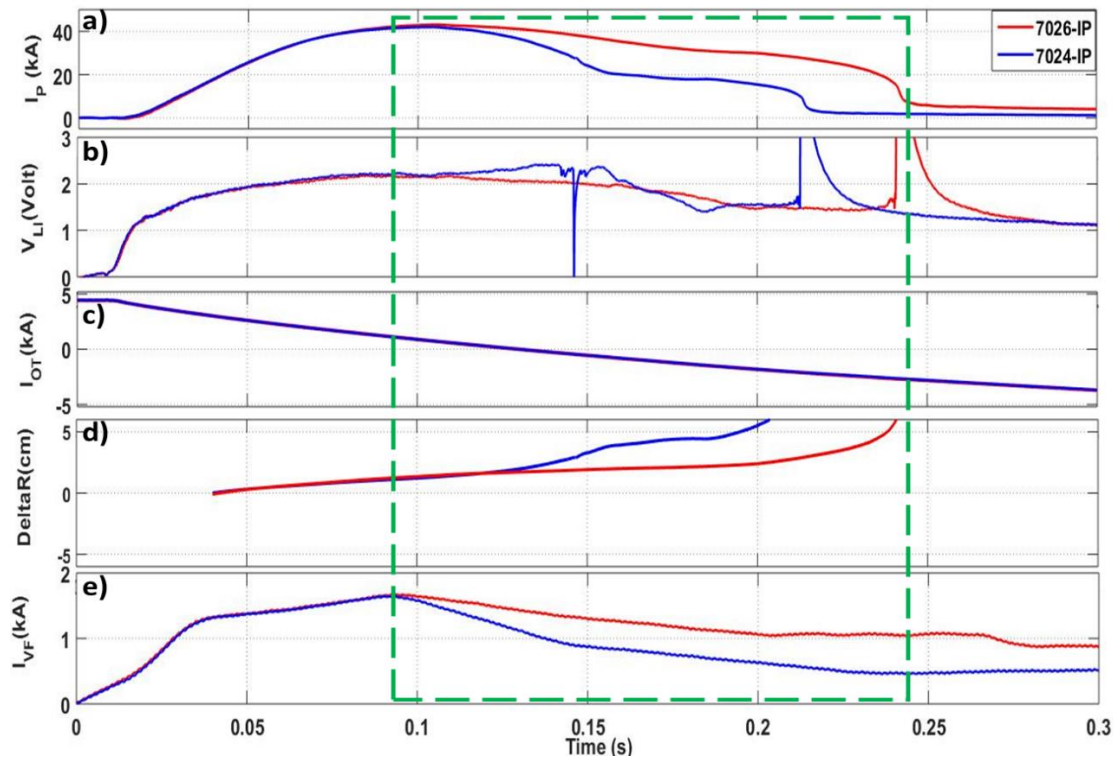


Figure 7. 7 Comparison of plasma shot # 7024(blue) and shot#7026(red) (position control loop applied). The Subplots represent a) plasma current b) Loop voltage c) OT current d) Radial shift and e) vertical field current.

In shot#7026(red), the plasma position control loop is applied at 90ms as I_p is reached at maximum current. The aim was to maintain plasma position and current subsequently. The vertical field coil current is maintained proportional to the plasma current signal and the error signal is generated from the shift of the position signal. In this experiment, our efforts were directed towards maintaining plasma position within a limit of ± 2 cm from the magnetic axis or the position where the maximum plasma current has been achieved. On the contrary, in Shot # 7024, without the plasma position control loop, the plasma moves towards the outward region. The plasma current has reduced because of the interaction of plasma with the limiter. The situation has improved in subsequent shots during the experiment (shown in Figure 7. 8) by enhanced optimization techniques.

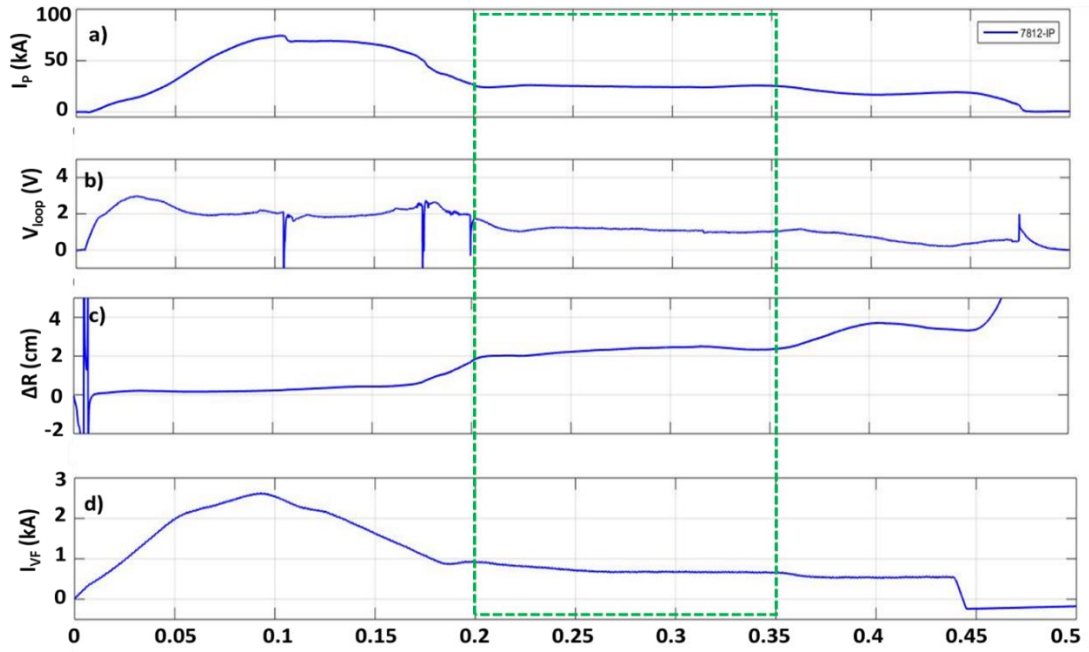


Figure 7. 8 A longer duration plasma shot using position control loop. SST-1 plasma shot # 7812. The subplots represent a) plasma current b) Loop voltage c) Radial shift and d) vertical field current.

In shot #7812, the plasma position control loop is applied at 190ms to maintain plasma position and to increase the duration of plasma. From the computed plasma shift, we can observe that the plasma is comparatively stable as the plasma center staying at a fixed position for a longer duration (during 200ms to 350ms for this particular shot marked with a green square.). Plasma position is stabilized in its shifted position. The overall situation has been improved during this experiment. A longer duration (450ms) of plasma has been achieved successfully. Hence, the successful application of a plasma position control loop can help towards achieving a long duration plasma with the initial implementation of feedback control.

7.6 Observations & Conclusions

In this chapter, a general methodology of plasma position and control has been discussed. The basic concepts of plasma shaping and its importance in plasma stability and equilibrium have also been discussed. A basic implementation of the position control loop in SST-1 tokamak aimed at achieving a long duration plasma has been initiated. The computed real-time position has been used to generate the error function. Subsequently, plasma position is stabilized using the position controller output controlling vertical field current. The implementation of this basic feedback loop has helped to stabilize the plasma position in a particular position for a longer duration. The total plasma flat-top duration has been increased. The longest plasma duration in excess of 450ms has been achieved using the initial implementation of the position feedback loop with the prevailing constraints. As per the present status of the SST-1 machine, the vertical field current profile control had been used with the consideration of the vessel time constant due to the non-availability of the in-vessel fast feedback coil. The upgradation towards advanced position control implementation using the vertical magnetic field and in-vessel fast feedback coil would be considered for SST-1 tokamak in future.

C_{CHAPTER} – **VIII**

Summary and future work

8.1 Summary and Conclusion

This thesis is fundamentally based on the operational aspects of the first Indian Steady State Superconducting Tokamak (SST-1) in its first phase of operation. This addresses the basis of plasma initiation and ramp-up by elaborating the technically favourable and unfavourable combinations of the vacuum error fields. It also addresses some of the basic studies on the initial shape of the poloidal magnetic null and its subsequent evolution. Thereafter, some of the basic characteristics of the formed plasma column have been studied from established formulations. This work also explains electromagnetic diagnostics, which comprises of designing, fabricating additional electromagnetic diagnostics particularly probes that have enabled characterizations of the plasma column better. Finally, with the knowledge of satisfactory information on the shift of the plasma column, this work has contributed towards some of the basic aspects of control in SST-1 plasma. These had been implemented in SST-1 operation during the experimental campaign. The implementation of the vertical field control has in fact led to longer pulse length in SST-1 ohmic shots.

At the beginning, in **chapter-I**, basic details of nuclear fusion, plasma and the detail description of the SST-1 device has been discussed for the sake of completeness and ease of understanding. In this section, a short description of the important subsystems of SST-1 such as the superconducting toroidal field magnets, the poloidal field magnets, the resistive central solenoids and compensating coils and the vertical field equilibrium coils has been discussed with important operating parameters.

As the SST-1 cryostat and the vacuum vessel are electrically continuous, a large eddy current flows through it during the start-up operation. In **chapter II**, vessel eddy currents have been computed from the in-vessel flux loops using a simple circuit model. This model is able to calculate eddy current that flows through the electrically

continuous and conducting SST-1 vacuum vessel and cryostat during start-up. The eddy current evolution has been observed for plasma as well as vacuum experiment with an identical central solenoid current and equilibrium field. The maximum eddy current ($I_{\text{EDDY max}}$) is about $\sim 20\text{kA}$ in the present operating scenarios. The rate of change of current in the central solenoid ($(dI_{\text{OT}})/dt$) and sudden disappearance of plasma current during the disruptions are main reasons for the production of eddy currents. The eddy current patterns seriously influence the field null and hence the plasma breakdown characteristics.

In **chapter III**, an electromagnetic model for SST-1 tokamak has been elaborately described. The electromagnetic fields for different current carrying coils have been investigated using finite element method. The simulation results have been validated using the known vertical field (VF) coil current pulse. The comparison results are in good agreement with each other. The magnetic field status for each active coil during start-up has been studied. An accurate computation of the vacuum field contributed by ohmic coils alone has been studied initially. The contribution of ohmic coils with combinations of equilibrium coils, and the vessel eddy current have also been carried out during plasma start-up.

The time evolution of the eddy current profiles and observations from this electromagnetic modeling have contributed to optimizing the initial start-up condition. This study significantly helps to increase the plasma current from 60kA to 110kA in the recent campaigns.

In **Chapter IV**, important magnetic diagnostics such as Rogowski coil, diamagnetic coil, flux loop and magnetic probes diagnostics have been presented for the SST-1 machine. The position, orientation, challenge, applicability and compensation

techniques have been explained with their principles. The plasma position has been measured using magnetic probes and flux loops signal following a standard methodology for SST-1 tokamak. The detailed description of this methodology is presented in **chapter V**. The shift computed from this methodology using the flux loops and magnetic probes are in good agreement, repeatable and reliable. The magnetic probes and flux loops were calibrated using a simple and reliable calibration technique. The main advantages of this technique is dependent on the experimental magnetic probes signals of vacuum shot. Comparison and repeatability tests with imaging signal has been also carried out. It has been observed that the plasma movement trend from imaging is identical with the shift calculated from magnetic diagnostics.

In **Chapter VI**, an experimental method has been presented to compute the magnetic flux surface contours of the SST-1 tokamak from the data of the magnetic loops, probes and analytical solution of the Grad-Shafranov equation. The theoretical and experimental flux surfaces are computed for the present operating conditions with prevailing constraints. Magnetic flux surface contours of the SST-1 tokamak plasma have been computed from the analytical solution of the Grad-Shafranov equation (GSE) by fitting experimental measurements obtained from magnetic probes and flux loops measurements. Here, we have used the Solov'ev equilibrium solution with linear profiles of flux function and pressure, using circular plasma cross section criteria.

In **chapter VII**, a short summary of plasma position feedback control has been discussed. The basic concepts of plasma shaping and its importance in plasma stability and equilibrium have also been discussed. A basic implementation of position control loop for the SST-1 tokamak has been initiated. The computed real-time position has been used to generate the error function and subsequently used to feed through vertical field current. The implementation of this basic feedback loop has helped to stabilize

the plasma position in a particular position for a longer duration. The total plasma flat-top duration has been increased. The longest plasma duration (~500ms) has been achieved using the initial implementation of the position feedback loop.

As per the present status of the SST-1 machine, due to the non-availability of the in-vessel fast feedback coil only the vertical field current profile control had been used with the consideration of vessel time constant. The upgradation towards advanced position control implementation using vertical magnetic field and in-vessel fast feedback coil would be considered for SST-1 tokamak in future.

In conclusion, the work performed in this thesis gives an insight into several newly observed work related to plasma start-up and plasma position and control related aspects of the SST-1 tokamak. This study significantly helps to increase the plasma current from 60kA to 110kA in recent campaigns and achieve longest plasma duration (~450ms) yet using initial implementation of the position feedback loop.

8.2 Future Work

Developing an enhanced plasma start-up model

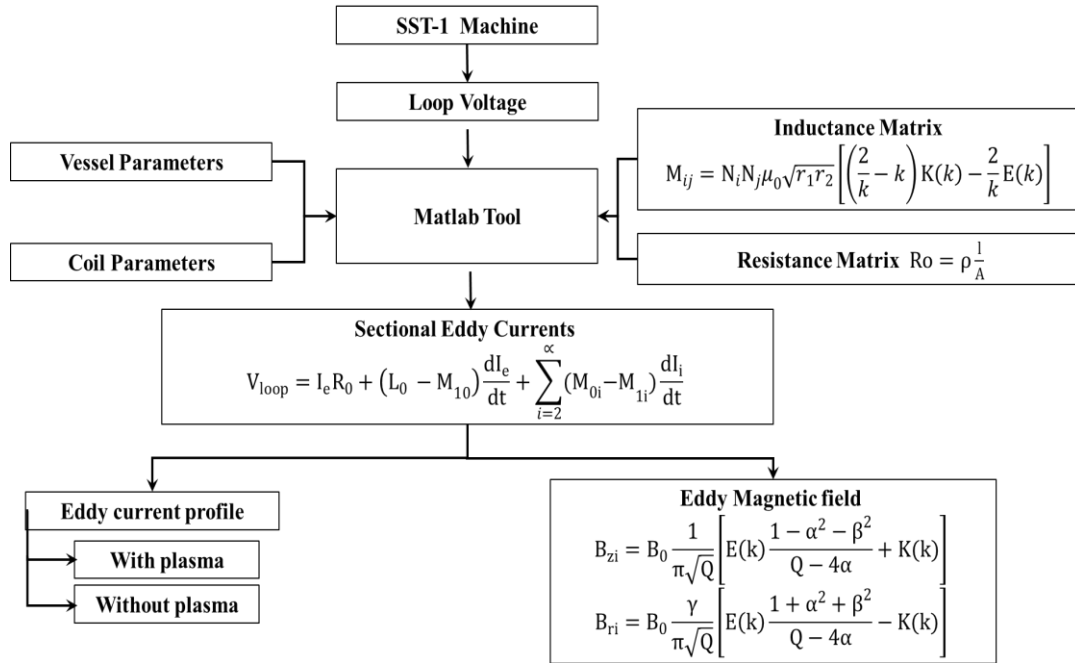
An enhanced plasma start-up model will be developed using magnetic field analysis. The main purpose of this work would be to compute and validate breakdown characteristics for the SST-1 tokamak. This plasma startup model will implement some of the known techniques which are already implemented in different other tokamaks.

Implementation of advanced position and shape control

Development of advanced model of the SST-1 control system, including power systems, vessel, and poloidal coils is going on. The aim of this work is to achieve the long duration plasma (>1 sec) using advanced position control. This work will be continued for the development of advanced model to control the plasma. After the successful implementation of the initial plasma position control, the work towards plasma shaping to produce D-shaped elongated plasma will be performed to solve several challenging control problems in the future.

Appendix I

Algorithms.



In this appendix section, a algorithm of overall computation process for eddy current calculation has been described. At first, the overall SST-1 Vacuum vessel has been divided into small segments. The experimentally measured loop voltage has been used to compute the sectional eddy current. The important vessel and coil parameter has been initialized. The inductance and resistance matrix has been calculated for the segmented section and active current carrying coils. The using a simple circuit model and MATLAB based tools we have calculated the sectional eddy current and to calculate the overall induce effects. Computation of segmental eddy current from the circuit model equation and flux loop experimental data. The eddy current measurement in SST-1 and the subsequent B-field evolution has been carried out using standard formulation.

Appendix II

An electromagnetic circuit based model has been considered with all active coil currents such as I_{OT} component I_{VF} component and vessel eddy currents components.

The induced flux loop voltage ($V_{loop\ i(R,Z)}$) at coordinate (R, Z) can be written for a vacuum shot as;

$$V_{loop\ i(R,Z)} = -M_{iOH_total} \frac{dI_{OH}}{dt} - M_{iBV_total} \frac{dI_{BV}}{dt} - \sum \left[\frac{d(M_{ji}I_j)}{dt} - I_j R_j \right] \quad (i)$$

The flux loop voltage for plasma shot can be similarly written as

$$V_{loop\ i(R,Z)} = -M_{iOH_total} \frac{dI_{OH}}{dt} - M_{iBV_total} \frac{dI_{BV}}{dt} - \sum \left[\frac{d(M_{ji}I_j)}{dt} - I_j R_j \right] - I_P R_P \quad (ii)$$

Where, $\frac{dI_{OH}}{dt}$ and $\frac{dI_{BV}}{dt}$ are the rate of change of currents in ohmic coils and vertical field coils respectively. The M_{iOH_total} is the total mutual inductance between i^{th} flux loop and ohmic coil whereas M_{iBV_total} is the total mutual inductance between i^{th} flux loop and vertical field coil. M_{ji} is the mutual inductance between the j^{th} vessel segment and i^{th} flux loop. I_j and R_j are the induced eddy current and resistance in the j^{th} vessel segment respectively. I_P is the plasma current and R_P is the plasma resistance. The eddy current has been computed for SST-1 tokamak from a standard circuit model.

The mutual inductance between two circular loops is given by the standard formulation.

$$M_{ij} = N_i N_j \mu_0 \sqrt{r_1 r_2} \left[\left(\frac{2}{k} - k \right) K(k) - \frac{2}{k} E(k) \right] \quad (iii)$$

$$\text{where } k = \sqrt{4r_1 r_2 / [(r_1 + r_2)^2 + (z_1 + z_2)^2]}$$

Where, N_i and N_j are the number of turns in respective circular loops. r_1 and r_2 are the radius of the first and second loop respectively with z_1, z_2 are the corresponding vertical

positions. $K(k)$ & $E(k)$ are the complete elliptic integral function of the first kind and second kind.

Comparison of computed flux loop signals using above equation is in excellent agreement with observed experimental signals. Result for one of the flux loop signal for inboard and outboard is shown in [Figure ii](#)). Following these, flux loop signal has been reproduced at the desired (R, Z) location which has been subsequently used in [chapter V](#) and [VI](#).

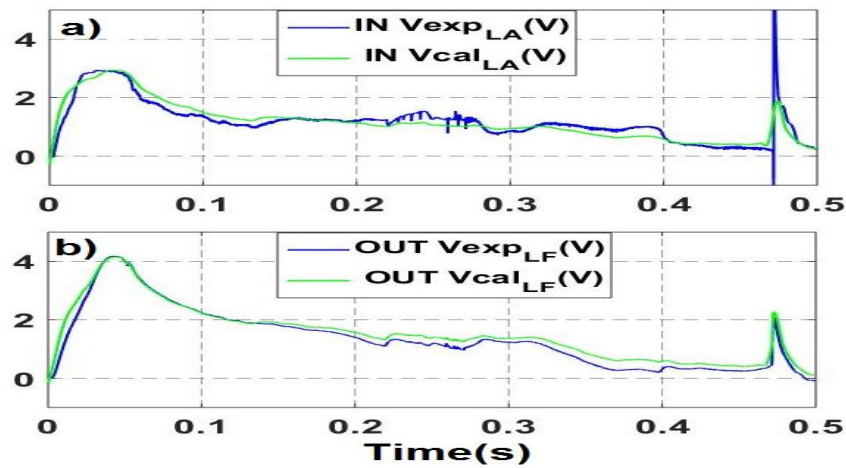


[Figure. ii](#) a). The comparison between computed signals and experimentally obtained flux loop signals (Inboard). b).The comparison between computed signals and experimentally obtained flux loop signals (Outboard).

Bibliography

Chapter I

- [1.1] Joaquin Sanchez, Nuclear fusion as a massive, clean, and inexhaustible energy source for the second half of the century: a brief history, status, and perspective, *Energy Science and Engineering* 2(4) (2014) 165–176.
- [1.2] Laila A. El-Guebaly, Fifty Years of Magnetic Fusion Research (1958–2008): Brief Historical Overview and Discussion of Future Trends, *Energies* 3 (2010) 1067-1086.
- [1.3] John Wesson, Tokamak, Third edition, Oxford university press, (2004)
- [1.4] F. Romanelli et al., Overview of JET results, *Nucl. Fusion* 49 (2009) 104006 (22pp)
- [1.5] M. Keilhacker and the JET team, Overview of results from the JET tokamak using beryllium first wall, *Physics of Fluids B: Plasma Physics* 2 (1990) 1291.
- [1.6] M. Mori and the JT-60 team, Latest Results from JT-60U, *Plasma Phys. Control Fusion* 36 (1994) B181-B191.
- [1.7] N. Oyama and the JT-60 Team, Overview of JT-60U results towards the establishment of advanced tokamak operation, *Nucl. Fusion* 49 (2009) 104007.
- [1.8] H. Takenaga1 and the JT-60 Team, Overview of JT-60U results for the development of a steady-state advanced tokamak scenario, *Nucl. Fusion* 47 (2007) S563–S578. (JT-60)
- [1.9] T. Hamacher and A.M. Bradshaw., Fusion as a future power source: Recent achievements and prospects, *The proceedings of the 18th World Energy Congress*.
- [1.10] Philippe Magaud et al., Nuclear Fusion Reactors, *Encyclopaedia of Energy*, Volume 4 (2004) 365-381.
- [1.11] Kingshuk Ghosh and Gautam Ghosh, The Saha ionization equation, *Eur. J. Phys.* 19 (1998) 7
- [1.12] S. Pradhan et al., The first experiments in SST-1, *Nucl. Fusion* 55 (2015) 104009.
- [1.13] S. Pradhan and SST-1 Mission Team, SST-1 magnet system refurbishment: An update, *Phys. Procedia*, 36 (2012), 791–796,
- [1.14] S. Pradhan., “SST-1 toroidal field magnet tests: Some results and lessons learned, *IEEE Trans. Appl. Superconductivity*, 22(3) (2012) 9501804
- [1.15] A. N. Sharma et. al., Thesis on ‘Studies on Quench characteristics of superconducting magnets of SST-1’ HBNI, February 2015
- [1.16] A. N. Sharma et. al., Cryogenic Acceptance Tests of SST-1 Superconducting Coils, *IEEE Transactions on Applied Superconductivity*, 25(2) (2015) 4200107
- [1.17] V. L. Tanna et al., Upgradation plans of SST-1 Cryogenics system at IPR. *IOP Conf. Series: Journal of Physics: Conf. Series* 18234 (526071879) (2017) 0012002
- [1.18] B. Sarkar et al., Cryogenic system of steady state superconducting Tokamak SST-1: Operational experience and controls, *Fusion Engineering and Design* 81 (2006) 2633–2641.
- [1.19] Z. Khan et al., Vacuum system of SST-1 tokamak, *Fusion Engineering and Design* 88 (2013) 692–695. .
- [1.20] Z. Khan et al., Validation of SST-1 components at low temperature under a vacuum environment, *Indian Journal of Cryogenics*, 38(1) (2013) 138–143.
- [1.21] Z. Khan et al., Nitrogen Gas Heating and Supply System for SST-1 tokamak, *Plasma Science, and Technology*, 15(2) (2013) 157.
- [1.22] Yuvakiran Paravastu et al., New design aspects of the cooling scheme for SST-1 plasma facing components, *Fusion Engineering and Design* 98–99 (2015) 1375-1379.
- [1.23] B. K. Shukla, J. Patel, R. Babu, et al., “Commissioning of 42 GHz/500kW ECRH System on tokamak SST-1”, *Fusion Eng. (SOFE)* (2013).

- [1.24] M. Sharma et al., Overview of data acquisition system for SST-1 diagnostics, *Fusion Engineering and Design* 112 (2016) 872–876
- [1.25] Kirti Mahajan et al., CORBA-based solution for remote participation in SST-1 tokamak control and operation, *Fusion Engineering and Design* 81 (2006) 2069–2072
- [1.26] Kirit Patel et al., Design and Architecture of SST-1 basic plasma control system, *Fusion Engineering and Design* 112 (2016) 703–709.

Chapter II

- [2.1] Mohammad Reza Nabavi et al., Eddy-Current Sensor Interface for Advanced Industrial Applications, *IEEE Transactions on Industrial Electronics*, 58(9) (2011)4414
- [2.2] V. Amoskov et al., Simulation and analysis of eddy currents induced in the GLOBUS-M tokamak, *Plasma Devices and Operations*, 13(1) (2005) 25–38.
- [2.3] I. Z. Abidin et al., Advantages and Applications of Eddy Current Thermography Testing for Comprehensive and Reliable Defect Assessment, *18th World Conference on Non-destructive Testing*, 16-20 April, Durban, South Africa.
- [2.4] D. A Humphreys et al., Development of ITER-relevant plasma control solutions at DIII-D, *Nucl. Fusion* 47 (2007) 943–951
- [2.5] D. A Humphreys et al., Filament-Circuit Model Analysis of Alcator C-Mod Vertical Stability, *PFC/JA-89-28*.
- [2.6] J Blum et al., Eddy current calculations for the Tore Supra tokamak, *IEEE Transactions on Magnetics*, 19(6) 1983 2461
- [2.7] G. Rubinaci, Numerical computation of the eddy currents on the vacuum vessel of a tokamak, *IEEE Transactions on Magnetics*, 19(6) 1983 2478
- [2.8] S. Nishio et al., a computer program system for transient electromagnetic analysis on a tokamak device, *IEEE Transactions on Magnetics*, 26(2) 1990 865
- [2.9] A. Zolfaghari et al., Calculation of Eddy Currents in the CTH Vacuum Vessel and Coil Frame for Use in MHD Equilibrium Reconstruction of the Plasma Discharge, *Fusion Science and Technology* 64(3) (2013) 498-501
- [2.10] M. Mattei et al., H-infinity Estimation of Eddy Currents in a tokamak, *3rd IFAC International Conference on Intelligent Control and Automation Science*, September 2-4, 2013. Chengdu, China.
- [2.11] G. A. Evans et al., Computing time-dependent eddy current in a tokamak, *computer physics communication* 69 (1992) 243 252.
- [2.12] D.A. Gates, J. E. Menard and R. J. Marsala., Vessel eddy current measurement for the National Spherical Torus Experiment, *Review of scientific instruments* 75(12) (2004) 5090-5093.
- [2.13] Ziauddin Khan et al., Vacuum system of SST-1 tokamak, *Fusion engineering and design* 88 (2013) 692-695.
- [2.14] Ziauddin Khan et al., Overall Performance of SST-1 tokamak Vacuum System, *IEEE transactions on plasma science*, 42(4) (2014) 1006-1011.
- [2.15] L.L. Lao, et al., Equilibrium Analysis of Current Profiles in tokamaks, *Nucl. Fusion* 30 (1990) 1035.

Chapter III

- [3.1] R. Papoular., The genesis of toroidal discharges, *Nuclear fusion* 16 1 (1976) 37-45.
- [3.2] B Lloyd et al, Low voltage ohmic and electron cyclotron heating assisted startup in DIII-D, *Nucl. Fusion* 31 (1991) 2031.
- [3.3] G. L. Jackson et al., Second harmonic electron cyclotron pre-ionization in the DIII-D tokamak, *Nucl. Fusion* 47 (2007) 257–263.

- [3.4] G. L. Jackson et al., ITER start-up studies in the DIII-D tokamak, *Nucl. Fusion* 48 (2008) 125002.
- [3.5] G. Granucci et al., Experiments and modeling on FTU tokamak for EC assisted plasma start-up studies in ITER-like configuration, *Nucl. Fusion* 55 (2015) 093025 (10pp)
- [3.6] R. Albanese et al., Experimental results with an optimized magnetic field configuration for the JET breakdown, *Nucl. Fusion* 52 (2012) 123010.
- [3.7] J. Liu et al., Investigation of field null for HL-2M tokamak start-up, *2013 IEEE 25th Symposium on Fusion Engineering (SOFE)*.
- [3.8] B. Lloyd et al., ECRH-assisted start-up in ITER, *Plasma Phys. Control. Fusion* 38 (1996) 1627–1643.
- [3.9] Aveg Kumar et al., 0-D modeling of SST-1 plasma break-down & start-up using ECRH assisted pre-ionization, *Fusion Engineering, and Design* 105 (2016) 22–28.
- [3.10] Kirit Patel et al., Observation on fundamental and second harmonic mode ECRH assisted plasma start-up in SST-1 experiments, *Fusion Engineering and Design* 106 (2016) 99–102.
- [3.11] YoungHwa An et al., Efficient ECH- assisted plasma start-up using trapped particle configuration in the versatile experiment spherical torus, *Nuclear Fusion* 57(2017) 016001(11pp)
- [3.12] H. Urano et al., Development of operation scenarios for plasma break down and current ramp-up phases in JT-60SA tokamak, *Fusion engineering and design* 100 (2015) 345-356.
- [3.13] K. Kajiwara et al., Electron cyclotron heating assisted startup in JT-60U, *Nucl. Fusion* 45 (2005) 694–705.
- [3.14] J. A. Leuer et al., Plasma Startup Design of Fully Superconducting tokamaks EAST and KSTAR with Implications for ITER, *IEEE transactions on plasma science* 38(3) (2010) 333-340.
- [3.15] J. A. Leuer et al., Tokamak start-up modeling and design for EAST first plasma campaign, *Fusion Sci. Tech.* 57 (2010) 48–65.
- [3.16] J. Havicek and O. Hronova., Characterization of the Magnetic field in the COMPASS tokamak, *WDS,08 Proceedings of Contributed papers, part II (2008) 110-114*.
- [3.17] Wonho Choe et al., solenoid free toroidal plasma start-up concepts utilizing only the outer poloidal field coils and a conducting center-post, *Nuclear Fusion* 45 (2005) 1463-1473.
- [3.18] V.F. Shevchenko et al., Long Pulse EBW Start-up Experiments in MAST, *Nuclear Fusion* 50, (2010) 022004
- [3.19] O. Kaneko et al., Plasma startup by neutral beam injection in the Large Helical Device, *Nucl. Fusion* 39 (1999) 1087.
- [3.20] D. Gradic et al., Assessment of the plasma start-up in Wendelstein 7-X with neutral beam injection, *Nucl. Fusion* 55 (2015) 033002.
- [3.21] T. Ozeki et al., Physics issues of high bootstrap current tokamaks, *Plasma Phys. Control. Fusion* 39 (1997) A371–A380
- [3.22] R. Raman et al., Non-inductive solenoid-free plasma start-up using coaxial helicity injection, *Nucl. Fusion* 45 (2005) L15–L19
- [3.23] M. Nagata et al., Coaxial helicity injection plasma start-up and magnetic reconnection on HIST, *2016 IEEE International Conference on Plasma Science (ICOPS)*, 16211410
- [3.24] S. Pradhan et al., The First Experiment in SST-1, *Nuclear Fusion* 55 (2015) 104009 (10pp).
- [3.25] Ashoo N. Sharma, Thesis: Studies on quench characteristics of superconducting magnets of SST-1 (2015).

- [3.26] ANSYS Maxwell FEM Tools. <http://www.ansys.com/>
- [3.27] S. Jana et al., Vessel Eddy current characteristics in SST-1 tokamak, *Fusion engineering and design* 112 (2016) 380-387.
- [3.28] S. Jana et al., Magnetic flux surfaces and radial Shafranov shifts in SST-1 tokamak plasma, *Fusion engineering and design* 120 (2017) 39–48.
- [3.29] Chandan Dhanani and Sishir Deshpande, Effect of eddy currents on the magnetic null during SST-1 start-up, *IPR Report (2006)*.

Chapter IV

- [4.1] Peter E. Stott, Alan Wootton, Giuseppe Gorini, Elio Sindoni, Dimitri Batani., Advanced Diagnostics for Magnetic and Inertial Fusion, Springer Science and Business Media New York (2002)
- [4.2] Ian H. Hutchinson., Principles of Plasma Diagnostics, Cambridge University Press, (1987)
- [4.3] EQUIPE TFR et al., tokamak plasma diagnostics, *Nucl. Fusion* 18 (1978) 647.
- [4.4] D.V. Orlinskij and G. Magyar., Plasma diagnostics on large tokamaks, *Nucl. Fusion* 28 (1988) 611.
- [4.5] G F Matthews., tokamak plasma diagnosis by electrical probes, *Plasma Phys. Control. Fusion* 36 (1994) 1595.
- [4.6] T R Hodapp et al., Magnetic Diagnostics for Future tokamaks, *IEEE transactions on plasma science* (1995) 0-7803-2969.
- [4.7] J G Bak et al., Electrical Probe Diagnostics for KSTAR, *Contributions to Plasma Physics*, 50(9) (2010) 892–897
- [4.8] E J Strait., the Magnetic diagnostic system of the DIII-D tokamak, *Review OF Scientific Instruments* 77 (2006) 023502.
- [4.9] E J Strait. et al, Spatial and temporal analysis of DIII-D 3D magnetic diagnostic data, *Review OF Scientific Instruments* 87 (2016) 11D423.
- [4.10] G Vayakis et al., Magnetic diagnostics for ITER/BPX Plasmas, *Review of Scientific Instruments* 74 (2003) 2409.
- [4.11] P Moreau et al., A magnetic diagnostic on Tore Supra, *Review of Scientific Instruments* 74(2003) 4324
- [4.12] D. Testa et al., The magnetic diagnostic set for ITER, *Proceedings of the 23rd SOFE conference*, San Diego (USA), 01-05 June 2009.
- [4.13] L.C.J.M. De Kock et al., Magnetic diagnostics for fusion plasmas, *Nuclear Fusion*, 36(3) (1996) 387
- [4.14] D. Raju, et al., Design of magnetic diagnostics for SST-1, *Fusion Engineering and design* 34-35 (1997) 717-720
- [4.15] Ruo-Yu Han et al., Hybrid PCB Rogowski Coil for Measurement of Nanosecond-Risetime Pulsed Current, *IEEE Transactions on Plasma Science* 43(10) (2015) 3555
- [4.16] G. Tonetti, J. P. Christiansen, and L. de Kock, Measurement of the energy content of the JET tokamak plasma with a diamagnetic loop, *Rev.Sci. Instrum.* 57, 2087 (1986).
- [4.17] S. Besshou et al., Diamagnetic double-loop method for a highly sensitive measurement of energy stored in a Stellarator plasma, *Review of Scientific Instruments*, 72(10) 2001 0 3859-3863.
- [4.18] J. G. Bak, S. G. Lee, and H. S. Kim., Diamagnetic loop measurement in Korea Superconducting Tokamak Advanced Research machine, *Review of Scientific Instruments* 82, 063504 (2011)

- [4.19] E. Joffrin and P. Defrasne, Differential method for the real time measurement of the diamagnetic beta and internal inductance in Tore Supra *Rev.Sci. Instrum.* 73, 2266 (2002).
- [4.20] J.M. Moret, F. Bühlmann, and G. Tonetti, Fast single loop diamagnetic measurements on the tcv tokamak *Rev.Sci. Instrum.* 74, 4634 (2003).
- [4.21] B. Shen, B. N. Wan, and X. Q. Zhang, Poloidal beta and internal inductance measurement on HT-7 superconducting tokamak, *Fusion Eng. Des.* 70, 311 (2004).
- [4.22] A. Salar Elahi, et al., Estimation of plasma horizontal displacement using Flux loops and comparison with analytical solution in IR-T1 tokamak, *Journal of Nuclear and Particle Physics* 2(6) (2012) 142
- [4.23] H. Ninomiya and Norio Suzuki, Estimation of plasma position and $\beta_p + I_i/2$ from magnetic measurements under High $-\beta$ condition in JFT-2, *Japanese Journal of Applied Physics* (1982) 21(9) 1323-1327.
- [4.24] J. C. Schmitt et al., Magnetic diagnostics for equilibrium reconstructions with eddy currents on the lithium tokamak experiment, *Review of Scientific Instruments* 85 (2014)11E817
- [4.25] J. D. King et al., An upgrade of the magnetic diagnostic system of the DIII-D tokamak for non-axisymmetric measurements, *Review of Scientific Instruments* 85 (2014) 083503
- [4.26] R. Kaita et al., Diagnostics for initial plasma operations on the National Spherical Torus Experiment, *Review of Scientific Instruments* 70 (1999) 480.
- [4.27] F. De Marco et al., High magnetic field tokamaks, *Nucl. Fusion* 26 (1986) 1193.

Chapter V

- [5.1] R. Lopez- Callejas, et al., Plasma position measurement on Novillo tokamak, *Fusion Eng. Des.* 54 (2001) 21-29.
- [5.2] Seong-Heon Seo., Plasma current Position measurement in the Korea Superconducting Tokamak Advanced research device, *Physics of Plasmas* (2009),16032501.
- [5.3] H. Grad and H. Rubin., Hydromagnetic equilibria and force-free fields, *Proceedings of the Second United Nations Conference on the Peaceful Uses of Atomic Energy*, United Nations, Geneva, Vol. 31 (1958) 190-197.
- [5.4] V. D. Shafranov., On magnetohydrodynamical equilibrium configurations, *Soviet J. Exp. Theor. Phys.* 6(1958) 545-554.
- [5.5] V. D. Shafranov, Equilibrium of a toroidal plasma in a magnetic field, *Journal of Nuclear energy* 5 (1963) 251-258.
- [5.6] S. V. Mirnov, A probe method for measuring the displacement of the current channel in the cylindrical and toroidal discharge vessel, *Journal of Nuclear Energy* 7 (1965) 7325.
- [5.7] H. Ninomiya and Norio Suzuki, Estimation of plasma position and $\beta_p + I_i/2$ from magnetic measurements under High $-\beta$ condition in JFT-2, *Japanese Journal of Applied Physics* (1982) 21(9) 1323-1327.
- [5.8] A. Salar Elahi., et al., Measurement of plasma boundary shift and approximation of magnetic surfaces on the IR-T1 tokamak, *Brazilian journal of physics*, (2010) 40(3).
- [5.9] Rahimirad A., M. Ghoranneviss, Calculation of plasma horizontal displacement by using simulated plasma column in IR-T1 tokamak, *Phys. Sc.* 81 (2010) 045502
- [5.10] Gergo Pokol et al., Instructions for student measurements on the GOLEM tokamak, Internal Report on October 7, 2014
- [5.11] G De Tommasi et al., Current, Position, and Shape Control in tokamaks, *Fusion Science, and Technology* 59 (3) (2011) 486-498.

- [5.12] G. Hommen, et al., Optical boundary reconstruction of tokamak plasmas for feedback control of plasma position and shape, *Review of Scientific Instruments* (2010) 81113504.
- [5.13] G. Hommen, et al., Real-Time optical plasma boundary reconstruction for plasma position control at the TCV tokamak, *Nucl. Fusion* 54 (2014) 073018.
- [5.14] P. Hacek, et al., Plasma boundary reconstruction using the Fast camera on COMPASS tokamak, *WDS 14 Proceedings of contributed paper-physics* (2014) 221-226.

Chapter VI

- [6.1] H. Grad and H. Rubin., Hydromagnetic equilibria and force-free fields, *Proceedings of the Second United Nations Conference on the Peaceful Uses of Atomic Energy*, United Nations, Geneva, Vol. 31 (1958) 190-197.
- [6.2] V. D. Shafranov., On magnetohydrodynamical equilibrium configurations, *Soviet J. Exp. Theor. Phys.* 6(1958) 545-554.
- [6.3] V. D. Shafranov, Equilibrium of a toroidal plasma in a magnetic field, *Journal of nuclear energy* 5 (1963) 251-258.
- [6.4] V. S. Mukhovatav and V. D. Shafranov, Plasma equilibrium in a tokamak, *Nucl. Fusion* 11 (1971) 605.
- [6.5] S. B Zheng, A.J. Wootton and E. R. Solano, Analytical tokamak equilibrium for shaped plasmas, *Phys. of Plasmas* 3 (1996) 1176.
- [6.6] C. V. Atanasiu, S. Gunter, K. Lackner, and I. G. Miron, Analytical solutions to the Grad Shafranov equation, *Physics of Plasmas* 11(7) (2004).
- [6.7] M.Asif, A. Asif, Study of poloidal beta and internal inductance by solving the simplest Grad Shafranov equation for a tokamak with a circular cross-section, *Journal of Applied Mechanics and Technical Physics* (2014) 55(6) 927.
- [6.8] Remi G. Lefrancois, et al., Numerical investigation of three-dimensional single-species plasma equilibria on magnetic surfaces, *Physics of Plasma* (2005)12 072105.
- [6.9] J.R. Ferron, et al., Real-time equilibrium reconstructions for tokamak discharge control, *Nuclear Fusion* 38(7) (1998).
- [6.10] L.L. Lao, et al., Equilibrium Analysis of Current Profiles in tokamaks, *Nucl. Fusion* 30 (1990) 1035.
- [6.11] Z. Amerian, et al., Control of heat and mass transfer processes by plasma equilibrium reconstruction in toroidal magnetic confinement nuclear fusion devices, *International Journal of Thermal Sciences* (2016) 110 299-303.
- [6.12] R. Lopez- Callejas, et al., Plasma position measurement on Novillo tokamak, *Fusion Eng. Des.* 54 (2001) 21-29.
- [6.13] Seong-Heon Seo., Plasma current Position measurement in the Korea Superconducting tokamak Advanced research device, *Physics of Plasmas* (2009), 16032501.
- [6.14] S. V. Mirnov, A probe method for measuring the displacement of the current channel in the cylindrical and toroidal discharge vessel, *Journal of nuclear energy* 7 (1965) 7325.
- [6.15] L. S. Solov'ev, et al., *Soviet Physics JETP* 26(2) (1968) 400.
- [6.16] A. Rahimirad, et al., Demonstration of Shafranov Shift by the Simplest Grad-Shafranov Equation Solution in IR-T1 tokamak, *Journal of fusion energy* 29 (2010) 73.

Chapter VII

- [7.1] D. C. Robinson and A. J. Wootton., An experimental study of tokamak plasmas with vertically elongated cross-sections. *Nuclear Fusion* 18 (1978) 1555–1567.

- [7.2] E. Rebhan and A Salat, Feedback stabilization of axisymmetric MHD instabilities in tokamaks. *Nuclear Fusion* 18 (1978) 1431–1444
- [7.3] S.C. Jardin, D.A. Larrabee, Feedback stabilization of rigid axisymmetric modes in tokamaks. *Nuclear Fusion* 22 (1982) 1095–1098
- [7.4] S. Moriyama et al., Analysis of optimal feedback control of vertical plasma position in a tokamak system. *Japanese Journal of Applied Physics* 24 (1985)849–855.
- [7.5] M. M. M. Al-Husari et al, Vertical Stabilization of tokamak Plasmas. *Proc. 30th IEEE Conference on Decision and Control*, Brighton (UK) (1991)
- [7.6] J. R. Gossner et al., Application of cautious stable predictive control to vertical positioning in COMPASS-D tokamak. *IEEE Trans. on Control Systems Technology* 7 (1999) 580–587.
- [7.7] M. Lennholm, D. Campbell, F. Milani, S. Puppini, F. Sartori, B. Tubbing, Plasma vertical stabilization at JET using adaptive gain adjustment. *Proc. 17th IEEE/NPSS Symposium on Fusion Engineering*, San Diego (CA) (1997).
- [7.8] R. Albanese, V. Coccolese, G. Rubinacci, Plasma modeling for the control of vertical instabilities. *Nuclear Fusion* 29 (1989) 1013–1023.
- [7.9] D.A. Humphreys, I. H. Hutchinson Axisymmetric magnetic control design in tokamaks using perturbed plasma equilibrium response modeling, *Fusion Technology* 23 (1993) 167–184.
- [7.10] P. Vyas, A.W. Morris, D. Mustafa, Vertical Position Control on COMPASS-D. *Fusion Technology* 33 (1998) 97–105.
- [7.11] L. Scibile, B. A Kouvaritakis, Discrete adaptive near-time optimum control for the plasma vertical position in a tokamak. *IEEE Transactions on Control Systems Technology* 9 (2001)148–162.
- [7.12] J.E. Morelli, A. Hirose, H.C. Wood, Fuzzy-Logic-Based Plasma-Position Controller for STOR-M. *IEEE Transactions on Control Systems Technology* 13 (2005)328–337.
- [7.13] M.L. Walker, D.A. Humphreys., A Multivariable Analysis of the Plasma Vertical Instability in tokamaks. *Proceedings of the 45th IEEE Conference on Decision and Control*, San Diego (CA) (2006)
- [7.14] M. Sharma et al., Overview of data acquisition system for SST-1 diagnostics, *Fusion Engineering and Design* 112 (2016) 872–876.
- [7.15] Kirti Mahajan et al., CORBA-based solution for remote participation in SST-1 tokamak control and operation, *Fusion Engineering and Design* 81 (2006) 2069–2072.
- [7.16] Kirit Patel et al., Design and Architecture of SST-1 basic plasma control system, *Fusion Engineering and Design* 112 (2016) 703–709.

